Logarithmic Expansions and the Stability of Periodic Patterns of Localized Spots for Reaction-Diffusion Systems in $\mathbb{R}^2$

D. IRON, J. RUMSEY, M. J. WARD, and J. WEI

David Iron; Department of Mathematics, Dalhousie University, Halifax, Nova Scotia, B3H 3J5, Canada,
John Rumsey; Faculty of Management, Dalhousie University, Halifax, Nova Scotia, B3H 3J5, Canada,
Michael Ward; Department of Mathematics, University of British Columbia, Vancouver, British Columbia, V6T 1Z2, Canada,
Juncheng Wei, Department of Mathematics, University of British Columbia, Vancouver, British Columbia, V6T 1Z2, Canada and
Department of Mathematics, Chinese University of Hong Kong, Shatin, New Territories, Hong Kong.

(*Received 4 March 2014*)

The linear stability of steady-state periodic patterns of localized spots in $\mathbb{R}^2$ for the two-component Gierer-Meinhardt (GM) and Schnakenburg reaction-diffusion models is analyzed in the semi-strong interaction limit corresponding to an asymptotically small diffusion coefficient ε^2 of the activator concentration. In the limit $\varepsilon \to 0$, localized spots in the activator are centered at the lattice points of a Bravais lattice with constant area $|\Omega|$. To leading order in $\nu = -1/\log\varepsilon$, the linearization of the steady-state periodic spot pattern has a zero eigenvalue when the inhibitor diffusivity satisfies $D = D_0/\nu$, for some D_0 independent of the lattice and the Bloch wavevector $\boldsymbol{k}$. From a combination of the method of matched asymptotic expansions, Floquet-Bloch theory, and the rigorous study of certain nonlocal eigenvalue problems, an explicit analytical formula for the continuous band of spectrum that lies within an $\mathcal{O}(\nu)$ neighborhood of the origin in the spectral plane is derived when $D = D_0/\nu + D_1$, where $D_1 = \mathcal{O}(1)$ is a de-tuning parameter. The periodic pattern is linearly stable when D_1 is chosen small enough so that this continuous band is in the stable left-half plane $\mathrm{Re}(\lambda) < 0$ for all $\boldsymbol{k}$. Moreover, for both the Schnakenburg and GM models, our analysis identifies a model-dependent objective function, involving the regular part of the Bloch Green's function, that must be maximized in order to determine the specific periodic arrangement of localized spots that constitutes a linearly stable steady-state pattern for the largest value of D. From a numerical computation, based on an Ewald-type algorithm, of the regular part of the Bloch Green's function that defines the objective function, it is shown within the class of oblique Bravais lattices that a regular hexagonal lattice arrangement of spots is optimal for maximizing the stability threshold in D.

Key words: singular perturbations, localized spots, logarithmic expansions, Bravais lattice, Floquet-Bloch theory, Green's function, nonlocal eigenvalue problem.

1 Introduction

Spatially localized spot patterns occur for various classes of reaction-diffusion (RD) systems with diverse applications to theoretical chemistry, biological morphogenesis, and applied physics. A survey of experimental and theoretical studies, through RD modeling, of localized spot patterns in various chemical contexts is given in [**30**]. Localized spot patterns have also been analyzed for complex-valued PDE models arising in the field of nonlinear optics. In this different context, the formation of clusters of localized spots of light in a driven optical cavity was analyzed in [**31**]. Owing to the widespread occurrence of localized patterns in various scientific applications, there has been considerable focus over the past decade on developing a theoretical understanding of the dynamics and stability of localized solutions to singularly perturbed RD systems. A brief survey of some open directions for the theoretical study of localized patterns in various applications is given in [**14**]. More generally, a wide range of topics in the analysis of far-from-equilibrium patterns modeled by PDE systems are discussed in [**22**].

In the singularly perturbed limit, many two-component reaction-diffusion (RD) systems allow for the existence of localized spot patterns where one or both of the solution components concentrate, or localize, at certain points in the domain. For the case where only one of the two solution components is localized, the spots are said to exhibit semi-strong interactions. The goal of this paper is to analyze the linear stability of steady-state periodic patterns of localized spots in $\mathbb{R}^2$ for two-component RD systems in the semi-strong interaction regime characterized by an asymptotically large diffusivity ratio. For concreteness, we will focus our analysis on two specific models. One model is a simplified Schnakenburg-type system

$$v_t = \varepsilon^2 \Delta v - v + uv^2\,, \qquad \tau u_t = D\Delta u + a - \varepsilon^{-2} uv^2\,, \tag{1.1}$$

where $0 < \varepsilon \ll 1$, $D > 0$, $\tau > 0$, and $a > 0$, are parameters. The second model is the prototypical Gierer-Meinhardt (GM) model formulated as

$$v_t = \varepsilon^2 \Delta v - v + v^2/u\,, \qquad \tau u_t = D\Delta u - u + \varepsilon^{-2} v^2\,, \tag{1.2}$$

where $0 < \varepsilon \ll 1$, $D > 0$, and $\tau > 0$, are parameters.

Our linear stability analysis for these two models will focus on the semi-strong interaction regime characterized by $\varepsilon \to 0$ with $D = \mathcal{O}(1)$. For $\varepsilon \to 0$, the localized spots for v are taken to be centered at the lattice points of a general Bravais lattice Λ, where the area $|\Omega|$ of the primitive cell is held constant. A brief outline of lattices and reciprocal lattices is given in §2.1. Our main goal for the Schnakenburg and GM models is to formulate an explicit objective function to be maximized that will identify the specific lattice arrangement of localized spots that is a linearly stable steady-state pattern for the largest value of D. Through a numerical computation of this objective function we will show that it is a regular hexagonal lattice arrangement of spots that yields this optimal stability threshold. This objective function is described in more detail below.

There is a rather extensive literature on the existence and stability of 1-D spike patterns for two-component RD systems in the semi-strong regime. In [**9**] and [**10**] the existence and stability of spike patterns for the GM and Gray-Scott models on the infinite line was analyzed using geometric singular perturbation theory and Evans function techniques. These techniques, together with a Floquet-based analysis, were used in [**29**] to analyze the stability of spatially periodic spikes for the GM model on the infinite line. On a bounded 1-D domain with homogeneous Neumann boundary conditions, the stability of N-spike steady-state solutions was analyzed in [**11**] and [**33**] through a detailed study of certain nonlocal eigenvalue problems. On a bounded $2-D$ domain with Neumann boundary conditions, a leading order in $\nu = -1/\log\varepsilon$ rigorous theory was developed to analyze the stability of multi-spot steady-state patterns for the GM model (cf. [**34**], [**36**]), the Schnakenburg model (cf. [**38**]), and the Gray-Scott (GS) model (cf. [**37**]), in the parameter regime where $D = D_0/\nu \gg 1$. For the Schnakenburg and GM models, the leading-order stability threshold for D_0 corresponding to a zero eigenvalue crossing was determined explicitly. A hybrid asymptotic-numerical theory to study the stability, dynamics, and self-replication patterns of spots, that is accurate to all powers in ν, was developed for the Schnakenburg model in [**12**] and for the GS model in [**8**]. In [**19**] and [**21**], the stability and self-replication behavior of a one-spot solution for the GS model was analyzed.

One of the key features of the finite domain problem in comparison with the periodic problem is that the spectrum of the linearization of the former is discrete rather than continuous. As far as we are aware, to date there has been no analytical study of the stability of periodic patterns of localized spots in $\mathbb{R}^2$ on Bravais lattices for singularly perturbed two-component RD systems. In the weakly nonlinear Turing regime, an analysis of the stability of patterns on Bravais lattices in $\mathbb{R}^3$ using group-theoretic tools of bifurcation theory with symmetry was done in [**5**] and [**6**].

By using the method of matched asymptotic expansions, in the limit $\varepsilon \to 0$ a steady-state localized spot solution is constructed for (1.1) and for (1.2) within the fundamental Wigner-Seitz cell of the lattice. The solution is then extended periodically to all of $\mathbb{R}^2$. The stability of this solution with respect to $\mathcal{O}(1)$ time-scale instabilities arising from zero eigenvalue crossings is then investigated by first using the Floquet-Bloch theorem (cf. [**15**], [**16**]) to formulate a singularly perturbed eigenvalue problem in the Wigner-Seitz cell Ω with quasi-periodic boundary conditions on $\partial\Omega$ involving the Bloch vector $\boldsymbol{k}$. In § 2.2, the Floquet-Bloch theory is formulated and a few key properties of the Bloch Green's function for the Laplacian are proved. In § 3 and § 4, the spectrum of the linearized eigenvalue problem is analyzed by using the method of matched asymptotic expansions combined with a spectral analysis based on perturbations of a nonlocal eigenvalue problem. More specifically, to leading-order in $\nu = -1/\log\varepsilon$ it is shown that a zero eigenvalue crossing occurs when $D \sim D_0/\nu$, where D_0 is a constant that depends on the parameters in the RD system, but is independent of the lattice geometry except through the area $|\Omega|$ of the Wigner-Seitz cell. Therefore, to leading-order in ν, the stability threshold is the same for any periodic spot pattern on a Bravais lattice Λ when $|\Omega|$ is held fixed. In order to determine the effect of the lattice geometry on the stability threshold, an expansion to higher-order in ν must be undertaken. In related singularly perturbed eigenvalue problems for the Laplacian in 2-D domains with holes, the leading-order eigenvalue asymptotics in the limit of small hole radius only depends on the number of holes and the area of the domain, and not on the arrangement of the holes within the domain. An analytical theory to calculate higher order terms in the eigenvalue asymptotics for these problems, which have applications to narrow-escape and capture phenomena in mathematical biology, is given in [**32**], [**13**], and [**24**].

To determine a higher-order approximation for the stability threshold for the periodic spot problem we perform a more refined perturbation analysis in order to calculate the continuous band $\lambda \sim \nu\lambda_1(\boldsymbol{k}, D_1, \Lambda)$ of spectra that lies within an $\mathcal{O}(\nu)$ neighborhood of the origin, i.e that satisfies $|\lambda(\boldsymbol{k}, D_1, \Lambda)| \leq \mathcal{O}(\nu)$, when $D = D_0/\nu + D_1$ for some de-tuning parameter $D_1 = \mathcal{O}(1)$. This band is found to depend on the lattice geometry Λ through the regular part of certain Green's functions. For the Schnakenburg model, λ_1 depends on the regular part $R_{b0}(\boldsymbol{k})$of the Bloch Green's function for the Laplacian, which depends on both $\boldsymbol{k}$ and the lattice. For the GM Model, λ_1 depends on both $R_{b0}(\boldsymbol{k})$ and the regular part R_{0p} of the periodic source-neutral Green's function on Ω. For both models, this band of continuous spectrum that lies near the origin when $D - D_0/\nu = \mathcal{O}(1)$ is proved to be real-valued.

For both the Schnakenburg and GM models, the de-tuning parameter D_1 on a given lattice is chosen so that $\lambda_1 < 0$ for all $\boldsymbol{k}$. Then, to determine the lattice for which the steady-state spot pattern is linearly stable for the largest possible value of D, we simply maximize D_1 with respect to the lattice geometry. In this way, for each of the two RD models, we derive a model-dependent objective function in terms of the regular parts of certain Green's functions that must be maximized in order to determine the specific periodic arrangement of localized spots that is linearly stable for the largest value of D. The model-dependent objective function $\mathcal{K}$ has the general form

$$\mathcal{K} \equiv a \min_{\boldsymbol{k}} R_{b0}(\boldsymbol{k}) - bR_{0p}\,,$$

for some constants $a > 0$ and $b \geq 0$. Here $R_{b0}(\boldsymbol{k})$ is the regular part of the Bloch Green's function for the Laplacian with Bloch wavevector $\boldsymbol{k}$, and R_{0p} is the regular part of the periodic source-neutral Green's function defined on the Wigner-Seitz cell. The calculation of the continuous band of spectra near the origin, and the derivation of the specific objective function to be maximized so as to identify the optimal lattice, is done for the Schnakenburg and GM models in § 3 and § 4, respectively.

In § 5.1 and § 5.2 we exhibit a very simple alternative method to readily identify this objective function for the Schnakenburg and GM models, respectively. In § 5.3, this simple alternative method is then used to determine an

optimal lattice arrangement of spots for the GS RD model by first calculating the objective function specific for the GS model.

In § 6 we show how to numerically compute the regular part $R_{b0}(\boldsymbol{k})$ of the Bloch Green's function for the Laplacian that is key for identifying the optimal lattice. Similar Green's functions, but for the Helmholtz operator, arise in the linearized theory of the scattering of water waves by a periodic arrangement of obstacles, and in related wave phenomena in electromagnetics and photonics. The numerical computation of Bloch Green's functions is well-known to be a challenging problem owing to the very slow convergence of their infinite series representations in the spatial domain, and methodologies to improve the convergence properties based on the Poisson summation formula are surveyed in [**17**] and [**18**]. The numerical approach we use to compute $R_{b0}(\boldsymbol{k})$ is an Ewald summation method, based on the Poisson summation formula involving the direct and reciprocal lattices, and follows closely the methodology developed in [**3**] and [**4**]. Our numerical results show that within the class of oblique Bravais lattices having a common area $|\Omega|$ of the primitive cell, it is a regular hexagonal lattice that optimizes the stability threshold for the Schnakneburg, GM, and GS models.

Finally, we remark that optimal lattice arrangements of localized structures in other PDE models having a variational structure, such as the study of vortices in Ginzburg-Landau theory (cf. [**26**]), the analysis of Abrikosov vortex lattices in the magnetic Ginzburg-Landau system (cf. [**27**, **28**]) and the study of droplets in diblock copolymer theory (cf. [**7**]), have been identified through the minimization of certain energy functionals. In contrast, for our RD systems having no variational structure, the optimal lattice is identified not through an energy minimization criterion, but instead from a detailed analysis that determines the spectrum of the linearization near the origin in the spectral plane when D is near a critical value.

2 Lattices and the Bloch Green's Functions

In this section we recall some basic facts about lattices and we introduce the Bloch-periodic Green's functions that plays a central role in the analysis in §3–5. A few key lemmas regarding this Green's function are established.

2.1 A Primer on Lattices and Reciprocal Lattices

Let $\boldsymbol{l}_1$ and $\boldsymbol{l}_2$ be two linearly independent vectors in $\mathbb{R}^2$, with angle θ between them, where without loss of generality we take $\boldsymbol{l}_1$ to be aligned with the positive x-axis. The Bravais lattice Λ is defined by

$$\Lambda = \left\{ m\boldsymbol{l}_1 + n\boldsymbol{l}_2 \;\middle|\; m,\, n \in \mathbb{Z} \right\}, \tag{2.1}$$

where $\mathbb{Z}$ denotes the set of integers. The *primitive* cell is the parallelogram generated by the vectors $\boldsymbol{l}_1$ and $\boldsymbol{l}_2$ of area $|\boldsymbol{l}_1 \times \boldsymbol{l}_2|$. We will set the area of the primitive cell to unity, so that $|\boldsymbol{l}_1||\boldsymbol{l}_2| \sin\theta = 1$.

We can also write $\boldsymbol{l}_1, \boldsymbol{l}_2 \in \mathbb{R}^2$ as complex numbers $\alpha, \beta \in \mathbb{C}$. Without loss of generality we set $\mathrm{Im}(\beta) > 0$, $\mathrm{Im}(\alpha) = 0$, and $\mathrm{Re}(\alpha) > 0$. In terms of α and β, the area of the primitive cell is $\mathrm{Im}(\overline{\alpha}\,\beta)$, which we set to unity. For a regular hexagonal lattice, $|\alpha| = |\beta|$, with $\beta = \alpha\, e^{i\theta}$, $\theta = \pi/3$, and $\alpha > 0$. This yields $\mathrm{Im}(\beta) = \alpha\sqrt{3}/2$ and the unit area requirement gives $\alpha^2\sqrt{3}/2 = 1$, which yields $\alpha = (4/3)^{1/4}$. For the square lattice, we have $\alpha = 1$, $\beta = i$, and $\theta = \pi/2$.

In terms of $\boldsymbol{l}_1, \boldsymbol{l}_2 \in \mathbb{R}^2$, we have that $\boldsymbol{l}_1 = \big(\mathrm{Re}(\alpha), \mathrm{Im}(\alpha)\big)$, $\boldsymbol{l}_2 = \big(\mathrm{Re}(\beta), \mathrm{Im}(\beta)\big)$ generate the lattice (2.1). For a regular hexagonal lattice of unit area for the primitive cell we have

$$\boldsymbol{l}_1 = \left(\left(\frac{4}{3}\right)^{1/4}, 0 \right) \qquad \text{and} \qquad \boldsymbol{l}_2 = \left(\frac{4}{3}\right)^{1/4} \left(\frac{1}{2}, \frac{\sqrt{3}}{2} \right). \tag{2.2}$$

In Fig. 1 we plot a portion of the hexagonal lattice generated with this $\boldsymbol{l}_1, \boldsymbol{l}_2$ pair.

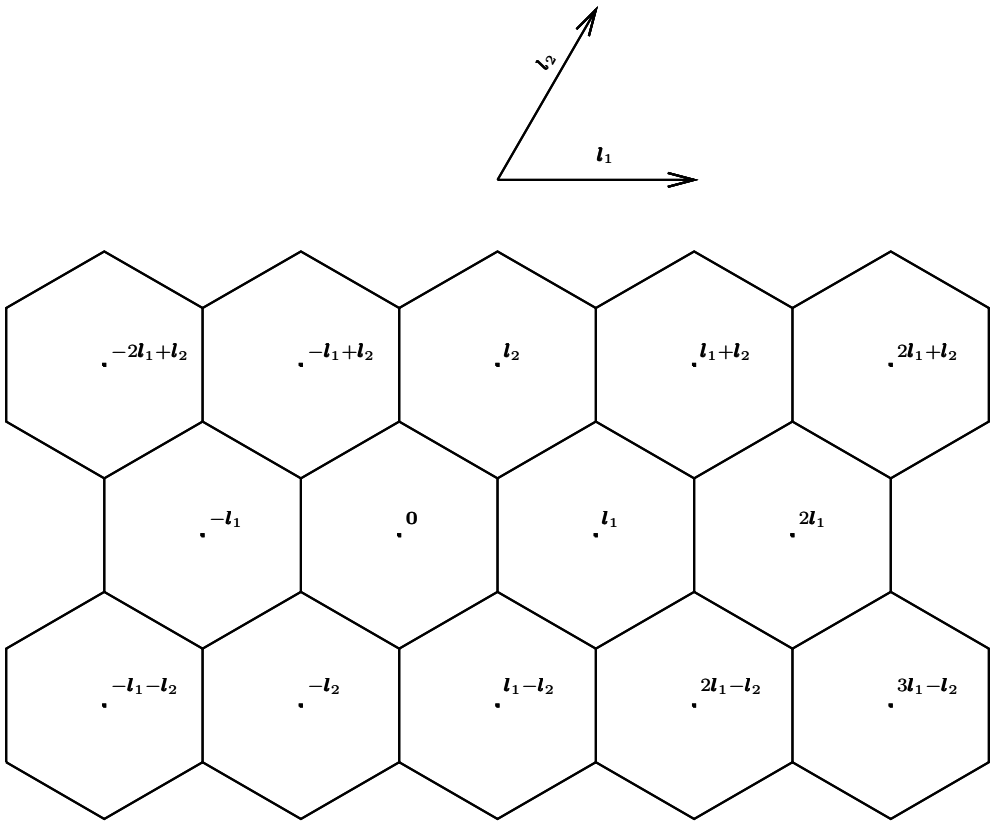

Figure 1. Hexagonal lattice generated by the lattice vectors (2.2). The fundamental Wigner-Seitz cell Ω for this lattice is the regular hexagon centered at the origin. The area Ω and the primitive cell are the same, and are set to unity.

The *Wigner-Seitz or Voronoi cell* centered at a given lattice point of Λ consists of all points in the plane that are closer to this point than to any other lattice point. It is constructed by first joining the lattice point by a straight line to each of the neighbouring lattice points. Then, by taking the perpendicular bisector to each of these lines, the Wigner-Seitz cell is the smallest area around this lattice point that is enclosed by all the perpendicular bisectors. The Wigner-Seitz cell is a convex polygon with the same area $|\boldsymbol{l}_1 \times \boldsymbol{l}_2|$ of the primitive cell $\mathcal{P}$. In addition, it is well-known that the union of the Wigner-Seitz cells for an arbitrary oblique Bravais lattice with arbitrary lattice vectors $\boldsymbol{l}_1, \boldsymbol{l}_2$, and angle θ, tile all of $\mathbb{R}^2$ (cf. [**2**]). In other words, there holds

$$\mathbb{R}^2 = \bigcup_{z \in \Lambda} (z + \Omega)\,. \tag{2.3}$$

By periodicity and the property (2.3), we need only consider the Wigner-Seitz cell centered at the origin, which we denote by Ω. In Fig. 1 we show the fundamental Wigner-Seitz cell for the hexagonal lattice. In Fig. 2 we plot the union of the Wigner-Seitz cells for an oblique Bravais lattice with $\boldsymbol{l}_1 = (1, 0)$, $\boldsymbol{l}_2 = (\cot\theta, 1)$ and $\theta = 74^\circ$.

As in [**3**], we define the reciprocal lattice $\Lambda^\star$ in terms of the two independent vectors $\boldsymbol{d}_1$ and $\boldsymbol{d}_2$, which are obtained from the lattice Λ by requiring that

$$\boldsymbol{d}_i \cdot \boldsymbol{l}_j = \delta_{ij}\,, \tag{2.4}$$

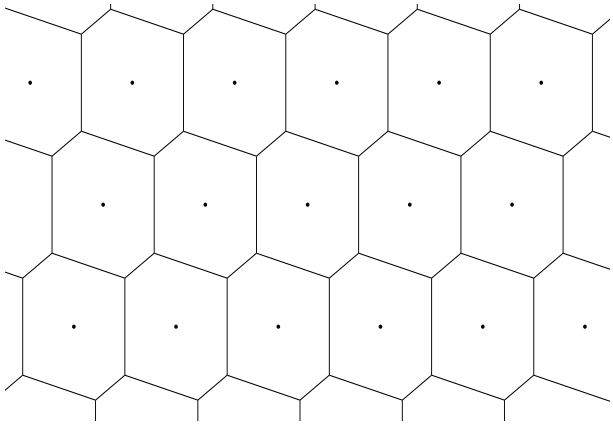

Figure 2. Wigner-Seitz cells for an oblique lattice with $\boldsymbol{l}_1 = (1, 0)$, $\boldsymbol{l}_2 = (\cot\theta, 1)$, and $\theta = 74°$, so that $|\Omega| = 1$. These cells tile the plane. The boundary of the Wigner-Seitz cells consist of three pairs of parallel lines of equal length.

where δ_{ij} is the Kronecker symbol. The reciprocal lattice $\Lambda^\star$ is defined by

$$\Lambda^\star = \left\{ m\boldsymbol{d}_1 + n\boldsymbol{d}_2 \;\middle|\; m,\, n \in \mathbb{Z} \right\}. \tag{2.5}$$

The first Brillouin zone, labeled by Ω_B, is defined as the Wigner-Seitz cell centered at the origin in the reciprocal space.

We remark that other authors (cf. [**17**], [**18**]) define the reciprocal lattice as $\Lambda^\star = \{2\pi m\,\boldsymbol{d}_1, 2\pi n\,\boldsymbol{d}_2\}_{m,n\in\mathbb{Z}}$. Our choice (2.5) for $\Lambda^\star$ is motivated by the form of the Poisson summation formula of [**3**] given in (6.4) below, and which is used in § 6 to numerically compute the Bloch Green's function.

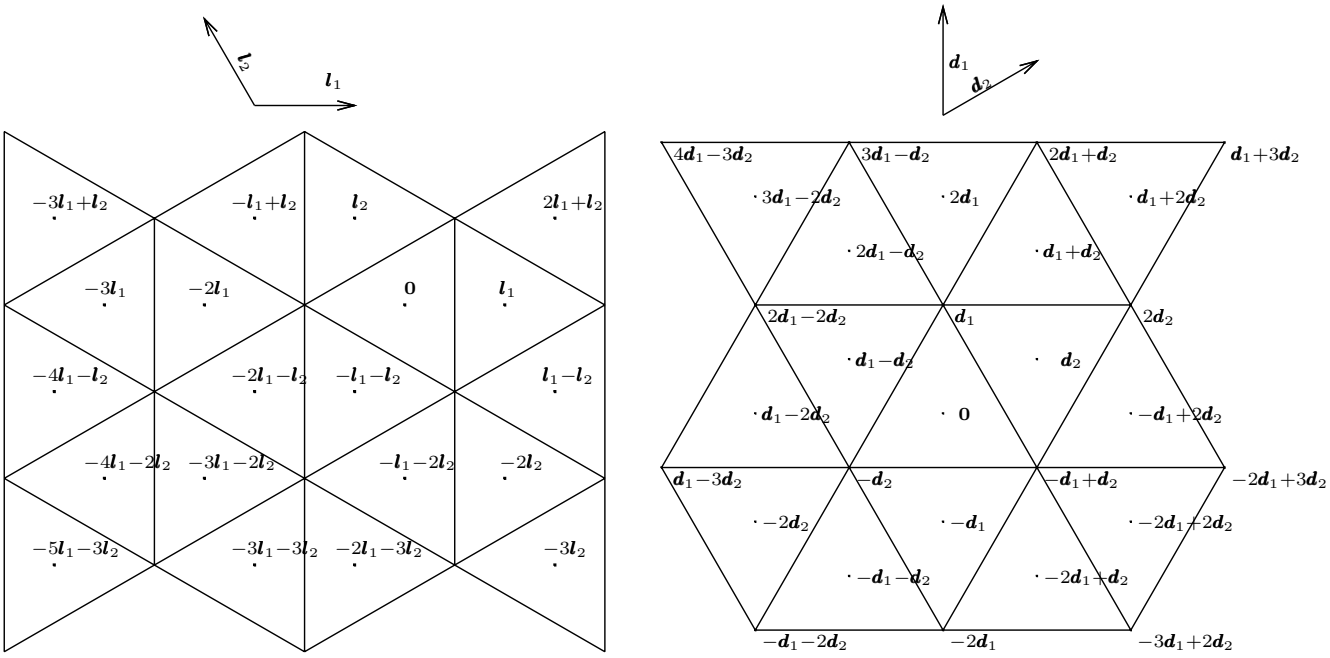

(a) Lattice Λ (b) Reciprocal Lattice Λ^*

Figure 3. Left panel: Triangular lattice Λ with unit area of the primitive cell generated by the lattice vectors in (2.6). Right panel: the corresponding reciprocal lattice Λ^* with reciprocal lattice vectors as in (2.9).

Finally we make some remarks on the equilateral triangular lattice which does not fall into the framework discussed above. As observed in [**7**], this special lattice requires a different treatment. For the equilateral triangle lattice, $\theta = 2\pi/3$ and $\mathrm{Im}\big(e^{2i\pi/3}\big) = \sqrt{3}/2$, so that the unit area requirement of the primitive cell again yields $\alpha = (4/3)^{1/4}$. Since $\mathrm{Re}\big(e^{2i\pi/3}\big) = -1/2$, it follows that in terms of $\boldsymbol{l}_i \in \mathbb{R}^2$ for $i = 1, 2$, an equilateral triangle cell structure has

$$\boldsymbol{l}_1 = \left(\left(\frac{4}{3}\right)^{1/4}, 0\right) \qquad \text{and} \qquad \boldsymbol{l}_2 = \left(\frac{4}{3}\right)^{1/4}\left(-\frac{1}{2}, \frac{\sqrt{3}}{2}\right). \tag{2.6}$$

This triangular lattice is shown in Fig. 3. The centers of the triangular cells are generated by (2.1), but there are points in Λ which are not cell centers (see Fig. 3). For example, $(3n+1)\boldsymbol{l}_1+\boldsymbol{l}_2$, $(3n+2)\boldsymbol{l}_1$, $3n\boldsymbol{l}_1-\boldsymbol{l}_2$, and $(3n+1)\boldsymbol{l}_1-2\boldsymbol{l}_2$ are not centers of cells of equilateral triangles. In general, for integers p and q the point $p\boldsymbol{l}_1 + q\boldsymbol{l}_2$ will be a vertex instead of a cell center when

$$(p \mod 3) + (q \mod 3) = 2\,, \tag{2.7}$$

where the positive representation of the mod function is used, i.e. $(-1) \mod 3 = 2$. Thus, for the equilateral triangular lattice the set of lattice points is

$$\Lambda_{tri} = \left\{ m\boldsymbol{l}_1 + n\boldsymbol{l}_2 \;\middle|\; m,\, n \in \mathbb{Z}\,,\ (m \mod 3) + (n \mod 3) \neq 2 \right\}. \tag{2.8}$$

The corresponding Wigner-Seitz cell is also an equilateral triangle.

Regarding the reciprocal lattice for the equilateral triangular lattice with $\boldsymbol{l}_1$ and $\boldsymbol{l}_2$ given by (2.6), the defining vectors for $\Lambda^\star$ are

$$\boldsymbol{d}_1 = \frac{1}{12^{1/4}}\left(\sqrt{3}, 1\right) \qquad \text{and} \qquad \boldsymbol{d}_2 = \frac{1}{12^{1/4}}\,(0, 2)\,, \tag{2.9}$$

as can be verified by substitution into (2.4). A plot of a portion of this reciprocal lattice for the equilateral triangle lattice is shown in the right panel of Fig. 3. From this plot it follows that, for integer p and q, $p\boldsymbol{d}_1 + q\boldsymbol{d}_2$ will be a vertex, not a centre, when

$$(p - q) \mod 3 = 1\,. \tag{2.10}$$

Therefore the reduced reciprocal lattice becomes

$$\Lambda^\star_{tri} = \left\{ m\boldsymbol{d}_1 + n\boldsymbol{d}_2 \;\middle|\; m,\, n \in \mathbb{Z}\,,\ (m - n) \mod 3 \neq 1 \right\}. \tag{2.11}$$

Unfortunately for the equilateral triangular lattice the property (2.3) does not hold. In other words, the whole $\mathbb{R}^2$ is not the union of cells translated on the Bravais lattice, and thus one can not restrict to one Wigner-Seitz cell at the origin. As such, it is unclear whether the corresponding Poisson summation formula in (6.4) below still holds. However, if a homogeneous Neumann boundary condition is imposed on the cell, it is possible to reflect through the edges and fill the whole $\mathbb{R}^2$. (This fact has been used in [**7**].) Therefore, the equilibrium contruction of a periodic spot pattern presented in Section 3.1 and Section 4.1 still applies for the equilateral triangular lattice. However, the stability of periodic spot patterns on the triangular lattice is an open problem.

2.2 A Few Key Properties of the Bloch Green's Functions

In our analysis of the stability of spot patterns in § 3.2 and § 4.2 below, the Bloch Green's function $G_{b0}(\mathbf{x})$ for the Laplacian plays a prominent role. In the Wigner-Seitz cell Ω, $G_{b0}(\mathbf{x})$ for $\boldsymbol{k}/(2\pi) \in \Omega_B$, satisfies

$$\Delta G_{b0} = -\delta(\mathbf{x})\,; \qquad \mathbf{x} \in \Omega\,, \tag{2.12 a}$$

subject to the quasi-periodicity condition on $\mathbb{R}^2$ that

$$G_{b0}(\mathbf{x}+\boldsymbol{l}) = e^{-i\boldsymbol{k}\cdot\boldsymbol{l}}\, G_{b0}(\mathbf{x})\,, \qquad \boldsymbol{l}\in\Lambda\,, \tag{2.12 b}$$

where Λ is the Bravais lattice (2.1). As we show below, (2.12 b) indirectly yields boundary conditions on the boundary $\partial\Omega$ of the Wigner-Seitz cell. The regular part $R_{b0}(\boldsymbol{k})$ of this Bloch Green's function is defined by

$$R_{b0}(\boldsymbol{k}) \equiv \lim_{\mathbf{x}\to 0}\left(G_{b0}(\mathbf{x}) + \frac{1}{2\pi}\log|\mathbf{x}|\right)\,. \tag{2.12 c}$$

In order to study the properties of $G_{b0}(\mathbf{x})$ and $R_{b0}(\boldsymbol{k})$, we first require a more refined description of the Wigner-Seitz cell. To do so, we observe that there are eight nearest neighbor lattice points to $\mathbf{x}=0$ given by the set

$$P \equiv \{\, m\boldsymbol{l}_1 + n\boldsymbol{l}_2 \mid m\in\{0,1,-1\}\,,\ n\in\{0,1,-1\}\,,\ (m,n)\neq 0\}\,. \tag{2.13}$$

For each (vector) point $\boldsymbol{P}_i\in P$, for $i=1,\ldots,8$, we define a Bragg line L_i. This is the line that crosses the point $\boldsymbol{P}_i/2$ orthogonally to $\boldsymbol{P}_i$. We define the unit outer normal to L_i by $\boldsymbol{\eta}_i \equiv \boldsymbol{P}_i/|\boldsymbol{P}_i|$. The convex hull generated by these Bragg lines is the Wigner-Seitz cell Ω, and the boundary $\partial\Omega$ of the Wigner-Seitz cell is, generically, the union of six Bragg lines. For a square lattice, $\partial\Omega$ has four Bragg lines. The centers of the Bragg lines generating $\partial\Omega$ are re-indexed as $\boldsymbol{P}_i$ for $i=1,\ldots,L$, where $L\in\{4,6\}$ is the number of Bragg lines de-marking $\partial\Omega$. The boundary $\partial\Omega$ of Ω is the union of the re-indexed Bragg lines L_i, for $i=1,\ldots,L$, and is parametrized segment-wise by a parameter t as

$$\partial\Omega = \Big\{ \mathbf{x}\in \bigcup_i \{\frac{\boldsymbol{P}_i}{2} + t\boldsymbol{\eta}_i^{\perp}\} \ \Big|\ -t_i\le t\le t_i\,,\ \ i=1,\ldots,L\,,\ \ L=\{4,6\}\Big\}\,. \tag{2.14}$$

Here $2t_i$ is the length of L_i, and $\boldsymbol{\eta}_i^{\perp}$ is the direction perpendicular to $\boldsymbol{P}_i$, and therefore tangent to L_i.

The following observation is central to the analysis below: Suppose that $\boldsymbol{P}$ is a neighbor of 0 and that the Bragg line crossing $\boldsymbol{P}/2$ lies on $\partial\Omega$. Then, by symmetry, the Bragg line crossing $-\boldsymbol{P}/2$ must also lie on $\partial\Omega$. In other words, Bragg lines on $\partial\Omega$ must come in pairs. This fact is evident from the plot of the Wigner-Seitz cell for the oblique lattice shown in Fig. 2. With this more refined description of the Wigner-Seitz cell, we now state and prove two key Lemmas that are needed in § 3.2 and § 4.2 below.

Lemma 2.1 *The regular part $R_{b0}(\boldsymbol{k})$ of the Bloch Green's function $G_{b0}(\mathbf{x})$ satisfying (2.12) is real-valued for $|\boldsymbol{k}|\neq 0$.*

Proof: Let $0<\rho\ll 1$ and define $\Omega_\rho \equiv \Omega - B_\rho(0)$, where $B_\rho(0)$ is the ball of radius ρ centered at $\mathbf{x}=0$. We multiply (2.12 a) by $\bar{G}_{b0}$, where the bar denotes conjugation, and we integrate over Ω_ρ using the divergence theorem to get

$$\int_{\Omega_\rho} \bar{G}_{b0}\Delta G_{b0}\,d\mathbf{x} + \int_{\Omega_\rho}\nabla\bar{G}_{b0}\cdot\nabla G_{b0}\,d\mathbf{x} = \int_{\partial\Omega_\rho}\bar{G}_{b0}\,\partial_\nu G_{b0}\,d\mathbf{x} = \int_{\partial\Omega}\bar{G}_{b0}\,\partial_\nu G_{b0}\,d\mathbf{x} - \int_{\partial B_\rho(0)}\bar{G}_{b0}\,\partial_{|\mathbf{x}|}G_{b0}\,d\mathbf{x}\,. \tag{2.15}$$

Here $\partial_\nu G_{b0}$ denotes the outward normal derivative of G_{b0} on $\partial\Omega$. For $\rho\ll 1$, we use (2.12 c) to calculate

$$\int_{\partial B_\rho(0)}\bar{G}_{b0}\,\partial_{|\mathbf{x}|}G_{b0}\,d\mathbf{x} \sim \int_0^{2\pi}\left(-\frac{1}{2\pi}\log\rho + R_{b0}(\boldsymbol{k}) + o(1)\right)\left(-\frac{1}{2\pi\rho}+\mathcal{O}(1)\right)\rho\,d\theta \sim \frac{1}{2\pi}\log\rho - R_{b0}(\boldsymbol{k}) + \mathcal{O}(\rho\log\rho)\,. \tag{2.16}$$

Upon using (2.16), together with $\Delta G_{b0}=0$ in Ω_ρ, in equation (2.15), we let $\rho\to 0$ to obtain

$$R_{b0}(\boldsymbol{k}) = -\int_{\partial\Omega}\bar{G}_{b0}(\mathbf{x})\,\partial_\nu G_{b0}(\mathbf{x})\,d\mathbf{x} + \lim_{\rho\to 0}\Big[\int_{\Omega_\rho}|\nabla G_{b0}|^2\,d\mathbf{x} + \frac{1}{2\pi}\log\rho\Big]\,. \tag{2.17}$$

From (2.17), to show that $R_{b0}(\boldsymbol{k})$ is real-valued it suffices to establish that the boundary integral term in (2.17) vanishes. To show this, we observe that since the Bragg lines come in pairs, we have

$$\int_{\partial\Omega} \bar{G}_{b0}(\mathbf{x})\,\partial_\nu G_{b0}(\mathbf{x})\,d\mathbf{x} = \sum_{i=1}^{L/2}\left(\int_{\frac{\boldsymbol{P}_i}{2}+t\boldsymbol{\eta}_i^\perp} \bar{G}_{b0}(\mathbf{x})\nabla_{\mathbf{x}}G_{b0}(\mathbf{x})\cdot\boldsymbol{\eta}_i\,d\mathbf{x} - \int_{\frac{-\boldsymbol{P}_i}{2}+t\boldsymbol{\eta}_i^\perp} \bar{G}_{b0}(\mathbf{x})\nabla_{\mathbf{x}}G_{b0}(\mathbf{x})\cdot\boldsymbol{\eta}_i\,d\mathbf{x}\right). \tag{2.18}$$

Here we have used the fact that the outward normals to the Bragg line pairs $\boldsymbol{P}_i/2 + t\boldsymbol{\eta}_i^\perp$ and $-\boldsymbol{P}_i/2 + t\boldsymbol{\eta}_i^\perp$ are in opposite directions. We then translate $\mathbf{x}$ by $\boldsymbol{P}_i$ to get

$$\int_{\frac{\boldsymbol{P}_i}{2}+t\boldsymbol{\eta}_i^\perp} \bar{G}_{b0}(\mathbf{x})\nabla_{\mathbf{x}}G_{b0}(\mathbf{x})\cdot\boldsymbol{\eta}_i\,d\mathbf{x} = \int_{\frac{-\boldsymbol{P}_i}{2}+t\boldsymbol{\eta}_i^\perp+\boldsymbol{P}_i} \bar{G}_{b0}(\mathbf{x})\nabla_{\mathbf{x}}G_{b0}(\mathbf{x})\cdot\boldsymbol{\eta}_i\,d\mathbf{x} = \int_{\frac{-\boldsymbol{P}_i}{2}+t\boldsymbol{\eta}_i^\perp} \bar{G}_{b0}(\mathbf{x}+\boldsymbol{P}_i)\nabla_{\mathbf{x}}G_{b0}(\mathbf{x}+\boldsymbol{P}_i)\cdot\boldsymbol{\eta}_i\,d\mathbf{x}\,. \tag{2.19}$$

Then, since $\boldsymbol{P}_i \in \Lambda$, we have by the quasi-periodicity condition (2.12 b) that

$$\bar{G}_{b0}(\mathbf{x}+\boldsymbol{P}_i)\nabla_{\mathbf{x}}G_{b0}(\mathbf{x}+\boldsymbol{P}_i) = \left(\bar{G}_{b0}(\mathbf{x})e^{i\boldsymbol{k}\cdot\boldsymbol{P}_i}\right)\left(\nabla_{\mathbf{x}}G_{b0}(\mathbf{x})e^{-i\boldsymbol{k}\cdot\boldsymbol{P}_i}\right) = \bar{G}_{b0}(\mathbf{x})\nabla_{\mathbf{x}}G_{b0}(\mathbf{x})\,.$$

Therefore, from (2.19) we conclude that

$$\int_{\frac{\boldsymbol{P}_i}{2}+t\boldsymbol{\eta}_i^\perp} \bar{G}_{b0}(\mathbf{x})\nabla_{\mathbf{x}}G_{b0}(\mathbf{x})\cdot\boldsymbol{\eta}_i\,d\mathbf{x} = \int_{\frac{-\boldsymbol{P}_i}{2}+t\boldsymbol{\eta}_i^\perp} \bar{G}_{b0}(\mathbf{x})\nabla_{\mathbf{x}}G_{b0}(\mathbf{x})\cdot\boldsymbol{\eta}_i\,d\mathbf{x}\,,$$

which establishes from (2.18) that $\int_{\partial\Omega} \bar{G}_{b0}(\mathbf{x})\,\partial_\nu G_{b0}(\mathbf{x})\,d\mathbf{x} = 0$. From (2.17) we conclude that $R_{b0}(\boldsymbol{k})$ is real. ■

Next, we determine the asymptotic behavior of $R_{b0}(\boldsymbol{k})$ as $|\boldsymbol{k}| \to 0$. Since (2.12) has no solution if $\boldsymbol{k} = 0$, it suggests that $R_{b0}(\boldsymbol{k})$ is singular as $|\boldsymbol{k}| \to 0$. To determine the asymptotic behavior of G_{b0} as $|\boldsymbol{k}| \to 0$, we introduce a small parameter $\sigma \ll 1$, and define $\boldsymbol{k} = \sigma\boldsymbol{\kappa}$ where $|\boldsymbol{\kappa}| = \mathcal{O}(1)$. For $\sigma \ll 1$, we expand $G_{b0}(\mathbf{x})$ as

$$G_{b0}(\mathbf{x}) = \sigma^{-2}\mathcal{U}_0(\mathbf{x}) + \sigma^{-1}\mathcal{U}_1(\mathbf{x}) + \mathcal{U}_2(\mathbf{x}) + \cdots\,. \tag{2.20}$$

For any $\boldsymbol{l} \in \Omega$, and for $\sigma \ll 1$, we have from (2.12 b) that

$$\frac{\mathcal{U}_0(\mathbf{x}+\boldsymbol{l})}{\sigma^2} + \frac{\mathcal{U}_1(\mathbf{x}+\boldsymbol{l})}{\sigma} + \mathcal{U}_2(\mathbf{x}+\boldsymbol{l}) + \cdots = \left[1 - i\sigma(\boldsymbol{\kappa}\cdot\boldsymbol{l}) - \frac{\sigma^2}{2}(\boldsymbol{\kappa}\cdot\boldsymbol{l})^2 + \cdots\right]\left(\frac{\mathcal{U}_0(\mathbf{x})}{\sigma^2} + \frac{\mathcal{U}_1(\mathbf{x})}{\sigma} + \mathcal{U}_2(\mathbf{x}) + \cdots\right). \tag{2.21}$$

Upon substituting (2.20) into (2.12 a), and then equating powers of σ in (2.21), we obtain the sequence of problems

$$\Delta\mathcal{U}_0 = 0\,; \qquad \mathcal{U}_0(\mathbf{x}+\boldsymbol{l}) = \mathcal{U}_0(\mathbf{x})\,, \tag{2.22 a}$$

$$\Delta\mathcal{U}_1 = 0\,; \qquad \mathcal{U}_1(\mathbf{x}+\boldsymbol{l}) = \mathcal{U}_1(\mathbf{x}) - i\,(\boldsymbol{\kappa}\cdot\boldsymbol{l})\,\mathcal{U}_0(\mathbf{x})\,, \tag{2.22 b}$$

$$\Delta\mathcal{U}_2 = -\delta(\mathbf{x})\,; \qquad \mathcal{U}_2(\mathbf{x}+\boldsymbol{l}) = \mathcal{U}_2(\mathbf{x}) - i\,(\boldsymbol{\kappa}\cdot\boldsymbol{l})\,\mathcal{U}_1(\mathbf{x}) - \frac{(\boldsymbol{\kappa}\cdot\boldsymbol{l})^2}{2}\mathcal{U}_0(\mathbf{x})\,. \tag{2.22 c}$$

The solution to (2.22 a) is that $\mathcal{U}_0$ is an arbitrary constant, while the solution to (2.22 b) is readily calculated as $\mathcal{U}_1(\mathbf{x}) = -i\,(\boldsymbol{\kappa}\cdot\mathbf{x})\,\mathcal{U}_0 + \mathcal{U}_{10}$, where $\mathcal{U}_{10}$ is an arbitrary constant. Upon substituting $\mathcal{U}_0$ and $\mathcal{U}_1$ into (2.22 c), we obtain for any $\boldsymbol{l} \in \Lambda$ that $\mathcal{U}_2$ satisfies

$$\Delta\mathcal{U}_2 = -\delta(\mathbf{x})\,; \qquad \mathcal{U}_2(\mathbf{x}+\boldsymbol{l}) = \mathcal{U}_2(\mathbf{x}) - (\boldsymbol{\kappa}\cdot\boldsymbol{l})\,(\boldsymbol{\kappa}\cdot\mathbf{x})\,\mathcal{U}_0 - i\,(\boldsymbol{\kappa}\cdot\boldsymbol{l})\,\mathcal{U}_{10} - \frac{(\boldsymbol{\kappa}\cdot\boldsymbol{l})^2}{2}\mathcal{U}_0\,. \tag{2.23}$$

By differentiating the periodicity condition in (2.23) with respect to $\mathbf{x}$, we have for any $\boldsymbol{l} \in \Lambda$ that

$$\nabla_{\mathbf{x}}\mathcal{U}_2(\mathbf{x}+\boldsymbol{l}) = \nabla_{\mathbf{x}}\mathcal{U}_2(\mathbf{x}) - \boldsymbol{\kappa}\,(\boldsymbol{\kappa}\cdot\boldsymbol{l})\,\mathcal{U}_0\,. \tag{2.24}$$

Next, to determine $\mathcal{U}_0$, we integrate $\Delta\mathcal{U}_2 = 0$ over Ω to obtain from the divergence theorem and a subsequent decomposition of the boundary integral over the Bragg line pairs, as in (2.18), that

$$-1 = \int_{\partial\Omega} \partial_\nu \mathcal{U}_2 \, d\mathbf{x} = \sum_{i=1}^{L/2} \left(\int_{\frac{\boldsymbol{P}_i}{2}+t\boldsymbol{\eta}_i^\perp} \nabla_{\mathbf{x}}\mathcal{U}_2(\mathbf{x})\cdot\boldsymbol{\eta}_i \, d\mathbf{x} - \int_{\frac{-\boldsymbol{P}_i}{2}+t\boldsymbol{\eta}_i^\perp} \nabla_{\mathbf{x}}\mathcal{U}_2(\mathbf{x})\cdot\boldsymbol{\eta}_i \, d\mathbf{x} \right). \tag{2.25}$$

Then, as similar to the derivation in (2.19), we calculate the boundary integrals as

$$\int_{\frac{\boldsymbol{P}_i}{2}+t\boldsymbol{\eta}_i^\perp} \nabla_{\mathbf{x}}\mathcal{U}_2(\mathbf{x})\cdot\boldsymbol{\eta}_i \, d\mathbf{x} = \int_{\frac{-\boldsymbol{P}_i}{2}+t\boldsymbol{\eta}_i^\perp+\boldsymbol{P}_i} \nabla_{\mathbf{x}}\mathcal{U}_2(\mathbf{x})\cdot\boldsymbol{\eta}_i \, d\mathbf{x} = \int_{\frac{-\boldsymbol{P}_i}{2}+t\boldsymbol{\eta}_i^\perp} \nabla_{\mathbf{x}}\mathcal{U}_2(\mathbf{x}+\boldsymbol{P}_i)\cdot\boldsymbol{\eta}_i \, d\mathbf{x}\,. \tag{2.26}$$

Upon using (2.26) in (2.25), we obtain

$$-1 = \sum_{i=1}^{L/2} \int_{-\frac{\boldsymbol{P}_i}{2}+t\boldsymbol{\eta}_i^\perp} \left(\nabla_{\mathbf{x}}\mathcal{U}_2(\mathbf{x}+\boldsymbol{P}_i) - \nabla_{\mathbf{x}}\mathcal{U}_2(\mathbf{x})\right)\cdot\boldsymbol{\eta}_i \, d\mathbf{x}\,. \tag{2.27}$$

Since $\boldsymbol{P}_i \in \Lambda$ and $\boldsymbol{\eta}_i = \boldsymbol{P}_i/|\boldsymbol{P}_i|$, we calculate the integrand in (2.27) by using (2.24) as

$$\left(\nabla_{\mathbf{x}}\mathcal{U}_2(\mathbf{x}+\boldsymbol{P}_i) - \nabla_{\mathbf{x}}\mathcal{U}_2(\mathbf{x})\right)\cdot\boldsymbol{\eta}_i = -\left(\boldsymbol{\kappa}\cdot\boldsymbol{\eta}_i\right)\left(\boldsymbol{\kappa}\cdot\boldsymbol{P}_i\right)\mathcal{U}_0 = -\left(\boldsymbol{\kappa}\cdot\boldsymbol{P}_i\right)^2 \frac{\mathcal{U}_0}{|\boldsymbol{P}_i|}\,. \tag{2.28}$$

Then, upon substituting (2.28) into (2.27), and by integrating the constant integrand over the Bragg lines, we obtain that $\mathcal{U}_0$ satisfies

$$-1 = -\mathcal{U}_0 \sum_{i=1}^{L/2} \frac{\left(\boldsymbol{\kappa}\cdot\boldsymbol{P}_i\right)^2}{|\boldsymbol{P}_i|} 2t_i = -\mathcal{U}_0 \sum_{i=1}^{L} \frac{\left(\boldsymbol{\kappa}\cdot\boldsymbol{P}_i\right)^2}{|\boldsymbol{P}_i|} t_i = -\mathcal{U}_0 \sum_{i=1}^{L} \left(\boldsymbol{\kappa}\cdot\boldsymbol{\eta}_i\right)^2 t_i |\boldsymbol{P}_i|\,, \tag{2.29}$$

where $2t_i$ is the length of the Bragg line L_i. Upon solving for $\mathcal{U}_0$, we obtain that

$$\mathcal{U}_0 = \frac{1}{\boldsymbol{\kappa}^T\mathcal{Q}\boldsymbol{\kappa}}\,, \qquad \text{where} \quad \mathcal{Q} \equiv \sum_{i=1}^{L} \boldsymbol{\eta}_i\omega_i\boldsymbol{\eta}_i^T\,, \quad \text{and} \quad \omega_i \equiv t_i|\boldsymbol{P}_i|\,. \tag{2.30}$$

Since $\omega_i > 0$, for $i = 1, \ldots, L$, we have $\mathbf{y}^T\mathcal{Q}\mathbf{y} = \sum_{i=1}^{L} \left(\boldsymbol{\eta}_i^T\mathbf{y}\right)^2 \omega_i > 0$ for any $\mathbf{y} \neq 0$, which proves that the matrix $\mathcal{Q}$ is positive definite. We summarize the results of this perturbation calculation in the following (formal) lemma:

Lemma 2.2 *For $|\boldsymbol{k}| \to 0$, the regular part $R_{b0}(\boldsymbol{k})$ of the Bloch Green's function of (2.12) has the leading-order singular asymptotic behavior*

$$R_{b0}(\boldsymbol{k}) \sim \frac{1}{\boldsymbol{k}^T\mathcal{Q}\boldsymbol{k}}\,, \tag{2.31}$$

where the positive definite matrix $\mathcal{Q}$ is defined in terms of the parameters of the Wigner-Seitz cell by (2.30).

We remark that a similar analysis can be done for the quasi-periodic reduced-wave Green's function, which satisfies

$$\Delta G(\mathbf{x}) - \sigma^2 G = -\delta(\mathbf{x})\,; \qquad \mathbf{x} \in \Omega\,; \qquad G(\mathbf{x}+\boldsymbol{l}) = e^{-i\boldsymbol{k}\cdot\boldsymbol{l}}\, G(\mathbf{x})\,, \qquad \boldsymbol{l} \in \Lambda\,, \tag{2.32 a}$$

where Λ is the Bravais lattice (2.1) and $\boldsymbol{k}/(2\pi) \in \Omega_B$. The regular part $R(\boldsymbol{k})$ of this Green's function is defined by

$$R(\boldsymbol{k}) \equiv \lim_{\mathbf{x}\to 0} \left(G(\mathbf{x}) + \frac{1}{2\pi}\log|\mathbf{x}| \right). \tag{2.32 b}$$

By a simple modification of the derivation of Lemma 2.1 and 2.2, we obtain the following result:

Lemma 2.3 *Let $\boldsymbol{k}/(2\pi) \in \Omega_B$. For the regular part $R(\boldsymbol{k})$ of the reduced-wave Bloch Green's function satisfying (2.32), we have the following:*

- *(i) Let σ^2 be real. Then $R(\boldsymbol{k})$ is real-valued.*
- *(ii) $R(\boldsymbol{k}) \sim R_{b0}(\boldsymbol{k}) + \mathcal{O}(\sigma^2)$ for $\sigma \to 0$ when $|\boldsymbol{k}| > 0$ with $|\boldsymbol{k}| = \mathcal{O}(1)$. Here $R_{b0}(\boldsymbol{k})$ is the regular part of the Bloch Green's function (2.12).*
- *(iii) Let $\sigma \to 0$, and consider the long-wavelength regime $|\boldsymbol{k}| = \mathcal{O}(\sigma)$, where $\boldsymbol{k} = \sigma\boldsymbol{\kappa}$ with $|\boldsymbol{\kappa}| = \mathcal{O}(1)$. Then,*

$$R(\boldsymbol{k}) \sim \frac{1}{\sigma^2\left[|\Omega| + \boldsymbol{\kappa}^T\mathcal{Q}\boldsymbol{\kappa}\right]}\,, \tag{2.33}$$

where the positive definite matrix $\mathcal{Q}$ is defined in (2.30).

Proof: To prove (i) we proceed as in the derivation of Lemma 2.1 to get

$$R(\boldsymbol{k}) = \lim_{\rho\to 0}\Big[\int_{\Omega_\rho}\left(|\nabla G|^2 + \sigma^2|G|^2\right)\,d\mathbf{x} + \frac{1}{2\pi}\log\rho\Big]\,, \tag{2.34}$$

which is real-valued. The second result (ii) is simply a regular perturbation result for the solution to (2.32) for $\sigma \to 0$ when $|\boldsymbol{k}|$ is bounded away from zero and $\boldsymbol{k}/(2\pi) \in \Omega_B$, so that $\boldsymbol{k}\cdot\boldsymbol{l} \neq 2\pi N$. Therefore, when $\boldsymbol{k}/(2\pi) \in \Omega_B$, $R(\boldsymbol{k})$ is unbounded only as $|\boldsymbol{k}| \to 0$. To establish the third result, we proceed as in (2.20)–(2.24), with the modification that $\Delta\mathcal{U}_2 = \mathcal{U}_0 - \delta(\mathbf{x})$ in Ω, Therefore, we must add the term $\mathcal{U}_0|\Omega|$ to the left-hand sides of (2.25), (2.27), and (2.29). By solving for $\mathcal{U}_0$ we get (2.33). ■

In §3.2 and §4.2 below, we will analyze the spectrum of the linearization around a steady-state periodic spot pattern for the Schnakenburg and GM models. For $\varepsilon \to 0$, it is the eigenfunction Ψ corresponding to the long-range solution component u that satisfies an elliptic PDE with coefficients that are spatially periodic on the lattice. As such, by the Floquet-Bloch theorem (cf. [**16**] and [**15**]), this eigenfunction must satisfy the quasi-periodic boundary conditions $\Psi(\mathbf{x}+\boldsymbol{l}) = e^{-i\boldsymbol{k}\cdot\boldsymbol{l}}\Psi(\mathbf{x})$ for $\boldsymbol{l} \in \Lambda$, $\mathbf{x} \in \mathbb{R}^2$ and $\boldsymbol{k}/(2\pi) \in \Omega_B$. This quasi-periodicity condition can be used to formulate a boundary operator on the boundary $\partial\Omega$ of the fundamental Wigner-Seitz cell Ω. Let L_i and L_{-i} be two parallel Bragg lines on opposite sides of $\partial\Omega$ for $i = 1, \ldots, L/2$. Let $\mathbf{x}_{i1} \in L_i$ and $\mathbf{x}_{i2} \in L_{-i}$ be any two opposing points on these Bragg lines. We define the boundary operator $\mathcal{P}_k\Psi$ by

$$\mathcal{P}_k\Psi = \Big\{\Psi \,\Big|\, \begin{pmatrix}\Psi(\mathbf{x}_{i1})\\ \partial_n\Psi(\mathbf{x}_{i1})\end{pmatrix} = e^{-i\boldsymbol{k}\cdot\boldsymbol{l}_i}\begin{pmatrix}\Psi(\mathbf{x}_{i2})\\ \partial_n\Psi(\mathbf{x}_{i2})\end{pmatrix}\,,\quad \forall\,\mathbf{x}_{i1}\in L_i\,,\ \forall\,\mathbf{x}_{i2}\in L_{-i}\,,\ \boldsymbol{l}_i\in\Lambda\,,\ i=1,\ldots,L/2\Big\}\,. \tag{2.35}$$

The boundary operator $\mathcal{P}_0\Psi$ simply corresponds to a periodicity condition for Ψ on each pair of parallel Bragg lines. These boundary operators are used in §3 and §4 below.

3 Periodic Spot Patterns for the Schnakenburg Model

We study the linear stability of a steady-state periodic pattern of localized spots for the Schnakenburg model (1.1) where the spots are centered at the lattice points of (2.1). The analysis below is based on the fundamental Wigner-Seitz cell Ω, which contains exactly one spot centered at the origin.

3.1 The Steady-State Solution

We use the method of matched asymptotic expansions to construct a steady-state one-spot solution to (1.1) centered at $\mathbf{x} = 0 \in \Omega$. The construction of such a solution consists of an outer region where v is exponentially small and $u = \mathcal{O}(1)$, and an inner region of extent $\mathcal{O}(\varepsilon)$ centered at the origin where both v and u have localized.

In the inner region we look for a locally radially symmetric steady-state solution of the form

$$u = \frac{1}{\sqrt{D}}\, U\,, \qquad v = \sqrt{D} V\,, \qquad \mathbf{y} = \varepsilon^{-1}\mathbf{x}\,. \tag{3.1}$$

Then, substituting (3.1) into the steady-state equations of (1.1), we obtain that $V \sim V(\rho)$ and $U \sim U(\rho)$, with $\rho = |\mathbf{y}|$, satisfy the following *core problem* in terms of an unknown source strength $S \equiv \int_0^\infty UV^2 \rho\, d\rho$ to be determined:

$$\Delta_\rho V - V + UV^2 = 0\,, \qquad \Delta_\rho U - UV^2 = 0\,, \qquad 0 < \rho < \infty\,, \tag{3.2 a}$$

$$U'(0) = V'(0) = 0\,; \qquad V \to 0\,, \qquad U \sim S\log\rho + \chi(S) + o(1)\,, \quad \text{as} \quad \rho \to \infty\,. \tag{3.2 b}$$

Here we have defined $\Delta_\rho V \equiv V'' + \rho^{-1}V'$.

The core problem (3.2), without the explicit far-field condition (3.2 b) was first identified and its solutions computed numerically in §5 of [**19**]. In [**12**], the function $\chi(S)$ was computed numerically, and solutions to the core problem were shown to closely related to the phenomena of self-replicating spots.

The unknown source strength S is determined by matching the the far-field behavior of the core solution to an outer solution for u valid away from $\mathcal{O}(\varepsilon)$ distances from 0. In the outer region, v is exponentially small, and from (3.1) we get $\varepsilon^{-2}uv^2 \to 2\pi\sqrt{D}S\delta(\mathbf{x})$. Therefore, from (1.1), the outer steady-state problem for u is

$$\begin{aligned} &\Delta u = -\frac{a}{D} + \frac{2\pi}{\sqrt{D}} S\,\delta(\mathbf{x})\,, \quad \mathbf{x} \in \Omega\,; \qquad \mathcal{P}_0 u = 0\,, \quad \mathbf{x} \in \partial\Omega\,, \\ &u \sim \frac{1}{\sqrt{D}}\left[S\log|\mathbf{x}| + \chi(S) + \frac{S}{\nu}\right]\,, \quad \text{as} \quad \mathbf{x} \to 0\,, \end{aligned} \tag{3.3}$$

where $\nu \equiv -1/\log\varepsilon$ and Ω is the fundamental Wigner-Seitz cell. The divergence theorem then yields

$$S = \frac{a|\Omega|}{2\pi\sqrt{D}}\,. \tag{3.4}$$

The solution to (3.3) is then written in terms of the periodic Green's function $G_{0p}(\mathbf{x})$ as

$$u(x) = -\frac{2\pi}{\sqrt{D}}\left[S G_{0p}(\mathbf{x};0) - u_c\right]\,, \qquad u_c \equiv \frac{1}{2\pi\nu}\left[S + 2\pi\nu S R_{0p} + \nu\chi(S)\right]\,, \tag{3.5}$$

where the periodic source-neutral Green's function $G_{0p}(\mathbf{x})$ and its regular part R_{0p} satisfy

$$\begin{aligned} &\Delta G_{0p} = \frac{1}{|\Omega|} - \delta(\mathbf{x})\,, \quad \mathbf{x} \in \Omega\,; \qquad \mathcal{P}_0 G_{0p} = 0 \quad \mathbf{x} \in \partial\Omega\,, \\ &G_{0p} \sim -\frac{1}{2\pi}\log|\mathbf{x}| + R_{0p} + o(1)\,, \quad \text{as} \quad \mathbf{x} \to 0\,; \qquad \int_\Omega G_{0p}\, d\mathbf{x} = 0\,. \end{aligned} \tag{3.6}$$

An explicit expression for R_{0p} on an oblique Bravais lattice was derived in Theorem 1 of [**7**]. A periodic pattern of spots is then obtained through periodic extension to $\mathbb{R}^2$ of the one-spot solution constructed within Ω.

Since the stability threshold occurs when $D = \mathcal{O}(1/\nu)$, for which $S = \mathcal{O}(\nu^{1/2}) \ll 1$ from (3.4), we must calculate an asymptotic expansion in powers of ν for the solution to the core problem (3.2). This result, which is required for the stability analysis in §3.2, is as follows:

Lemma 3.1 *For $S = S_0\nu^{1/2} + S_1\nu^{3/2} + \cdots$, where $\nu \equiv -1/\log\varepsilon \ll 1$, the asymptotic solution to the core problem (3.2) is*

$$V \sim \nu^{1/2}\left(V_0 + \nu V_1 + \cdots\right), \qquad U \sim \nu^{-1/2}\left(U_0 + \nu U_1 + \nu^2 U_2 + \cdots\right), \qquad \chi \sim \nu^{-1/2}\left(\chi_0 + \nu\chi_1 + \cdots\right), \tag{3.7 a}$$

where U_0, $U_1(\rho)$, $V_0(\rho)$, and $V_1(\rho)$ are defined by

$$U_0 = \chi_0\,, \qquad U_1 = \chi_1 + \frac{1}{\chi_0}U_{1p}\,, \qquad V_0 = \frac{w}{\chi_0}\,, \qquad V_1 = -\frac{\chi_1}{\chi_0^2}w + \frac{1}{\chi_0^3}V_{1p}\,. \tag{3.7 b}$$

Here $w(\rho)$ is the unique ground-state solution to $\Delta_\rho w - w + w^2 = 0$ with $w(0) > 0$, $w'(0) = 0$, and $w \to 0$ as $\rho \to \infty$. In terms of $w(\rho)$, the functions U_{1p} and V_{1p} are the unique solutions on $0 \le \rho < \infty$ to

$$\begin{aligned} &L_0 V_{1p} = -w^2 U_{1p}\,, \qquad V_{1p}'(0) = 0\,, \quad V_{1p} \to 0\,, \quad \text{as} \quad \rho \to \infty\,, \\ &\Delta_\rho U_{1p} = w^2\,, \qquad U_{1p}'(0) = 0\,, \quad U_{1p} \to b\log\rho + o(1)\,, \quad \text{as} \quad \rho \to \infty\,; \qquad b \equiv \int_0^\infty w^2\rho\,d\rho\,, \end{aligned} \tag{3.7 c}$$

where the linear operator L_0 is defined by $L_0 V_{1p} \equiv \Delta_\rho V_{1p} - V_{1p} + 2wV_{1p}$. Finally, in (3.7 a), the constants χ_0 and χ_1 are related to S_0 and S_1 by

$$\chi_0 = \frac{b}{S_0}\,, \qquad \chi_1 = -\frac{S_1 b}{S_0^2} + \frac{S_0}{b^2}\int_0^\infty V_{1p}\rho\,d\rho\,. \tag{3.7 d}$$

The derivation of this result was given in §6 of [**12**] and is outlined in Appendix A below. We remark that the $o(1)$ condition in the far-field behavior of U_{1p} in (3.7 *c*) eliminates an otherwise arbitrary constant in the determination of U_{1p}. This condition, therefore, ensures that the solution to the linear BVP system (3.7 *c*) is unique.

3.2 The Spectrum of the Linearization Near the Origin

To study the stability of the periodic pattern of spots with respect to fast $\mathcal{O}(1)$ time-scale instabilities, we use the Floquet-Bloch theorem that allows us to only consider the Wigner-Seitz cell Ω, centered at the origin, with quasi-periodic boundary conditions imposed on its boundaries.

We linearize around the steady-state u_e and v_e, as calculated in §3.1, by introducing the perturbation

$$u = u_e + \mathrm{e}^{\lambda t}\eta\,, \qquad v = v_e + \mathrm{e}^{\lambda t}\phi\,. \tag{3.8}$$

By substituting (3.8) into (1.1) and linearizing, we obtain the following eigenvalue problem for ϕ and η:

$$\begin{aligned} &\varepsilon^2\Delta\phi - \phi + 2u_e v_e\phi + v_e^2\eta = \lambda\phi\,, \quad \mathbf{x} \in \Omega\,; \qquad \mathcal{P}_{\boldsymbol{k}}\phi = 0\,, \quad \mathbf{x} \in \partial\Omega\,, \\ &D\Delta\eta - 2\varepsilon^{-2}u_e v_e\phi - \varepsilon^{-2}v_e^2\eta = \lambda\tau\eta\,, \quad \mathbf{x} \in \Omega\,; \qquad \mathcal{P}_{\boldsymbol{k}}\eta = 0\,, \quad \mathbf{x} \in \partial\Omega\,, \end{aligned} \tag{3.9}$$

where $\mathcal{P}_{\boldsymbol{k}}$ is the quasi-periodic boundary operator of (2.35).

In the inner region near $\mathbf{x} = 0$ we introduce the local variables $N(\rho)$ and $\Phi(\rho)$ by

$$\eta = \frac{1}{D}N(\rho)\,, \qquad \phi = \Phi(\rho)\,, \qquad \rho = |\mathbf{y}|\,, \qquad \mathbf{y} = \varepsilon^{-1}\mathbf{x}\,. \tag{3.10}$$

Upon substituting (3.10) into (3.9), and by using $u_e \sim U(\rho)/\sqrt{D}$ and $v_e \sim \sqrt{D}V(\rho)$, where U and V satisfy the core problem (3.2), we obtain on $0 < \rho < \infty$ that

$$\begin{aligned} &\Delta_\rho\Phi - \Phi + 2UV\Phi + NV^2 = \lambda\Phi\,, \qquad \Phi \to 0\,, \quad \text{as} \quad \rho \to \infty\,, \\ &\Delta_\rho N = 2UV\Phi + NV^2\,, \qquad N \sim C\log\rho + B\,, \quad \text{as} \quad \rho \to \infty\,, \end{aligned} \tag{3.11}$$

with $\Phi'(0) = N'(0) = 0$, and where $B = B(S;\lambda)$. We remark that for $\mathrm{Re}(\lambda+1) > 0$, Φ in (3.11) decays exponentially as $\rho \to \infty$. However, in contrast, we cannot apriori impose that N in (3.11) is bounded as $\rho \to \infty$. Instead we must allow for the possibility of a logarithmic growth for N as $\rho \to \infty$. Upon using the divergence theorem we identify C as $C = \int_0^\infty \left(2UV\Phi + NV^2\right) \rho \, d\rho$. The constant C will be determined by matching N to an outer eigenfunction η, valid away from $\mathbf{x} = 0$, that satisfies (3.9).

To formulate this outer problem, we obtain since v_e is localized near $\mathbf{x} = 0$ that, in the sense of distributions,

$$\varepsilon^{-2}\left(2u_e v_e \phi + \eta v_e^2\right) \to \left(\int_{\mathbb{R}^2} \left(2UV\Phi + NV^2\right) \, d\mathbf{y}\right) \delta(\mathbf{x}) = 2\pi C \delta(\mathbf{x})\,. \tag{3.12}$$

By using this expression in (3.9), we conclude that the outer problem for η is

$$\begin{aligned} &\Delta\eta - \frac{\tau\lambda}{D}\eta = \frac{2\pi C}{D}\delta(\mathbf{x})\,, \quad \mathbf{x} \in \Omega\,; \qquad \mathcal{P}_{\boldsymbol{k}}\eta = 0\,, \quad \mathbf{x} \in \partial\Omega\,, \\ &\eta \sim \frac{1}{D}\left(C\log|\mathbf{x}| + \frac{C}{\nu} + B\right)\,, \quad \text{as} \quad \mathbf{x} \to 0\,. \end{aligned} \tag{3.13}$$

The solution to (3.13) is $\eta = -2\pi C D^{-1} G_{b\lambda}(\mathbf{x})$, where $G_{b\lambda}$ satisfies

$$\begin{aligned} &\Delta G_{b\lambda} - \frac{\tau\lambda}{D}G_{b\lambda} = -\delta(\mathbf{x})\,, \quad \mathbf{x} \in \Omega\,; \qquad \mathcal{P}_{\boldsymbol{k}} G_{b\lambda} = 0\,, \quad \mathbf{x} \in \partial\Omega\,, \\ &G_{b\lambda} \sim -\frac{1}{2\pi}\log|\mathbf{x}| + R_{b\lambda}\,, \quad \text{as} \quad \mathbf{x} \to 0\,. \end{aligned} \tag{3.14}$$

From the requirement that the behavior of η as $\mathbf{x} \to 0$ agree with that in (3.13), we conclude that $B + C/\nu = -2\pi C R_{b\lambda}$. Finally, since the stability threshold occurs in the regime $D = \mathcal{O}(\nu^{-1}) \gg 1$, we conclude from Lemma 2.3 (ii) that for $|\boldsymbol{k}| \neq 0$ and $\boldsymbol{k}/(2\pi) \in \Omega_B$,

$$\left(1 + 2\pi\nu R_{b0} + \mathcal{O}(\nu^2)\right) C = -\nu B\,, \tag{3.15}$$

where R_{b0} is the regular part of the Bloch Green's function G_{b0} defined by (2.12) on Ω.

We now proceed to determine the portion of the continuous spectrum of the linearization that lies within an $\mathcal{O}(\nu)$ neighborhood of the origin, i. e. that satisfies $|\lambda| \leq \mathcal{O}(\nu)$, when D is close to a certain critical value. To do so, we first must calculate an asymptotic expansion for the solution to (3.11) together with (3.15).

By using (3.7 *a*) we first calculate the coefficients in the differential operator in (3.11) as

$$\begin{aligned} UV &= w + \nu\left(U_0 V_1 + U_1 V_0\right) + \cdots = w + \frac{\nu}{\chi_0^2}\left[V_{1p} + w U_{1p}\right] + \cdots\,, \\ V^2 &= \nu\left(V_0^2 + 2\nu V_0 V_1\right) + \cdots = \nu\frac{w^2}{\chi_0^2} + \frac{2\nu^2}{\chi_0^3}\left(-\chi_1 w^2 + \frac{w V_{1p}}{\chi_0}\right) + \cdots\,, \end{aligned}$$

so that the local problem (3.11) on $0 < \rho < \infty$ becomes

$$\begin{aligned} &\Delta_\rho \Phi - \Phi + \left[2w + \frac{2\nu}{\chi_0^2}\left(V_{1p} + w U_{1p}\right) + \cdots\right]\Phi = -\nu\left[\frac{w^2}{\chi_0^2} + \frac{2\nu}{\chi_0^3}\left(-\chi_1 w^2 + \frac{w V_{1p}}{\chi_0}\right) + \cdots\right] N + \lambda\Phi\,, \\ &\Delta_\rho N = \left[2w + \frac{2\nu}{\chi_0^2}\left(V_{1p} + w U_{1p}\right) + \cdots\right]\Phi + \nu\left[\frac{w^2}{\chi_0^2} + \frac{2\nu}{\chi_0^3}\left(-\chi_1 w^2 + \frac{w V_{1p}}{\chi_0}\right) + \cdots\right] N\,, \\ &\Phi \to 0\,, \qquad N \sim C\log\rho + B\,, \quad \text{as} \quad \rho \to \infty\,; \qquad \Phi'(0) = N'(0) = 0\,. \end{aligned} \tag{3.16}$$

We then introduce the appropriate expansions

$$\begin{aligned} &N = \frac{1}{\nu}\left(\hat{N}_0 + \nu\hat{N}_1 + \cdots\right)\,, \qquad B = \frac{1}{\nu}\left(\hat{B}_0 + \nu\hat{B}_1 + \cdots\right)\,, \qquad C = C_0 + \nu C_1 + \cdots\,, \\ &\Phi = \Phi_0 + \nu\Phi_1 + \cdots\,, \qquad \lambda = \lambda_0 + \nu\lambda_1 + \cdots\,, \end{aligned} \tag{3.17}$$

into (3.16) and collect powers of ν.

To leading order, we obtain on $0 < \rho < \infty$ that

$$
\begin{aligned}
&L_0\Phi_0 \equiv \Delta_\rho\Phi_0 - \Phi_0 + 2w\Phi_0 = -\frac{w^2}{\chi_0^2}\hat{N}_0 + \lambda_0\Phi_0\,, \qquad \Delta_\rho\hat{N}_0 = 0\,,\\
&\Phi_0 \to 0\,, \qquad \hat{N}_0 \to \hat{B}_0 \quad \text{as} \quad \rho\to\infty\,; \qquad \Phi_0'(0) = 0\,, \quad \hat{N}_0'(0) = 0\,,
\end{aligned}
\tag{3.18}
$$

where L_0 is referred to as the local operator. We conclude that $\hat{N}_0 = \hat{B}_0$ for $\rho \geq 0$.

At next order, we obtain on $\rho > 0$ that Φ_1 satisfies

$$
L_0\Phi_1 + \frac{2}{\chi_0^2}\left(V_{1p} + wU_{1p}\right)\Phi_0 + \frac{2}{\chi_0^3}\left(-\chi_1 w^2 + \frac{wV_{1p}}{\chi_0}\right)\hat{N}_0 = -\frac{w^2}{\chi_0^2}\hat{N}_1 + \lambda_1\Phi_0\,; \qquad \Phi_1 \to 0\,, \quad \text{as} \quad \rho\to\infty\,,
\tag{3.19}
$$

with $\Phi_1'(0) = 0$, and that $\hat{N}_1$ on $\rho > 0$ satisfies

$$
\Delta_\rho\hat{N}_1 = 2w\Phi_0 + \frac{w^2}{\chi_0^2}\hat{N}_0\,; \qquad \hat{N}_1 \sim C_0\log\rho + \hat{B}_1\,, \quad \text{as} \quad \rho\to\infty\,; \qquad \hat{N}_1'(0) = 0\,.
\tag{3.20}
$$

In our analysis we will also need the problem for $\hat{N}_2$ given by

$$
\begin{aligned}
&\Delta_\rho\hat{N}_2 = 2w\Phi_1 + \frac{2}{\chi_0^2}\left(V_{1p} + wU_{1p}\right)\Phi_0 + \frac{2}{\chi_0^3}\left(-\chi_1 w^2 + \frac{wV_{1p}}{\chi_0}\right)\hat{N}_0 + \frac{w^2}{\chi_0^2}\hat{N}_1\,,\\
&\hat{N}_2 \sim C_1\log\rho + \hat{B}_2\,, \quad \text{as} \quad \rho\to\infty\,; \qquad \hat{N}_2'(0) = 0\,.
\end{aligned}
\tag{3.21}
$$

In addition, by substituting (3.17) into (3.15), we obtain upon collecting powers of ν that

$$
C_0 = -\hat{B}_0\,, \qquad C_1 + 2\pi R_{b0}C_0 = -\hat{B}_1\,.
\tag{3.22}
$$

Next, we proceed to analyze (3.18)–(3.21). From the divergence theorem, we obtain from (3.20) that

$$
C_0 = \int_0^\infty 2w\Phi_0\rho\,d\rho + \frac{b}{\chi_0^2}\hat{N}_0\,, \qquad b \equiv \int_0^\infty w^2\rho\,d\rho\,.
\tag{3.23}
$$

Since $C_0 = -\hat{B}_0$ and $\hat{B}_0 = \hat{N}_0$, (3.23) yields that

$$
\hat{N}_0 = \hat{B}_0 = -2\left[1 + \frac{b}{\chi_0^2}\right]^{-1}\int_0^\infty w\Phi_0\rho\,d\rho\,.
\tag{3.24}
$$

With $\hat{N}_0$ known, (3.18) provides the leading-order nonlocal eigenvalue problem (NLEP)

$$
L_0\Phi_0 - \frac{2w^2 b}{\chi_0^2 + b}\frac{\int_0^\infty w\Phi_0\,\rho\,d\rho}{\int_0^\infty w^2\rho\,d\rho} = \lambda_0\Phi_0\,; \qquad \Phi_0 \to 0\,, \quad \text{as} \quad \rho\to\infty\,; \qquad \Phi_0'(0) = 0\,.
\tag{3.25}
$$

For this NLEP, the rigorous result of [**34**] (see also Theorem 3.7 of the survey article [**35**]) proves that $\mathrm{Re}(\lambda_0) < 0$ if and only if $2b/(\chi_0^2 + b) > 1$. At the stability threshold where $2b/(\chi_0^2 + b) = 1$, we have from the identity $L_0 w = w^2$ that $\Phi_0 = w$ and $\lambda_0 = 0$. From (3.24) and (3.23) we can then calculate $\hat{B}_0$ and C_0 at this leading-order stability threshold. In summary, to leading order in ν, we obtain at $\lambda_0 = 0$ that

$$
\frac{b}{\chi_0^2} = 1\,, \qquad \Phi_0 = w\,, \qquad \hat{B}_0 = \hat{N}_0 = -b = -\int_0^\infty w^2\rho\,d\rho\,, \qquad C_0 = b\,.
\tag{3.26}
$$

Upon substituting (3.26) into (3.20) we obtain at $\lambda_0 = 0$ that $\hat{N}_1$ on $\rho > 0$ satisfies

$$
\Delta_\rho\hat{N}_1 = w^2\,; \qquad \hat{N}_1 \sim b\log\rho + \hat{B}_1\,, \quad \text{as} \quad \rho\to\infty\,; \qquad \hat{N}_1'(0) = 0\,.
\tag{3.27}
$$

Upon comparing (3.27) with the problem for U_{1p}, as given in (3.7 c), we conclude that

$$\hat{N}_1 = U_{1p} + \hat{B}_1 \,. \tag{3.28}$$

Next, we observe that for $D = D_0/\nu \gg 1$, it follows from (3.4) that $S = \nu^{1/2} S_0 + \cdots$, where $S_0 = a|\Omega|/(2\pi\sqrt{D_0})$. Then, since $S_0 = b/\chi_0$ from (3.7 d), and $b/\chi_0^2 = 1$ when $\lambda_0 = 0$ from (3.26), the critical value of D_0 at the leading-order stability threshold $\lambda_0 = 0$ is

$$D_0 = D_{0c} \equiv \frac{a^2|\Omega|^2}{4\pi^2 b} \,. \tag{3.29 a}$$

This motivates the definition of the bifurcation parameter μ by

$$\mu \equiv \frac{4\pi^2 D\nu b}{a^2|\Omega|^2} \,, \tag{3.29 b}$$

so that at criticality where $\chi_0 = \sqrt{b}$, we have $\mu = 1$.

We then proceed to analyze the effect of the higher order terms in powers of ν on the stability threshold. In particular, we determine the continuous band of spectrum that is contained within an $\mathcal{O}(\nu)$ ball near $\lambda = 0$ when the bifurcation parameter μ is $\mathcal{O}(\nu)$ close to its leading-order critical value $\mu = 1$. As such, we set

$$\lambda = \nu\lambda_1 + \cdots \,, \qquad \text{for} \qquad \mu = 1 + \nu\mu_1 + \cdots \,, \tag{3.30}$$

and we derive an expression for λ_1 in terms of μ_1, the Bloch vector $\boldsymbol{k}$, the lattice structure, and certain correction terms to the core problem.

To determine an expression for μ_1 in terms of χ_0 and χ_1 we first set $D = D_0/\nu$ and write the two term expansion for the source strength S as

$$S = \frac{a|\Omega|}{2\pi\sqrt{D}} = \nu^{1/2}\left(S_0 + \nu S_1 + \cdots\right) \,,$$

where S_0 and S_1 are given in (3.7 d) in terms of χ_0 and χ_1. By using (3.7 d) and (3.29 b), this expansion for S becomes

$$\sqrt{\frac{b}{\mu}} = \left(\frac{b}{\chi_0} + \nu \left[-\frac{\chi_1 b}{\chi_0} + \frac{1}{\chi_0^3} \int_0^\infty V_{1p}\rho \, d\rho \right] + \cdots \right) \,. \tag{3.31}$$

As expected, to leading order we have $\mu = 1$ when $b = \chi_0^2$. At $\lambda_0 = 0$ where $\chi_0 = \sqrt{b}$, we use $\mu^{-1/2} \sim 1 - \nu\mu_1/2 + \cdots$ to relate μ_1 to χ_1 as

$$\frac{\chi_1}{\sqrt{b}} = \frac{\mu_1}{2} + \frac{1}{b^2} \int_0^\infty V_{1p}\rho \, d\rho \,. \tag{3.32}$$

Next, we substitute $\Phi_0 = w$, $\hat{N}_0 = -b$, $\chi_0^2 = b$, and $\hat{N}_1 = U_{1p} + \hat{B}_1$ from (3.28), into the equation (3.19) for Φ_1. After some algebra, we conclude that Φ_1 at $\lambda_0 = 0$ satisfies

$$L_0\Phi_1 + \frac{w^2}{b}\hat{B}_1 = -\frac{2\chi_1\chi_0}{b}w^2 - \frac{3}{b}w^2 U_{1p} + \lambda_1 w \,; \qquad \Phi_1 \to 0 \,, \quad \text{as} \quad \rho \to \infty \,, \tag{3.33}$$

with $\Phi_1'(0) = 0$. In a similar way, at the leading-order stability threshold, the problem (3.21) for $\hat{N}_2$ on $\rho > 0$ becomes

$$\begin{aligned} \Delta_\rho \hat{N}_2 &= 2w\Phi_1 + \frac{w^2}{b}\hat{B}_1 + \frac{3}{b}w^2 U_{1p} + \frac{2\chi_0\chi_1}{b}w^2 \,, \\ \hat{N}_2 &\sim C_1 \log\rho + \hat{B}_2 \,, \quad \text{as} \quad \rho \to \infty \,; \qquad \hat{N}_2'(0) = 0 \,. \end{aligned} \tag{3.34}$$

To determine $\hat{B}_1$, as required in (3.33), we use the divergence theorem on (3.34) to obtain that

$$C_1 = 2\int_0^\infty w\Phi_1\rho\,d\rho + \hat{B}_1 + \frac{3}{b}\int_0^\infty w^2 U_{1p}\rho\,d\rho + 2\chi_0\chi_1\,.$$

Upon combining this expression with $C_1 + 2\pi R_{b0}C_0 = -\hat{B}_1$, as obtained from (3.22), where $C_0 = b$, we obtain $\hat{B}_1$ as

$$\hat{B}_1 = -\int_0^\infty w\Phi_1\rho\,d\rho - \pi b R_{b0} - \frac{3}{2b}\int_0^\infty w^2 U_{1p}\rho\,d\rho - \chi_0\chi_1\,.$$

Upon substituting this expression into (3.33), we conclude that Φ_1 satisfies

$$\mathcal{L}\Phi_1 \equiv L_0\Phi_1 - w^2\frac{\int_0^\infty w\Phi_1\rho\,d\rho}{\int_0^\infty w^2\rho\,d\rho} = \mathcal{R}_s + \lambda_1 w\,; \qquad \Phi_1 \to 0\,, \quad \text{as} \quad \rho\to\infty\,, \tag{3.35 a}$$

with $\Phi_1'(0) = 0$, where the residual $\mathcal{R}_s$ is defined by

$$\mathcal{R}_s \equiv \pi w^2 R_{b0} + \frac{3}{2b^2}w^2\int_0^\infty w^2 U_{1p}\rho\,d\rho - \frac{\chi_0\chi_1 w^2}{b} - \frac{3}{b}w^2 U_{1p}\,. \tag{3.35 b}$$

Finally, λ_1 is determined by imposing a solvability condition on (3.35). The homogeneous adjoint operator $\mathcal{L}^\star$ corresponding to (3.35) is

$$\mathcal{L}^\star\Psi \equiv L_0\Psi - w\frac{\int_0^\infty w^2\Psi\rho\,d\rho}{\int_0^\infty w^2\rho\,d\rho}\,. \tag{3.36}$$

We define $\Psi^\star = w + \rho w'/2$ and readily verify that $L_0\Psi^\star = w$ and $L_0 w = w^2$ (see [**34**]). Then, we use Green's second identity to obtain $\int_0^\infty [wL_0\Psi^\star - \Psi^\star L_0 w]\,\rho\,d\rho = \int_0^\infty \left(w^2 - \Psi^\star w^2\right)\rho\,d\rho$. By the decay of w and $\Psi^\star$ as $\rho\to\infty$, we obtain that $\int_0^\infty w^2\rho\,d\rho = \int_0^\infty \Psi^\star w^2\rho\,d\rho$. Therefore, since the ratio of the two integrals in (3.36) is unity when $\Psi = \Psi^\star$, we conclude that $\mathcal{L}^\star\Psi^\star = 0$.

Finally, we impose the solvability condition that the right hand side of (3.35) is orthogonal to $\Psi^\star$ in the sense that $\lambda_1\int_0^\infty w\Psi^\star\rho\,d\rho + \int_0^\infty \mathcal{R}_s\Psi^*\rho\,d\rho = 0$. By using (3.35 *b*) for $\mathcal{R}_s$, this solvability condition yields that

$$\lambda_1 = -\frac{\int_0^\infty w^2\Psi^\star\rho\,d\rho}{b\int_0^\infty w\Psi^\star\rho\,d\rho}\left(b\pi R_{b0} - \chi_1\chi_0 + \frac{3}{2b}\int_0^\infty w^2 U_{1p}\rho\,d\rho - 3\frac{\int_0^\infty w^2 U_{1p}\Psi^\star\rho\,d\rho}{\int_0^\infty w^2\Psi^\star\rho\,d\rho}\right)\,. \tag{3.37}$$

Equation (3.37) is simplified by first calculating the following integrals by using integration by parts:

$$\begin{aligned}
&\int_0^\infty w^2\Psi^\star\rho\,d\rho = \int_0^\infty (L_0 w)\left(L_0^{-1}w\right) = \int_0^\infty w^2\rho\,d\rho = b\,,\\
&\int_0^\infty w\Psi^\star\rho\,d\rho = \int_0^\infty \rho w\left(w + \frac{\rho}{2}w'\right)\,d\rho = \int_0^\infty w^2\rho\,d\rho + \frac{1}{4}\int_0^\infty \left[w^2\right]'\rho^2\,d\rho = \frac{b}{2}\,.
\end{aligned} \tag{3.38}$$

In addition, since $L_0 V_{1p} = -w^2 U_{1p}$ from (3.7 *c*) and $\Psi^\star = L_0^{-1}w$, we obtain upon integrating by parts that

$$\int_0^\infty w^2 U_{1p}\Psi^\star\rho\,d\rho = -\int_0^\infty (L_0 V_{1p})\left(L_0^{-1}w\right)\rho\,d\rho = -\int_0^\infty V_{1p}w\rho\,d\rho\,.$$

By substituting this expression and (3.38) into (3.37), we obtain

$$\frac{\lambda_1}{2} = -\frac{1}{b}\left[b\pi R_{b0} - \chi_0\chi_1 + \frac{3}{2b}\int_0^\infty w^2 U_{1p}\rho\,d\rho + \frac{3}{b}\int_0^\infty w V_{1p}\rho\,d\rho\right]. \tag{3.39}$$

Next, we use (3.7 *c*) to calculate $\int_0^\infty w^2 U_{1p}\rho\,d\rho = \int_0^\infty (V_{1p} - 2wV_{1p})\,\rho\,d\rho$. Finally, we substitute this expression together with $\chi_0 = \sqrt{b}$ and (3.32), which relates μ_1 to χ_1, into (3.39) to obtain our final expression for λ_1. We summarize our result as follows:

Principal Result 3.1 *In the limit $\varepsilon \to 0$, consider a steady-state periodic pattern of spots for the Schnakenburg model (1.1) on the Bravais lattice Λ when $D = \mathcal{O}(\nu^{-1})$, where $\nu = -1/\log\varepsilon$. Then, when*

$$D = \frac{a^2|\Omega|^2}{4\pi^2 b\nu}\,(1 + \mu_1\nu)\,, \tag{3.40 a}$$

where $\mu_1 = \mathcal{O}(1)$, the portion of the continuous spectrum of the linearization that lies within an $\mathcal{O}(\nu)$ neighborhood of the origin $\lambda = 0$, i. e. that satisfies $|\lambda| \le \mathcal{O}(\nu)$, is given by

$$\lambda = \nu\lambda_1 + \cdots, \qquad \lambda_1 = 2\left[\frac{\mu_1}{2} - \pi R_{b0} - \frac{1}{2b^2}\int_0^\infty \rho V_{1p}\,d\rho\right]. \tag{3.40 b}$$

Here $|\Omega|$ is the area of the Wigner-Seitz cell and $R_{b0} = R_{b0}(\boldsymbol{k})$ is the regular part of the Bloch Green's function G_{b0} defined on Ω by (2.12), with $\boldsymbol{k} \neq 0$ and $\boldsymbol{k}/(2\pi) \in \Omega_B$.

The result (3.40 *b*) determines how the portion of the band of continuous spectrum that lies near the origin depends on the de-tuning parameter μ_1, the correction V_{1p} to the solution of the core problem, and the lattice structure and Bloch wavevector $\boldsymbol{k}$ as inherited from $R_{b0}(\boldsymbol{k})$.

Remark 3.1 *We need only consider $\boldsymbol{k}/(2\pi)$ in the first Brillouin zone Ω_B, defined as the Wigner-Seitz cell centered at the origin for the reciprocal lattice. Since R_{b0} is real-valued from Lemma 2.1, it follows that the band of spectrum (3.40 b) lies on the real axis in the λ-plane. Furthermore, since by Lemma 2.2, $R_{b0} = \mathcal{O}\left(1/(\boldsymbol{k}^T\mathcal{Q}\boldsymbol{k})\right) \to +\infty$ as $|\boldsymbol{k}| \to 0$ for some positive definite matrix $\mathcal{Q}$, the continuous band of spectrum that corresponds to small values of $|\boldsymbol{k}|$ is not within an $\mathcal{O}(\nu)$ neighborhood of $\lambda = 0$, but instead lies at an $\mathcal{O}\left(\nu/\boldsymbol{k}^T\mathcal{Q}\boldsymbol{k}\right)$ distance from the origin along the negative real axis in the λ-plane.*

We conclude from (3.40 *b*) that a periodic arrangement of spots with a given lattice structure is linearly stable when

$$\mu_1 < 2\pi R_{b0}^\star + \frac{1}{b^2}\int_0^\infty V_{1p}\rho\,d\rho\,, \qquad R_{b0}^\star \equiv \min_{\boldsymbol{k}} R_{b0}(\boldsymbol{k})\,. \tag{3.41}$$

For a fixed area $|\Omega|$ of the Wigner-Seitz cell, the optimal lattice geometry is defined as the one that allows for stability for the largest inhibitor diffusivity D. This leads to one of our main results.

Principal Result 3.2 *The optimal lattice arrangement for a periodic pattern of spots for the Schnakenburg model (1.1) is the one for which $\mathcal{K}_s \equiv R_{b0}^*$ is maximized. Consequently, this optimal lattice allows for stability for the largest*

possible value of D. For $\nu = -1/\log\varepsilon \ll 1$, a two-term asymptotic expansion for this maximal stability threshold for D is given explicitly by in terms of an objective function $\mathcal{K}_s$ by

$$D_{optim} \sim \frac{a^2|\Omega|^2}{4\pi^2 b\nu}\left[1+\nu\left(2\pi\max_{\Lambda}\mathcal{K}_s + \frac{1}{b^2}\int_0^\infty V_{1p}\rho\,d\rho\right)\right], \qquad \mathcal{K}_s \equiv R^{\star}_{b0} = \min_{\boldsymbol{k}} R_{b0}\,, \tag{3.42}$$

where $\max_\Lambda \mathcal{K}_s$ is taken over all lattices Λ that have a common area $|\Omega|$ of the Wigner-Seitz cell. In (3.42), V_{1p} is the solution to (3.7c) and $b = \int_0^\infty w^2\rho\,d\rho$ where $w(\rho) > 0$ is the ground-state solution of $\Delta_\rho w - w + w^2 = 0$. Numerical computations yield $b \approx 4.93$ and $\int_0^\infty V_{1p}\rho\,d\rho \approx 0.481$.

The numerical method to compute $\mathcal{K}_{\rm s}$ is given in §6. In §6.1, we show numerically that within the class of oblique Bravais lattices, $\mathcal{K}_{\rm s}$ is maximized for a regular hexagonal lattice. Thus, the maximal stability threshold for D is obtained for a regular hexagonal lattice arrangement of spots.

4 Periodic Spot Patterns for the Gierer-Meinhardt Model

In this section we analyze the linear stability of a steady-state periodic pattern of spots for the GM model (1.2), where the spots are centered at the lattice points of the Bravais lattice (2.1).

4.1 The Steady-State Solution

We first use the method of matched asymptotic expansions to construct a steady-state one-spot solution to (1.2) centered at the origin of the Wigner-Seitz cell Ω.

In the inner region near the origin of Ω we look for a locally radially symmetric steady-state solution of the form

$$u = D\,U\,, \qquad v = DV\,, \qquad \mathbf{y} = \varepsilon^{-1}\mathbf{x}\,. \tag{4.1}$$

Then, substituting (4.1) into the steady-state equations of (1.2), we obtain that $V \sim V(\rho)$ and $U \sim U(\rho)$, with $\rho = |\mathbf{y}|$, satisfy the core problem

$$\Delta_\rho V - V + V^2/U = 0\,, \qquad \Delta_\rho U = -V^2\,, \qquad 0 < \rho < \infty\,, \tag{4.2a}$$

$$U'(0) = V'(0) = 0\,; \qquad V \to 0\,, \qquad U \sim -S\log\rho + \chi(S) + o(1)\,, \quad \text{as} \quad \rho\to\infty\,, \tag{4.2b}$$

where $\Delta_\rho V \equiv V'' + \rho^{-1}V'$ and $S = \int_0^\infty V^2\rho\,d\rho$. The unknown source strength S will be determined by matching the far-field behavior of the core solution to an outer solution for u valid away from $\mathcal{O}(\varepsilon)$ distances from the origin.

Since v is exponentially small in the outer region, we have in the sense of distributions that $\varepsilon^{-2}v^2 \to 2\pi D^2 S\delta(\mathbf{x})$. Therefore, from (1.2), the outer steady-state problem for u is

$$\begin{aligned} \Delta u - \frac{1}{D}u = -2\pi DS\,\delta(\mathbf{x})\,, \quad \mathbf{x}\in\Omega\,; \qquad \mathcal{P}_0 u = 0\,, \quad \mathbf{x}\in\partial\Omega\,, \\ u \sim -DS\log|\mathbf{x}| + D\left(-\frac{S}{\nu} + \chi(S)\right), \quad \text{as} \quad \mathbf{x}\to 0\,, \end{aligned} \tag{4.3}$$

where $\nu \equiv -1/\log\varepsilon$. We introduce the reduced-wave Green's function $G_p(\mathbf{x})$ and its regular part R_p, which satisfy

$$\begin{aligned} \Delta G_p - \frac{1}{D}G_p = -\delta(\mathbf{x})\,, \quad \mathbf{x}\in\Omega\,; \qquad \mathcal{P}_0 G_p = 0\,, \quad \mathbf{x}\in\partial\Omega\,, \\ G_p(\mathbf{x}) \sim -\frac{1}{2\pi}\log|\mathbf{x}| + R_p\,, \quad \text{as} \quad \mathbf{x}\to 0\,, \end{aligned} \tag{4.4}$$

where R_p is the regular part of G_p. The solution to (4.3) is $u(\mathbf{x}) = 2\pi DSG_p(\mathbf{x})$. Now as $\mathbf{x} \to 0$ we calculate the local behavior of $u(\mathbf{x})$ and compare it with the required behavior in (4.3). This yields that S satisfies

$$(1 + 2\pi\nu R_p)\, S = \nu\chi(S)\,. \tag{4.5}$$

Since the stability threshold occurs when $D = \mathcal{O}(\nu^{-1}) \gg 1$, we expand the solution to (4.4) for $D = D_0/\nu \gg 1$ with $D_0 = \mathcal{O}(1)$ to obtain

$$G_p = \frac{D_0}{|\Omega|\nu} + G_{0p} + \mathcal{O}(\nu)\,, \qquad R_p = \frac{D_0}{|\Omega|\nu} + R_{0p} + \mathcal{O}(\nu)\,, \tag{4.6}$$

where G_{0p} and R_{0p} is the periodic source-neutral Green's function and its regular part, respectively, defined by (3.6). By combining (4.5) and (4.6), we get that S satisfies

$$\left(1 + \mu + 2\pi\nu R_{0p} + \mathcal{O}(\nu^2)\right) S = \nu\chi(S)\,, \qquad \mu \equiv \frac{2\pi D_0}{|\Omega|}\,. \tag{4.7}$$

To determine the appropriate scaling for S in terms of $\nu \ll 1$ for a solution to (4.7), we use $\chi(S) = \mathcal{O}(S^{1/2})$ as $S \to 0$ from Appendix B. Thus, to balance the leading order terms in (4.7), we require that $S = \mathcal{O}(\nu^2)$ as $\nu \to 0$. The next result determines a two-term expansion for the solution to the core problem (4.2) for $\nu \to 0$ when $S = \mathcal{O}(\nu^2)$.

Lemma 4.1 *For $S = S_0\nu^2 + S_1\nu^3 + \cdots$, where $\nu \equiv -1/\log\varepsilon \ll 1$, the asymptotic solution to the core problem (4.2) is*

$$V \sim \nu\left(V_0 + \nu V_1 + \cdots\right), \qquad U \sim \nu\left(U_0 + \nu U_1 + \nu^2 U_2 + \cdots\right), \qquad \chi \sim \nu\left(\chi_0 + \nu\chi_1 + \cdots\right), \tag{4.8 a}$$

where U_0, $U_1(\rho)$, $V_0(\rho)$, and $V_1(\rho)$ are defined by

$$U_0 = \chi_0\,, \qquad U_1 = \chi_1 + S_0 U_{1p}\,, \qquad V_0 = \chi_0 w\,, \qquad V_1 = \chi_1 w + S_0 V_{1p}\,. \tag{4.8 b}$$

Here $w(\rho)$ is the unique ground-state solution to $\Delta_\rho w - w + w^2 = 0$ with $w(0) > 0$, $w'(0) = 0$, and $w \to 0$ as $\rho \to \infty$. In terms of $w(\rho)$, the functions U_{1p} and V_{1p} are the unique solutions on $0 \le \rho < \infty$ to

$$\begin{aligned} &L_0 V_{1p} = w^2 U_{1p}\,, \qquad V_{1p}'(0) = 0\,, \quad V_{1p} \to 0\,, \quad \text{as} \quad \rho \to \infty\,, \\ &\Delta_\rho U_{1p} = -w^2/b\,, \qquad U_{1p}'(0) = 0\,, \qquad U_{1p} \to -\log\rho + o(1)\,, \quad \text{as} \quad \rho \to \infty\,; \qquad b \equiv \int_0^\infty \rho w^2\, d\rho\,, \end{aligned} \tag{4.8 c}$$

where $L_0 V_{1p} \equiv \Delta_\rho V_{1p} - V_{1p} + 2wV_{1p}$. Finally, in (4.8 a), the constants χ_0 and χ_1 are related to S_0 and S_1 by

$$\chi_0 = \sqrt{\frac{S_0}{b}}\,, \qquad \chi_1 = \frac{S_1}{2\chi_0 b} - \frac{S_0}{b}\int_0^\infty w V_{1p}\rho\, d\rho\,. \tag{4.8 d}$$

The derivation of this result is given in Appendix B below. The $o(1)$ condition in the far-field behavior in (4.8 c) eliminates an otherwise arbitrary constant in the determination of U_{1p}. Therefore, this condition ensures that the solution to the linear BVP (4.8 c) is unique.

4.2 The Spectrum of the Linearization Near the Origin

We linearize around the steady-state solution u_e and v_e, as calculated in §4.1, by introducing the perturbation (3.8). This yields the following eigenvalue problem, where $\mathcal{P}_{\boldsymbol{k}}$ is the quasi-periodic boundary operator of (2.35):

$$\begin{aligned} \varepsilon^2\Delta\phi - \phi + \frac{2v_e}{u_e}\phi - \frac{v_e^2}{u_e^2}\eta = \lambda\phi\,, \quad \mathbf{x}\in\Omega\,; \qquad \mathcal{P}_{\boldsymbol{k}}\phi = 0\,, \quad \mathbf{x}\in\partial\Omega\,, \\ D\Delta\eta - \eta + 2\varepsilon^{-2}v_e\phi = \lambda\tau\eta\,, \quad \mathbf{x}\in\Omega\,; \qquad \mathcal{P}_{\boldsymbol{k}}\eta = 0\,, \quad \mathbf{x}\in\partial\Omega\,. \end{aligned} \tag{4.9}$$

In the inner region near $\mathbf{x}=0$ we introduce the local variables $N(\rho)$ and $\Phi(\rho)$ by

$$\eta = N(\rho)\,, \qquad \phi = \Phi(\rho)\,, \qquad \rho = |\mathbf{y}|\,, \qquad \mathbf{y} = \varepsilon^{-1}\mathbf{x}\,. \tag{4.10}$$

Upon substituting (4.10) into (4.9), and by using $u_e \sim DU$ and $v_e \sim DV$, where U and V satisfy the core problem (4.2), we obtain on $0<\rho<\infty$ that

$$\begin{aligned} \Delta_\rho\Phi - \Phi + \frac{2V}{U}\Phi - \frac{V^2}{U^2}N = \lambda\Phi\,, \qquad \Phi\to 0\,, \quad \text{as} \quad \rho\to\infty\,, \\ \Delta_\rho N = -2V\Phi\,, \qquad N\sim -C\log\rho + B\,, \quad \text{as} \quad \rho\to\infty\,, \end{aligned} \tag{4.11}$$

with $\Phi'(0)=N'(0)=0$ and where $B=B(S;\lambda)$. The divergence theorem yields the identity $C = 2\int_0^\infty V\Phi\rho\,d\rho$.

To determine the constant C we must match the far field behavior of the core solution to an outer solution for η, which is valid away from $\mathbf{x}=0$. Since v_e is localized near $\mathbf{x}=0$, we calculate in the sense of distributions that $2\varepsilon^{-2}v_e\phi \to 2D\left(\int_{\mathbb{R}^2} V\Phi\,d\mathbf{y}\right)\delta(\mathbf{x}) = 2\pi CD\delta(\mathbf{x})$. By using this expression in (4.9), we obtain that the outer problem for η is

$$\begin{aligned} \Delta\eta - \theta_\lambda^2\eta = -2\pi C\delta(\mathbf{x})\,, \quad \mathbf{x}\in\Omega\,; \qquad \mathcal{P}_{\boldsymbol{k}}\eta = 0\,, \quad \mathbf{x}\in\partial\Omega\,, \\ \eta\sim -C\log|\mathbf{x}| - \frac{C}{\nu} - B\,, \quad \text{as} \quad \mathbf{x}\to 0\,, \end{aligned} \tag{4.12}$$

where we have defined $\theta_\lambda \equiv \sqrt{(1+\tau\lambda)/D}$. The solution to (4.12) is $\eta = 2\pi C\mathcal{G}_{b\lambda}(\mathbf{x})$, where $\mathcal{G}_{b\lambda}$ satisfies

$$\begin{aligned} \Delta\mathcal{G}_{b\lambda} - \theta_\lambda^2\mathcal{G}_{b\lambda} = -\delta(\mathbf{x})\,, \quad \mathbf{x}\in\Omega\,; \qquad \mathcal{P}_{\boldsymbol{k}}\mathcal{G}_{b\lambda} = 0\,, \quad \mathbf{x}\in\partial\Omega\,, \\ \mathcal{G}_{b\lambda}\sim -\frac{1}{2\pi}\log|\mathbf{x}| + \mathcal{R}_{b\lambda}\,, \quad \text{as} \quad \mathbf{x}\to 0\,. \end{aligned} \tag{4.13}$$

By imposing that the behavior of η as $\mathbf{x}\to 0$ agrees with that in (4.12), we conclude that $(1+2\pi\nu\mathcal{R}_{b\lambda})\,C = \nu B$. Then, since $D = D_0/\nu \gg 1$, we have from Lemma 2.3(ii), upon taking the $D\gg 1$ limit in (4.13), that $R_{b\lambda}\sim R_{b0}+\mathcal{O}(\nu)$ for $|\boldsymbol{k}|>0$ and $\boldsymbol{k}/(2\pi)\in\Omega_B$. This yields,

$$\left(1 + 2\pi\nu R_{b0} + \mathcal{O}(\nu^2)\right)C = \nu B\,, \tag{4.14}$$

where $R_{b0} = R_{b0}(\boldsymbol{k})$ is the regular part of the Bloch Green's function G_{b0} defined on Ω by (2.12).

As in §3.2, we now proceed to determine the portion of the continuous spectrum of the linearization that lies within an $\mathcal{O}(\nu)$ neighborhood of the origin $\lambda=0$ when D is close to a certain critical value. To do so, we first must calculate an asymptotic expansion for the solution to (4.11) together with (4.14).

By using (4.8 *a*) we first calculate the coefficients in the differential operator in (4.11) as

$$\frac{V}{U} = w + \frac{\nu S_0}{\chi_0}\left(V_{1p} - wU_{1p}\right) + \cdots\,, \qquad \frac{V^2}{U^2} = w^2 + \frac{2\nu S_0}{\chi_0}w\left(V_{1p} - wU_{1p}\right) + \cdots\,,$$

so that the local problem (4.11) on $0<\rho<\infty$ becomes

$$
\begin{aligned}
&\Delta_\rho\Phi-\Phi+\left[2w+\frac{2\nu S_0}{\chi_0}w\left(V_{1p}-wU_{1p}\right)+\cdots\right]\Phi=\left[w^2+\frac{2\nu S_0}{\chi_0}w\left(V_{1p}-wU_{1p}\right)+\cdots\right]N+\lambda\Phi\,,\\
&\Delta_\rho N=-2\nu\left[\chi_0 w+\nu\left(\chi_1 w+S_0V_{1p}\right)+\cdots\right]\Phi\,,\\
&\qquad\Phi\to 0\,,\qquad N\sim -C\log\rho+B\,,\quad \text{as}\quad \rho\to\infty\,;\qquad \Phi'(0)=N'(0)=0\,.
\end{aligned}
\tag{4.15}
$$

To analyze (4.15) together with (4.14), we substitute the appropriate expansions

$$
\begin{aligned}
&N=\frac{1}{\nu}\left(\hat N_0+\nu\hat N_1+\cdots\right)\,,\quad B=\frac{1}{\nu}\left(\hat B_0+\nu\hat B_1+\cdots\right)\,,\quad C=C_0+\nu C_1+\cdots\,,\\
&\Phi=\frac{1}{\nu}\left(\Phi_0+\nu\Phi_1+\cdots\right)\,,\qquad \lambda=\lambda_0+\nu\lambda_1+\cdots\,,
\end{aligned}
\tag{4.16}
$$

into (4.15) and collect powers of ν.

To leading order, we obtain on $0<\rho<\infty$ that

$$
\begin{aligned}
&L_0\Phi_0\equiv\Delta_\rho\Phi_0-\Phi_0+2w\Phi_0=w^2\hat N_0+\lambda_0\Phi_0\,,\qquad \Delta_\rho\hat N_0=0\,,\\
&\qquad\Phi_0\to 0\,,\qquad \hat N_0\to\hat B_0\quad\text{as}\quad\rho\to\infty\,;\qquad \Phi_0'(0)=\hat N_0'(0)=0\,,
\end{aligned}
\tag{4.17}
$$

where L_0 is the local operator. We conclude that $\hat N_0=\hat B_0$ for $\rho\ge 0$.

At next order, we obtain on $\rho>0$ that Φ_1 satisfies

$$
L_0\Phi_1-w^2\hat N_1=-\frac{2S_0}{\chi_0}\left(V_{1p}-wU_{1p}\right)\Phi_0+\frac{2S_0}{\chi_0}w\left(V_{1p}-wU_{1p}\right)\hat N_0+\lambda_1\Phi_0\,;\qquad \Phi_1\to 0\,,\quad\text{as}\quad\rho\to\infty\,,
\tag{4.18}
$$

with $\Phi_1'(0)=0$, and that $\hat N_1$ on $\rho>0$ satisfies

$$
\Delta_\rho\hat N_1=-2\chi_0 w\Phi_0\,;\qquad \hat N_1\sim -C_0\log\rho+\hat B_1\,,\quad\text{as}\quad\rho\to\infty\,;\qquad \hat N_1'(0)=0\,.
\tag{4.19}
$$

At one higher order, the problem for $\hat N_2$ on $\rho>0$ is

$$
\Delta_\rho\hat N_2=-2\chi_0 w\Phi_1-2\left(\chi_1 w+S_0V_{1p}\right)\Phi_0\,;\qquad \hat N_2\sim -C_1\log\rho+\hat B_2\,,\quad\text{as}\quad\rho\to\infty\,;\qquad \hat N_2'(0)=0\,.
\tag{4.20}
$$

In addition, by substituting (4.16) into (4.14) we obtain, upon collecting powers of ν, that

$$
C_0=\hat B_0\,,\qquad C_1+2\pi R_{b0}\hat B_0=\hat B_1\,.
\tag{4.21}
$$

Next, we proceed to analyze (4.17)–(4.20). From the divergence theorem, we obtain from (4.19) that

$$
C_0=2\chi_0\int_0^\infty w\Phi_0\rho\,d\rho\,.
\tag{4.22}
$$

To identify χ_0 in (4.22), we substitute $S=\nu^2S_0+\cdots$ and $\chi\sim\nu\chi_0+\cdots$ into (4.7) to get $(1+\mu+\cdots)\left(\nu^2S_0+\cdots\right)\sim\nu^2(\chi_0+\cdots)$. From the leading order terms, we get $\chi_0=S_0(1+\mu)$. Then, since $S_0=b\chi_0^2$ from (4.8 *d*), we obtain

$$
\chi_0=\frac{1}{b(1+\mu)}\,,\qquad S_0=\frac{1}{b(1+\mu)^2}\,,\qquad C_0=\hat B_0=\hat N_0=\frac{2}{b(1+\mu)}\int_0^\infty w\Phi_0\rho\,d\rho\,.
\tag{4.23}
$$

From (4.17) we then obtain the leading-order NLEP on $\rho>0$,

$$
L_0\Phi_0-\frac{2w^2}{(1+\mu)}\frac{\int_0^\infty w\Phi_0\,\rho\,d\rho}{\int_0^\infty w^2\rho\,d\rho}=\lambda_0\Phi_0\,;\qquad \Phi_0\to 0\,,\quad\text{as}\quad\rho\to\infty\,;\qquad \Phi_0'(0)=0\,;\qquad \mu\equiv\frac{2\pi D_0}{|\Omega|}\,.
\tag{4.24}
$$

For this NLEP, Theorem 3.7 of [**35**] proves that $\mathrm{Re}(\lambda_0)<0$ if and only if $2/(1+\mu)>1$. Therefore, the stability

threshold where $\lambda_0 = 0$ and $\Phi_0 = w$ occurs when $\mu = 1$. At this stability threshold, we calculate from (4.23) that

$$\chi_0 = \frac{1}{2b}\,, \qquad S_0 = \frac{1}{4b}\,, \qquad \Phi_0 = w\,, \qquad C_0 = \hat{B}_0 = \hat{N}_0 = \frac{1}{b}\int_0^\infty w\Phi_0\rho\,d\rho = 1\,. \tag{4.25}$$

Upon substituting (4.25) into (4.19) we obtain at $\lambda_0 = 0$ that $\hat{N}_1$ on $\rho > 0$ satisfies

$$\Delta_\rho\hat{N}_1 = -2\chi_0 w^2 = -\frac{w^2}{b}\,; \qquad \hat{N}_1 \sim -\log\rho + \hat{B}_1\,, \quad \text{as} \quad \rho\to\infty\,; \qquad \hat{N}_1'(0) = 0\,. \tag{4.26}$$

Upon comparing (4.26) with the problem for U_{1p} in (4.8 *c*), we conclude that

$$\hat{N}_1 = U_{1p} + \hat{B}_1\,. \tag{4.27}$$

As in §3.2, we now proceed to analyze the effect of the higher order terms by determining the continuous band of spectrum that is contained within an $\mathcal{O}(\nu)$ ball near $\lambda = 0$ when the bifurcation parameter μ is $\mathcal{O}(\nu)$ close to the leading-order critical value $\mu = 1$. As such, we set

$$\lambda = \nu\lambda_1 + \cdots\,, \qquad \text{for} \qquad \mu = 1 + \nu\mu_1 + \cdots\,, \tag{4.28}$$

and we derive an expression for λ_1 in terms of the de-tuning parameter μ_1, the Bloch wavevector $\boldsymbol{k}$, the lattice structure, and certain correction terms to the core problem.

We first use (4.8 *d*) and (4.7) to calculate χ_1 in terms of μ_1. By substituting $\mu = 1+\nu\mu_1+\cdots$ together with (4.8 *a*) into (4.7), we obtain

$$\left[1 + (1+\nu\mu_1) + 2\pi\nu R_{0p} + \cdots\right]\left[\nu^2 S_0 + \nu^3 S_1 + \cdots\right] = \nu^2\left(\chi_0 + \nu\chi_1 + \cdots\right)\,.$$

From the $\mathcal{O}(\nu^3)$ terms, we obtain that $\chi_1 = \mu_1 S_0 + 2S_1 + 2\pi R_{0p}S_0$. Upon combining this result together with (4.8 *d*) for χ_1, and by using $\chi_0 = 1/(2b)$, we obtain at criticality where $\lambda_0 = 0$ that

$$\chi_1 = -\frac{\mu_1}{4b} - \frac{\pi R_{0p}}{2b} - \frac{1}{2b^2}\int_0^\infty wV_{1p}\rho\,d\rho\,. \tag{4.29}$$

This result is needed below in the evaluation of the solvability condition.

Next, we substitute (4.25) and (4.27) into (4.18) for Φ_1 to obtain, after some algebra, that (4.18) reduces at the leading-order stability threshold $\lambda_0 = 0$ to

$$L_0\Phi_1 - w^2\hat{B}_1 = \lambda_1 w + w^2 U_{1p}\,; \qquad \Phi_1 \to 0\,, \quad \text{as} \quad \rho\to\infty\,, \tag{4.30}$$

with $\Phi_1'(0) = 0$. In a similar way, at the leading-order stability threshold $\lambda_0 = 0$, the problem (4.20) for $\hat{N}_2$ on $\rho > 0$ reduces to

$$\Delta_\rho\hat{N}_2 = -\frac{w}{b}\Phi_1 - 2\left(\chi_1 w + \frac{1}{4b}V_{1p}\right)w\,; \qquad \hat{N}_2 \sim -C_1\log\rho + \hat{B}_2\,, \quad \text{as} \quad \rho\to\infty\,; \qquad \hat{N}_2'(0) = 0\,. \tag{4.31}$$

By applying the divergence theorem to (4.31) we get

$$C_1 = \frac{1}{b}\int_0^\infty w\Phi_1\rho\,d\rho + 2\chi_1 b + \frac{1}{2b}\int_0^\infty wV_{1p}\rho\,d\rho\,. \tag{4.32}$$

Then, by using (4.21) with $\hat{B}_0 = 1$ to relate C_1 to $\hat{B}_1$, we determine $\hat{B}_1$ as $\hat{B}_1 = C_1 + 2\pi R_{b0}$ where C_1 is given in (4.32). With $\hat{B}_1$ obtained in this way, we find from (4.30) that Φ_1 satisfies

$$\mathcal{L}\Phi_1 \equiv L_0\Phi_1 - w^2\frac{\int_0^\infty w\Phi_1\rho\,d\rho}{\int_0^\infty w^2\rho\,d\rho} = \mathcal{R}_g + \lambda_1 w\,; \qquad \Phi_1 \to 0\,, \quad \text{as} \quad \rho\to\infty\,, \tag{4.33 a}$$

with $\Phi_1'(0)=0$, where the residual $\mathcal{R}_g$ is defined by

$$\mathcal{R}_g \equiv 2\pi R_{b0}w^2 + 2\chi_1 b w^2 + \frac{1}{2b}w^2\int_0^\infty wV_{1p}\rho\,d\rho + w^2U_{1p}\,. \tag{4.33 b}$$

As discussed in §3.2, the solvability condition for (4.33) is that the right-hand side of (4.33 *a*) is orthogonal to the homogeneous adjoint solution $\Psi^\star = w + \rho w'/2$ in the sense that $\lambda_1\int_0^\infty w\Psi^\star\rho\,d\rho + \int_0^\infty \mathcal{R}_g\Psi^*\rho\,d\rho = 0$. Upon using (4.29), which relates χ_1 to μ_1, to simplify this solvability condition, we readily obtain by using (4.33 *b*) for $\mathcal{R}_g$ that

$$\lambda_1 = -\frac{\int_0^\infty w^2\Psi^\star\rho\,d\rho}{\int_0^\infty w\Psi^\star\rho\,d\rho}\left(2\pi R_{b0} - \frac{\mu_1}{2} - \pi R_{0p} - \frac{1}{2b}\int_0^\infty wV_{1p}\rho\,d\rho\right) - \frac{\int_0^\infty w^2U_{1p}\Psi^\star\rho\,d\rho}{\int_0^\infty w\Psi^\star\rho\,d\rho}\,. \tag{4.34}$$

To simplify the terms in (4.34), we use $L_0V_{1p} = w^2U_{1p}$ and $\Delta_\rho U_{1p} = -w^2/b$ from (4.8 *c*), together with $w = L_0^{-1}\Psi^\star$ to calculate, after an integration by parts, that

$$\int_0^\infty w^2U_{1p}\Psi^\star\rho\,d\rho = \int_0^\infty (L_0V_{1p})\left(L_0^{-1}w\right)\rho\,d\rho = \int_0^\infty V_{1p}w\rho\,d\rho\,.$$

By substituting this expression, together with $\int_0^\infty w^2\Psi^\star\rho\,d\rho = b$ and $\int_0^\infty w\Psi^\star\rho\,d\rho = b/2$, as obtained from (3.38), into (4.34) we obtain our final result for λ_1. We summarize our result as follows:

Principal Result 4.1 *In the limit $\varepsilon\to 0$, consider a steady-state periodic pattern of spots for the GM model (1.2) where $D=\mathcal{O}(\nu^{-1})$ with $\nu = -1/\log\varepsilon$. Then, when*

$$D \sim \frac{|\Omega|}{2\pi\nu}\left(1+\nu\mu_1\right)\,, \tag{4.35 a}$$

where $\mu_1=\mathcal{O}(1)$ and $|\Omega|$ is the area of the Wigner-Seitz cell, the portion of the continuous spectrum of the linearization that lies within an $\mathcal{O}(\nu)$ neighborhood of the origin $\lambda=0$ is given by

$$\lambda = \nu\lambda_1 + \cdots\,, \qquad \lambda_1 = 2\left[\frac{\mu_1}{2} - 2\pi R_{b0} + \pi R_{0p} - \frac{1}{2b}\int_0^\infty \rho w V_{1p}\,d\rho\right]\,. \tag{4.35 b}$$

Here $R_{b0}=R_{b0}(\boldsymbol{k})$ is the regular part of the Bloch Green's function G_{b0} defined on Ω by (2.12), $\boldsymbol{k}/(2\pi)\in\Omega_B$, and R_{0p} is the regular part of the periodic source-neutral Green's function G_{0p} satisfying (3.6).

Remark 4.1 *In comparison with the analogous result obtained in Principal Result 3.1 for the Schnakenburg model, λ_1 in (4.35 b) now depends on the regular parts of two different Green's functions. The term R_{0p} only depends on the geometry of the lattice, whereas $R_{b0}=R_{b0}(\boldsymbol{k})$ depends on both the lattice geometry and the Bloch wavevector $\boldsymbol{k}$. To calculate $R_{b0}(\boldsymbol{k})$ we again need only consider vectors $\boldsymbol{k}/(2\pi)$ in the first Brillouin zone Ω_B of the reciprocal lattice. Since R_{b0} is real-valued from Lemma 2.1, the band of spectrum (4.35 b) lies on the real axis in the λ-plane. Moreover, from Lemma 2.2 small values of $|\boldsymbol{k}|$ generate spectra that lie at an $\mathcal{O}\left(\nu/\boldsymbol{k}^T\mathcal{Q}\boldsymbol{k}\right)$ distance from the origin along the negative real axis in the λ-plane, where $\mathcal{Q}$ is a positive definite matrix.*

For a given lattice geometry, we seek to determine μ_1 so that $\lambda_1<0$ for all $\boldsymbol{k}$. From (4.35 *b*), we conclude that a

periodic arrangement of spots with a given lattice structure is linearly stable when

$$\mu_1 < 4\pi R_{b0}^\star - 2\pi R_{0p} + \frac{1}{b}\int_0^\infty w V_{1p}\rho\, d\rho\,, \qquad R_{b0}^\star \equiv \min_{\boldsymbol{k}} R_{b0}(\boldsymbol{k})\,. \tag{4.36}$$

We characterize the optimal lattice as the one with a fixed area $|\Omega|$ of the Wigner-Seitz cell that allows for stability for the largest inhibitor diffusivity D. This leads to our second main result.

Principal Result 4.2 *The optimal lattice arrangement for a periodic pattern of spots for the GM model (1.2) is the one for which the objective function $\mathcal{K}_{gm}$ is maximized, where*

$$\mathcal{K}_{gm} \equiv 4\pi R_{b0}^\star - 2\pi R_{0p}\,, \qquad R_{b0}^\star \equiv \min_{\boldsymbol{k}} R_{b0}(\boldsymbol{k})\,. \tag{4.37}$$

For $\nu = -1/\log\varepsilon \ll 1$, a two-term asymptotic expansion for this maximal stability threshold for D is given explicitly by

$$D_{optim} \sim \frac{|\Omega|}{2\pi\nu}\left[1 + \nu\left(\max_{\Lambda}\mathcal{K}_{gm} + \frac{1}{b}\int_0^\infty w V_{1p}\rho\, d\rho\right)\right]\,, \tag{4.38}$$

where $\max_\Lambda \mathcal{K}_{gm}$ is taken over all lattices Ω having a common area $|\Omega|$ of the Wigner-Seitz cell. In (4.38), V_{1p} is the solution to (4.8 c) and $b = \int_0^\infty w^2\rho\, d\rho \approx 4.93$ where $w(\rho) > 0$ is the ground-state solution of $\Delta_\rho w - w + w^2 = 0$. Numerical computations yield $\int_0^\infty w V_{1p}\rho\, d\rho \approx -0.945$.

The numerical method to compute $\mathcal{K}_{\rm gm}$ is given in §6. In §6.1, we show numerically that within the class of oblique Bravais lattices, the maximal stability threshold for D occurs for a regular hexagonal lattice.

5 A Simple Approach for Calculating the Optimal Value of the Diffusivity

In this section we implement a very simple alternative approach to calculate the stability threshold for the Schnakenburg (1.1) and GM Models (1.2) in §5.1 and §5.2, respectively. In §5.3 this method is then used to determine an optimal stability threshold for the GS model. In this alternative approach, we do not calculate the entire band of continuous spectrum that lies near the origin when the bifurcation parameter μ is $\mathcal{O}(\nu)$ close to its critical value. Instead, we determine the critical value of μ, depending on the Bloch wavevector $\boldsymbol{k}$, such that $\lambda = 0$ is in the spectrum of the linearization. We then perform a min-max optimization of this critical value of μ with respect to $\boldsymbol{k}$ and the lattice geometry Λ in order to find the optimal value of D.

5.1 The Schnakenburg Model

This alternative approach for calculating the stability threshold requires the following two-term expansion for $\chi(S)$ in terms of S as $S \to 0$:

Lemma 5.1 *For $S \to 0$, the asymptotic solution to the core problem (3.2) is*

$$\begin{aligned} &V \sim \frac{S}{b}w + \frac{S^3}{b^3}\left(-\hat\chi_1 b w + V_{1p}\right) + \cdots\,, \qquad U \sim \frac{b}{S} + S\left(\hat\chi_1 + \frac{U_{1p}}{b}\right) + \cdots\,, \\ &\chi \sim \frac{b}{S} + S\hat\chi_1 + \cdots\,; \qquad \hat\chi_1 \equiv \frac{1}{b^2}\int_0^\infty V_{1p}\rho\, d\rho\,. \end{aligned} \tag{5.1}$$

Here $w(\rho)$ is the unique positive ground-state solution to $\Delta_\rho w - w + w^2 = 0$ and $b \equiv \int_0^\infty w^2 \rho d\rho$. In terms of $w(\rho)$, the functions U_{1p} and V_{1p} are the unique solutions on $0 \le \rho < \infty$ to (3.7 c).

The derivation of this result, as outlined at the end of Appendix A, is readily obtained by setting $S_1 = 0$ and $S = S_0\nu^{1/2}$ in the results of Lemma 3.1.

The key step in the analysis is to note that at $\lambda = 0$, the solution to the inner problem (3.11) for Φ and N can be readily identified by differentiating the core problem (3.2) with respect to S. More specifically, at $\lambda = 0$, the solution to (3.11) is $\Phi = CV_S$, $N = CU_S$, and $B(S;0) = C\chi'(S)$. With B known at $\lambda = 0$, we obtain from (3.15) and (3.4) that the critical value of D at $\lambda = 0$ satisfies the nonlinear algebraic problem

$$1 + 2\pi\nu R_{b0} + \mathcal{O}(\nu^2) + \nu\chi'(S) = 0\,, \qquad \text{where} \quad S = \frac{a|\Omega|}{2\pi\sqrt{D}}\,. \tag{5.2}$$

To determine the critical threshold in D from (5.2) we use the two-term expansion for $\chi(S)$ in (5.1) to get $\chi'(S) \sim -b/S^2 + \hat{\chi}_1 + \cdots$. By using the relation for S in terms of D from (5.2) when $D = D_0/\nu \gg 1$, we obtain that

$$\chi'(S) \sim -\frac{\mu}{\nu} + \hat{\chi}_1 + \cdots\,, \qquad \mu \equiv \frac{4\pi^2 D_0 b}{a^2|\Omega|^2}\,, \qquad D = \frac{D_0}{\nu}\,. \tag{5.3}$$

Upon substituting this expression into (5.2), we obtain that

$$1 - \mu + \nu\hat{\chi}_1 = -2\pi\nu R_{b0} + \mathcal{O}(\nu^2)\,,$$

which determines μ as $\mu \sim 1 + \nu(2\pi R_{b0} + \hat{\chi}_1)$. Upon recalling the definition of μ in (5.3), we conclude that $\lambda = 0$ when $D = D^\star(\boldsymbol{k})$, where $D^\star(\boldsymbol{k})$ is given by

$$D^\star(\boldsymbol{k}) \equiv \frac{a^2|\Omega|^2}{4\pi^2 b\nu}\left[1 + \nu\left(2\pi R_{b0}(\boldsymbol{k}) + \hat{\chi}_1\right) + \mathcal{O}(\nu^2)\right]\,, \tag{5.4}$$

where $\hat{\chi}_1$ is defined in (5.1). By minimizing $R_{b0}(\boldsymbol{k})$ with respect to $\boldsymbol{k}$, and then maximizing the result with respect to the geometry of the lattice Λ, (5.4) recovers the main result (3.42) of Principal Result 3.2. This simple method, which relies critically on the observation that $B = \chi'(S)$ at $\lambda = 0$, provides a rather expedient approach for calculating the optimal threshold in D. However, it does not characterize the spectrum contained in the small ball $|\lambda| = \mathcal{O}(\nu) \ll 1$ near the origin when D is near the leading-order stability threshold $a^2|\Omega|^2/(4\pi^2 b\nu)$.

5.2 The Gierer-Meinhardt Model

Next, we use a similar approach as in §5.1 to re-derive the the stability result in (4.38) of Principal Result 4.2 for the GM model. We first need the following result that gives a two-term expansion in terms of S for $\chi(S)$ as $S \to 0$:

Lemma 5.2 *For $S \to 0$, the asymptotic solution to the core problem (4.2) is*

$$\begin{aligned} &V \sim \sqrt{\frac{S}{b}}\,w + S\left(\hat{\chi}_1 w + V_{1p}\right) + \cdots\,, \qquad U \sim \sqrt{\frac{S}{b}} + S\left(\hat{\chi}_1 + U_{1p}\right) + \cdots\,, \\ &\chi \sim \sqrt{\frac{S}{b}} + S\hat{\chi}_1 + \cdots\,, \qquad \hat{\chi}_1 \equiv -\frac{1}{b}\int_0^\infty w V_{1p}\rho\, d\rho\,. \end{aligned} \tag{5.5}$$

Here $w(\rho)$ is the unique positive ground-state solution to $\Delta_\rho w - w + w^2 = 0$ and $b \equiv \int_0^\infty w^2 \rho d\rho$. In terms of $w(\rho)$, the functions U_{1p} and V_{1p} are the unique solutions on $0 \le \rho < \infty$ to (4.8 c).

The derivation of this result, as outlined at the end of Appendix B, is readily obtained by setting $S_1 = 0$ and $S = S_0\nu^2$ in the results of Lemma 4.1.

As similar to the analysis in §5.1, the solution to (4.11) for Φ and N is readily identified by differentiating the core problem (4.2) with respect to S. In this way, we get $B(S,0) = C\chi'(S)$. Therefore, at $\lambda = 0$, we obtain from (4.14) and (4.7) that the critical values of D and S where $\lambda = 0$ satisfy the coupled nonlinear algebraic system

$$\begin{aligned} &\left(1 + \mu + 2\pi\nu R_{0p} + \mathcal{O}(\nu^2)\right) S = \nu\chi(S)\,, \qquad \mu \equiv \frac{2\pi D_0}{|\Omega|}\,, \qquad D = \frac{D_0}{\nu}\,, \\ &1 + 2\pi\nu R_{b0} + \mathcal{O}(\nu^2) - \nu\chi'(S) = 0\,. \end{aligned} \tag{5.6}$$

We then use the two term expansion in (5.5) for $\chi(S)$ as $S \to 0$ to find an approximate solution to (5.6).

In contrast to the related analysis for the Schnakenburg model in §5.1, this calculation is slightly more involved since S must first be calculated from a nonlinear algebraic equation. By substituting (5.5) for $\chi(S)$ into the first equation of (5.6), and expanding $\mu = \mu_0 + \nu\mu_1 + \cdots$, we obtain

$$\left[1 + \mu_0 + \nu\left(\mu_1 + 2\pi\nu R_{0p}\right)\right] S \sim \nu\left(\sqrt{\frac{S}{b}} + S\hat{\chi}_1\right)\,,$$

which can be solved asymptotically when $\nu \ll 1$ to get the two-term expansion for S in terms of μ_0 and μ_1 given by

$$S = \nu^2\left(\hat{S}_0 + \nu\hat{S}_1 + \cdots\right)\,; \qquad \hat{S}_0 \equiv \frac{1}{b(1+\mu_0)^2}\,, \qquad \hat{S}_1 \equiv \frac{2}{b(1+\mu_0)^3}\left(\hat{\chi}_1 - \mu_1 - 2\pi R_{0p}\right)\,. \tag{5.7}$$

From the two-term expansion (5.7) for S we calculate $\chi'(S)$ from (5.5) as

$$\chi'(S) \sim \frac{1}{2\sqrt{b}\nu}\left(\hat{S}_0 + \nu\hat{S}_1 + \cdots\right)^{-1/2} + \hat{\chi}_1 \sim \frac{\hat{S}_0^{-1/2}}{2\sqrt{b}\nu} + \left[\hat{\chi}_1 - \frac{\hat{S}_1}{4\sqrt{b}\hat{S}_0^{3/2}}\right] + \mathcal{O}(\nu)\,.$$

By using (5.7) for $\hat{S}_0$ and $\hat{S}_1$, the expression above becomes

$$\chi'(S) \sim \frac{1}{2\nu}\left[(1+\mu_0) + \nu\left(\hat{\chi}_1 + \mu_1 + 2\pi R_{0p}\right) + \mathcal{O}(\nu^2)\right]\,. \tag{5.8}$$

Then, upon substituting (5.8) into the second equation of (5.6) we obtain, up to $\mathcal{O}(\nu)$ terms, that

$$1 + 2\pi\nu R_{b0} \sim (1+\mu_0) + \frac{\nu}{2}\left(\hat{\chi}_1 + 2\pi R_{0p} + \mu_1\right)\,,$$

which determines μ_0 and μ_1 as

$$\mu_0 = 1\,, \qquad \mu_1 = -\hat{\chi}_1 - 2\pi R_{0p} + 4\pi R_{b0}\,. \tag{5.9}$$

Finally, by recalling the definition of μ and $\hat{\chi}_1$ in (5.6) and (5.5), respectively, and by using the two-term expansion $\mu = \mu_0 + \nu\mu_1$ from (5.9), we conclude that $\lambda = 0$ when $D = D^\star(\boldsymbol{k})$, where $D^\star(\boldsymbol{k})$ is given by

$$D^\star(\boldsymbol{k}) \equiv \frac{|\Omega|}{2\pi\nu}\left[1 + \nu\left(4\pi R_{b0}(\boldsymbol{k}) - 2\pi R_{0p} + \frac{1}{b}\int_0^\infty w V_{1p}\rho\, d\rho\right) + \mathcal{O}(\nu^2)\right]\,. \tag{5.10}$$

By minimizing $R_{b0}(\boldsymbol{k})$ with respect to $\boldsymbol{k}$, and then maximizing the result with respect to the geometry of the lattice Λ, (5.10) recovers the main result (4.38) of Principal Result 4.2.

5.3 The Gray-Scott Model

In this sub-section we employ the simple approach of §5.1 and §5.2 to optimize a stability threshold for a periodic pattern of localized spots for the GS model, where the spots are localized at the lattice points of the Bravais lattice

Λ of (2.1). In the Wigner-Seitz cell Ω, the GS model in the dimensionless form of [**19**] is

$$v_t = \varepsilon^2\,\Delta v - v + Auv^2\,, \quad \tau u_t = D\,\Delta u + (1-u) - uv^2\,, \quad \mathbf{x}\in\Omega\,; \qquad \mathcal{P}_0 u = \mathcal{P}_0 v = 0\,, \quad \mathbf{x}\in\partial\Omega\,, \tag{5.11}$$

where $\varepsilon > 0$, $D > 0$, $\tau > 1$, and the feed-rate parameter $A > 0$ are constants. In various parameter regimes of A and D, the stability and self-replication behavior of localized spots for (5.11) have been studied in [**19**], [**20**], [**21**], [**37**], and [**8**] (see also the references therein). We will consider the parameter regime $D = \mathcal{O}(\nu^{-1}) \gg 1$ and $A = \mathcal{O}(\varepsilon)$ of [**37**]. In this regime, and to leading order in ν, an existence and stability analysis of N-spot patterns in a finite domain was undertaken via a Lypanunov Schmidt reduction and a rigorous study of certain nonlocal eigenvalue problems. We briefly review the main stability result of [**37**] following (5.16 *b*) below.

We first construct a one-spot steady-state solution to (5.11) with spot centered at $\mathbf{x} = 0$ in Ω in the regime $D = \mathcal{O}(\nu^{-1})$ and $A = \mathcal{O}(\varepsilon)$ by using the approach in §2 of [**8**].

In the inner region near $\mathbf{x} = 0$ we introduce the local variables U, V, and $\mathbf{y}$, defined by

$$u = \frac{\varepsilon}{A\sqrt{D}}U\,, \qquad v = \frac{\sqrt{D}}{\varepsilon}V\,, \qquad \mathbf{y} = \varepsilon^{-1}\mathbf{x}\,, \tag{5.12}$$

into the steady-state problem for (5.11). We obtain that $U \sim U(\rho)$ and $V \sim V(\rho)$, with $\rho = |\mathbf{y}|$, satisfy the same core problem

$$\Delta_\rho V - V + UV^2 = 0\,, \qquad \Delta_\rho U - UV^2 = 0\,, \qquad 0 < \rho < \infty\,, \tag{5.13 a}$$

$$U'(0) = V'(0) = 0\,; \qquad V \to 0\,, \qquad U \sim S\log\rho + \chi(S) + o(1)\,, \quad \text{as} \quad \rho\to\infty\,, \tag{5.13 b}$$

as that for the Schnakenburg model studied in §3.1, where $S \equiv \int_0^\infty UV^2\rho\,d\rho$ and $\Delta_\rho V \equiv V'' + \rho^{-1}V'$. Therefore, for $S \to 0$, the two-term asymptotics of $\chi(S)$ is given in (5.1) of Lemma 5.1.

To formulate the outer problem for u, we observe that since v is localized near $\mathbf{x} = 0$ we have in the sense of distributions that $uv^2 \to \varepsilon^2\left(\int_{\mathbb{R}^2}\sqrt{D}\,(A\varepsilon)^{-1}\,UV^2\,d\mathbf{y}\right)\,\delta(\mathbf{x}) \sim 2\pi\varepsilon\sqrt{D}A^{-1}S\,\delta(\mathbf{x})$. Then, upon matching u to the core solution U, we obtain from (5.11) that

$$\begin{aligned} \Delta u + \frac{1}{D}(1-u) &= \frac{2\pi\,\varepsilon}{A\sqrt{D}}S\,\delta(\mathbf{x})\,, \quad \mathbf{x}\in\Omega\,; \qquad \mathcal{P}_0 u = 0\,, \quad \mathbf{x}\in\partial\Omega\,, \\ u &\sim \frac{\varepsilon}{A\sqrt{D}}\left(S\log|\mathbf{x}| + \frac{S}{\nu} + \chi(S)\right)\,, \quad \text{as} \quad \mathbf{x}\to 0\,, \end{aligned} \tag{5.14}$$

where $\nu \equiv -1/\log\varepsilon$. The solution to (5.14) is $u = 1 - 2\pi\varepsilon S G_p(\mathbf{x})/(A\sqrt{D})$, where $G_p(\mathbf{x})$ is the Green's function of (4.4). Next, we calculate the local behavior of u as $\mathbf{x}\to 0$ and compare it with the required behavior in (5.14). This yields that S satisfies

$$S + \nu\,[\chi(S) + 2\pi S R_p] = \frac{A\nu\sqrt{D}}{\varepsilon}\,, \tag{5.15}$$

where R_p is the regular part of G_p as defined in (4.4).

We consider the regime $D = D_0/\nu \gg 1$ with $D_0 = \mathcal{O}(1)$. By using the two-term expansion (4.6) for R_p in terms of the regular part R_{0p} of the periodic source-neutral Green's of (3.6), (5.15) becomes

$$S\,(1+\mu) + \nu\,[2\pi S R_{0p} + \chi(S)] + \mathcal{O}(\nu^2) = \mathcal{A}\sqrt{\nu\mu}\,, \tag{5.16 a}$$

where we have defined μ and $\mathcal{A} = \mathcal{O}(1)$ in terms of $A = \mathcal{O}(\varepsilon)$ by

$$\mathcal{A} = \frac{A}{\varepsilon}\sqrt{\frac{|\Omega|}{2\pi}}\,, \qquad \mu \equiv \frac{2\pi D_0}{|\Omega|}\,, \qquad D = \frac{D_0}{\nu}\,. \tag{5.16 b}$$

To illustrate the bifurcation diagram associated with (5.16 *a*), we use $\chi(S) \sim b/S$ as $S \to 0$ from (5.1) of Lemma 5.1. Upon writing $S = \nu^{1/2}\mathcal{S}$, with $\mathcal{S} = \mathcal{O}(1)$, we obtain from (5.16) that, to leading order in ν,

$$\mathcal{A}\sqrt{\mu} = \mathcal{S}(1+\mu) + \frac{b}{\mathcal{S}}\,; \qquad \mu = \frac{2\pi D_0}{|\Omega|}\,, \qquad b = \int_0^\infty w^2 \rho\, d\rho\,. \tag{5.17}$$

From Lemma 5.1 and (5.12), the spot amplitude $V(0)$ to leading order in ν is related to $\mathcal{S}$ by $V(0) = \varepsilon^{-1}\sqrt{D_0}\mathcal{S}w(0)/b$. In Fig. 4 we use (5.17) to plot the leading-order saddle-node bifurcation diagram of $\mathcal{S}$ versus $\mathcal{A}$, where the upper solution branch corresponds a pattern with large amplitude spots. The saddle-node point occurs when $\mathcal{S}_f = \sqrt{b/(1+\mu)}$ and $\mathcal{A}_f = 2\sqrt{b}\sqrt{(1+\mu)/\mu}$. As we show below, there is a zero eigenvalue crossing corresponding to an instability for some Bloch wavevector $\boldsymbol{k}$ with $|\boldsymbol{k}| > 0$ and $\boldsymbol{k}/(2\pi) \in \Omega_B$ that occurs within an $\mathcal{O}(\nu)$ neighborhood of the point $(\mathcal{S}_0, \mathcal{A}_0)$ on the upper branch of Fig. 4 given by $\mathcal{S}_0 = \sqrt{b}$ and $\mathcal{A}_0 = (2+\mu)\sqrt{b/\mu}$. Since $|\boldsymbol{k}| > 0$ for this instability, we refer to it as a competition instability. Below, we will expand $\mathcal{A} = \mathcal{A}_0 + \nu\mathcal{A}_1 + \cdots$, and determine the optimal lattice arrangement of spots that minimizes $\mathcal{A}_1$. This has the effect of maximizing the extent of the upper solution branch in Fig. 4 that is stable to competition instabilities.

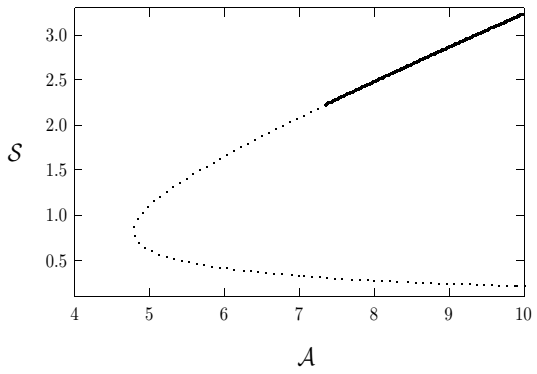

Figure 4. Plot, to leading-order in ν, of the saddle-node bifurcation diagram $\mathcal{S}$ versus $\mathcal{A}$, obtained from (5.17), for the GS model with $|\Omega| = 1$ and $D_0 = 1$. The leading-order spot amplitude $V(0) = \varepsilon^{-1}\sqrt{D_0}\mathcal{S}w(0)/b$ is directly proportional to $\mathcal{S}$. The heavy solid branch of large amplitude spots is linearly stable to competition instabilities, while the dotted branch is unstable to competition instabilities. To leading order in ν, the zero eigenvalue crossing corresponding to the competition instability threshold occurs at $\mathcal{A}_0 = (2+\mu)\sqrt{b/\mu} \approx 7.34$ where $\mathcal{S}_0 = \sqrt{b} \approx 2.22$.

Before proceeding with the calculation of the optimal lattice for the periodic problem, we recall some prior rigorous results of [**37**] for the finite domain problem with N localized spots in a finite domain Ω_N with homogeneous Neumann boundary conditions. From [**37**], the bifurcation diagram to leading order in ν is

$$\mathcal{A}\sqrt{\mu_N} = \mathcal{S}(1+\mu_N) + \frac{b}{\mathcal{S}}\,, \qquad b = \int_0^\infty w^2 \rho\, d\rho\,, \qquad \mu_N = \frac{2\pi N D_0}{|\Omega_N|}\,, \qquad \mathcal{A} = \frac{A}{\varepsilon}\sqrt{\frac{|\Omega_N|}{2\pi N}}\,,$$

which shows that we need only replace $|\Omega|$ in (5.17) with $|\Omega_N|/N$. From a rigorous NLEP analysis of the finite domain problem, it was proved in [**37**] that the lower solution branch in Fig. 4 is unstable to synchronous instabilities, while the upper branch is stable to such instabilities. In contrast, it is only the portion of the upper solution branch with $\mathcal{S} > \mathcal{S}_0$ that is stable to competition instabilities (see Fig. 4). Therefore, there is two zero eigenvalue crossings; one at

the saddle-node point corresponding to a synchronous instability, and one at the point $(\mathcal{S}_0, \mathcal{A}_0)$ on the upper branch corresponding to a competition instability.

Similarly, for the periodic spot problem we remark that there is also a zero eigenvalue crossing when $\boldsymbol{k} = 0$, i.e. the synchronous instability, which occurs at the saddle-node bifurcation point. However, since it is the zero eigenvalue crossing for the competition instability that sets the instability threshold for $\mathcal{A}$ (see Fig. 4), we will not analyze the effect of the lattice geometry on the zero eigenvalue crossing for the synchronous instability mode.

We now proceed to analyze the zero eigenvalue crossing for the competition instability. To determine the stability of the steady-state solution u_e and v_e, we introduce (3.8) into (5.11) to obtain the Floquet-Bloch eigenvalue problem

$$\begin{aligned} &\varepsilon^2\Delta\phi - \phi + 2Au_ev_e\phi + Av_e^2\eta = \lambda\phi\,, \quad \mathbf{x}\in\Omega\,; \qquad \mathcal{P}_{\boldsymbol{k}}\phi = 0\,, \quad \mathbf{x}\in\partial\Omega\,, \\ &D\Delta\eta - \eta - 2u_ev_e\phi - v_e^2\eta = \lambda\tau\eta\,; \qquad \mathcal{P}_{\boldsymbol{k}}\phi = 0\,, \quad \mathbf{x}\in\partial\Omega\,. \end{aligned} \tag{5.18}$$

In the inner region near $\mathbf{x} = 0$ we look for a locally radially symmetric eigenpair $N(\rho)$ and $\Phi(\rho)$, with $\rho = |\mathbf{y}|$, defined in terms of η and ϕ by

$$\eta = \frac{\varepsilon}{A\sqrt{D}}N(\rho)\,, \qquad \phi = \frac{\sqrt{D}}{\varepsilon}\Phi(\rho)\,, \qquad \rho = |\mathbf{y}|\,, \qquad \mathbf{y} = \varepsilon^{-1}\mathbf{x}\,. \tag{5.19}$$

From (5.18), we obtain to within negligible $\mathcal{O}(\varepsilon^2)$ terms that $N(\rho)$ and $\Phi(\rho)$ satisfy

$$\begin{aligned} &\Delta_\rho\Phi - \Phi + 2UV\Phi + NV^2 = \lambda\Phi\,, \qquad \Phi\to 0\,, \quad \text{as} \quad \rho\to\infty\,, \\ &\Delta_\rho N = 2UV\Phi + NV^2\,, \qquad N\sim C\log\rho + B\,, \quad \text{as} \quad \rho\to\infty\,, \end{aligned} \tag{5.20}$$

with $\Phi'(0) = N'(0) = 0$, $B = B(S;\lambda)$, and $C = \int_0^\infty \left(2UV\Phi + NV^2\right)\rho\,d\rho$.

To determine the outer problem for η, we first calculate in the sense of distributions that

$$2u_ev_e\phi + v_e^2\eta \to \frac{\sqrt{D}}{A\varepsilon}\left[\varepsilon^2\int_{\mathbb{R}^2}\left(2UV\Phi + V^2N\right)\,d\mathbf{y}\right]\delta(\mathbf{x}) = \frac{2\pi\varepsilon\sqrt{D}}{A}C\delta(\mathbf{x})\,. \tag{5.21}$$

Then, by asymptotically matching η as $\mathbf{x}\to 0$ with the far-field behavior of N in (5.20), we obtain from (5.21) and (5.18) that the outer problem for η is

$$\begin{aligned} &\Delta\eta - \theta_\lambda^2\eta = \frac{2\pi\varepsilon}{A\sqrt{D}}C\delta(\mathbf{x})\,, \quad \mathbf{x}\in\Omega\,; \qquad \mathcal{P}_{\boldsymbol{k}}\eta = 0\,, \quad \mathbf{x}\in\partial\Omega\,, \\ &\eta\sim\frac{\varepsilon}{A\sqrt{D}}\left[C\log|\mathbf{x}| + \frac{C}{\nu}B\right]\,, \quad \text{as} \quad \mathbf{x}\to 0\,. \end{aligned} \tag{5.22}$$

Here we have defined $\theta_\lambda \equiv \sqrt{(1+\tau\lambda)/D}$. The solution to (5.22) is $\eta = -2\pi\varepsilon C\mathcal{G}_{b\lambda}(\mathbf{x})/(A\sqrt{D})$, where $\mathcal{G}_{b\lambda}$ satisfies (4.13). By imposing that the behavior of η as $\mathbf{x}\to 0$ agrees with that in (5.22), we conclude that $(1 + 2\pi\nu\mathcal{R}_{b\lambda})\,C + \nu B = 0$, where $R_{b\lambda}$ is the regular part of $G_{b\lambda}$ defined in (4.13). Then, since $D = D_0/\nu \gg 1$, we have from Lemma 2.3(ii) upon taking the $D\gg 1$ limit in (4.13) that $R_{b\lambda}\sim R_{b0} + \mathcal{O}(\nu)$ for $|\boldsymbol{k}| > 0$ and $\boldsymbol{k}/(2\pi)\in\Omega_B$. Thus, we have

$$\left(1 + 2\pi\nu R_{b0} + \mathcal{O}(\nu^2)\right)C - \nu B = 0\,, \tag{5.23}$$

where $R_{b0} = R_{b0}(\boldsymbol{k})$ is the regular part of the Bloch Green's function G_{b0} defined on Ω by (2.12). We remark that if we were to consider zero-eigenvalue crossings for a synchronous instability where $\boldsymbol{k} = 0$, we would instead use $R_{b\lambda} = R_p \sim D_0/\nu|\Omega| + R_{0p} + \cdots$ from (4.6) to obtain $\left(1 + \mu + 2\pi\nu R_{p0} + \mathcal{O}(\nu^2)\right)C + \nu B = 0$ in place of (5.23).

As in §5.1 we use the key fact that at $\lambda = 0$, we have $B(S;0) = C\chi'(S)$. Therefore, at $\lambda = 0$, we obtain from (5.23) and (5.16 *a*) that the critical values of $\mathcal{A}$ and S where $\lambda = 0$ satisfy the coupled nonlinear algebraic system

$$S\,(1+\mu) + \nu\left[2\pi SR_{0p} + \chi(S)\right] + \mathcal{O}(\nu^2) = \mathcal{A}\sqrt{\nu\mu}\,, \qquad 1 + 2\pi\nu R_{b0} + \mathcal{O}(\nu^2) + \nu\chi'(S) = 0\,. \tag{5.24}$$

The final step in the calculation is to use the two term expansion for $\chi(S)$, as given in (5.1) of Lemma 5.1, to obtain a two-term approximate solution in powers of ν to (5.24). By substituting $\chi'(S) \sim -bS^{-2} + \hat{\chi}_1$ for $S \ll 1$ into the second equation of (5.24), we readily calculate a two-term expansion for S as

$$S \sim \sqrt{b\nu}\left(1 + \nu\hat{S}_1 + \cdots\right), \qquad \hat{S}_1 \equiv -\frac{1}{2}\left(\hat{\chi}_1 + 2\pi R_{b0}\right). \tag{5.25}$$

Then, we substitute (5.25), together with the two-term expansion

$$\mathcal{A} = \mathcal{A}_0 + \nu\mathcal{A}_1 + \cdots, \tag{5.26}$$

into the first equation of (5.24), and equate powers of ν. From the $\mathcal{O}(\nu^{1/2})$ terms in the resulting expression we obtain that $\mathcal{A}_0 = \sqrt{b}(2+\mu)/\sqrt{\mu}$, while at order $\mathcal{O}(\nu^{3/2})$ we get that $\mathcal{A}_1 = \mathcal{A}_1(\boldsymbol{k})$ satisfies

$$\frac{\mathcal{A}_1}{\sqrt{b\mu}} = \frac{2\pi R_{0p}}{\mu} + \frac{\hat{\chi}_1}{\mu} + \hat{S}_1 = \frac{2\pi R_{0p}}{\mu} - \pi R_{b0}(\boldsymbol{k}) + \hat{\chi}_1\frac{(2-\mu)}{2\mu}, \tag{5.27}$$

where $\hat{\chi}_1$ is given in (5.1) of Lemma 5.1.

To determine the optimal lattice that allows for stability for the smallest value of $\mathcal{A}$, we first fix a lattice Λ and then maximize $\mathcal{A}_1$ in (5.27) through minimizing $R_{b0}(\boldsymbol{k})$ with respect to the Bloch wavevector $\boldsymbol{k}$. Then, we minimize $\mathcal{A}_1$ with respect to the lattice geometry Λ while fixing $|\Omega|$. We summarize this third main result as follows:

Principal Result 5.1 *The optimal lattice arrangement for a steady-state periodic pattern of spots for the GS model (5.11) in the regime $D = D_0/\nu \gg 1$ and $A = \mathcal{O}(\varepsilon)$ is the one for which the objective function $\mathcal{K}_{gs}$ is maximized, where*

$$\mathcal{K}_{gs} \equiv \pi\mu R_{b0}^{\star} - 2\pi R_{0p}, \qquad R_{b0}^{\star} \equiv \min_{\boldsymbol{k}} R_{b0}(\boldsymbol{k}), \qquad \mu \equiv \frac{2\pi D_0}{|\Omega|}. \tag{5.28}$$

For $\nu = -1/\log\varepsilon \ll 1$, a two-term asymptotic expansion for the competition instability threshold of A on the optimal lattice is

$$A_{optim} = \varepsilon\sqrt{\frac{2\pi}{|\Omega|}}\mathcal{A}_{optim}, \qquad \mathcal{A}_{optim} \sim \frac{\sqrt{b}(2+\mu)}{\sqrt{\mu}} + \nu\sqrt{\frac{b}{\mu}}\left(-\max_{\Lambda}\mathcal{K}_{gs} + \frac{1}{b^2}\left(1-\frac{\mu}{2}\right)\int_0^{\infty} V_{1p}\rho\,d\rho\right) + \cdots, \tag{5.29}$$

where $\max_{\Lambda}\mathcal{K}_{gs}$ is taken over all lattices Λ having a common area $|\Omega|$ of the Wigner-Seitz cell. In (5.29), V_{1p} is the solution to (3.7 c), while $b = \int_0^{\infty} w^2\rho\,d\rho \approx 4.93$, where $w(\rho) > 0$ is the ground-state solution of $\Delta_\rho w - w + w^2 = 0$, and $\int_0^{\infty} V_{1p}\rho\,d\rho \approx 0.481$.

We remark that (5.29) can also be derived through the more lengthy but systematic approach given in § 3 and § 4 of first calculating the portion of the continuous spectrum that satisfies $|\lambda| \le \mathcal{O}(\nu)$ when $\mathcal{A} = \mathcal{A}_0 + \mathcal{O}(\nu)$.

The numerical method to compute $\mathcal{K}_{\rm gs}$ is given in §6. In §6.1, we show numerically that within the class of oblique Bravais lattices, $\mathcal{K}_{\rm gs}$ is maximized for a regular hexagonal lattice. Thus, the minimal stability threshold for the feed-rate A occurs for this hexagonal lattice.

6 Numerical Computation of the Bloch Green's Function

We seek a rapidly converging expansion for the Bloch Green's function G_{b0} satisfying (2.12) on the Wigner-Seitz cell Ω for the Bravais lattice Λ of (2.1). It is the regular part R_{b0} of this Green's function that is needed in Principal Results 3.2, 4.2, and 5.1. Since only one Green's function needs to be calculated numerically in this section, for clarity

of notation we remove its subscript. In §6.1 we will revert to the notation of § 2–5 to determine the optimal lattice for the stability thresholds in Principal Results 3.2, 4.2, and 5.1.

Instead of computing the Bloch Green's function on Ω, it is computationally more convenient to equivalently compute the Bloch Green's function $G \equiv G_{b0}$ on all of $\mathbb{R}^2$ that satisfies

$$\Delta G(\mathbf{x}) = -\delta(\mathbf{x})\,; \qquad G(\mathbf{x}+\boldsymbol{l}) = e^{-i\boldsymbol{k}\cdot\boldsymbol{l}}\, G(\mathbf{x})\,, \quad \boldsymbol{l} \in \Lambda\,, \tag{6.1}$$

where $\boldsymbol{k}/(2\pi) \in \Omega_B$. The regular part $R(0) \equiv R_{b0}(0)$ of this Bloch Green's function is defined

$$R(0) \equiv \lim_{\mathbf{x}\to 0} \left(G(\mathbf{x}) + \frac{1}{2\pi}\log|\mathbf{x}| \right). \tag{6.2}$$

To derive a computationally tractable expression for $R(0)$ we will follow closely the methodology of [**3**].

We construct the solution to (6.1) as the sum of free-space Green's functions

$$G(\mathbf{x}) = \sum_{\boldsymbol{l}\in\Lambda} G_{\rm free}(\mathbf{x}+\boldsymbol{l})\, e^{i\boldsymbol{k}\cdot\boldsymbol{l}}\,. \tag{6.3}$$

This sum guarantees that the quasi-periodicity condition in (6.1) is satisfied. That is, if $G(\mathbf{x}) = \sum_{\boldsymbol{l}\in\Lambda} G_{\rm free}(\mathbf{x}+\boldsymbol{l})\, e^{i\boldsymbol{k}\cdot\boldsymbol{l}}$, then, upon choosing any $\boldsymbol{l}^\star \in \Lambda$, it follows that $G(\mathbf{x}+\boldsymbol{l}^\star) = e^{-i\boldsymbol{k}\cdot\boldsymbol{l}^\star}\, G(\mathbf{x})$. To show this, we use $\boldsymbol{l}^\star + \boldsymbol{l} \in \Lambda$ and calculate

$$G(\mathbf{x}+\boldsymbol{l}^*) = \sum_{\boldsymbol{l}\in\Lambda} G_{\rm free}(\mathbf{x}+\boldsymbol{l}^*+\boldsymbol{l})\, e^{i\boldsymbol{k}\cdot\boldsymbol{l}} = \sum_{\boldsymbol{l}\in\Lambda} G_{\rm free}(\mathbf{x}+\boldsymbol{l}^*+\boldsymbol{l})\, e^{i\boldsymbol{k}\cdot(\boldsymbol{l}^*+\boldsymbol{l})}\, e^{-i\boldsymbol{k}\cdot\boldsymbol{l}^*} = e^{-i\boldsymbol{k}\cdot\boldsymbol{l}^*}\, G(\mathbf{x})\,.$$

In order to analyze (6.3), we will use the Poisson summation formula with converts a sum over Λ to a sum over the reciprocal lattice $\Lambda^\star$ of (2.5). In the notation of [**3**], we have (see Proposition 2.1 of [**3**])

$$\sum_{\boldsymbol{l}\in\Lambda} f(\mathbf{x}+\boldsymbol{l})\, e^{i\boldsymbol{k}\cdot\boldsymbol{l}} = \frac{1}{V}\sum_{\boldsymbol{d}\in\Lambda^*} \hat{f}(2\pi\boldsymbol{d}-\boldsymbol{k})\, e^{i\mathbf{x}\cdot(2\pi\boldsymbol{d}-\boldsymbol{k})}\,, \quad \mathbf{x}\,, \boldsymbol{k} \in \mathbb{R}^2\,, \tag{6.4}$$

where $\hat{f}$ is the Fourier transform of f, and $V = |\Omega|$ is the area of the primitive cell of the lattice.

Remark 6.1 *Other authors (cf. [**17**], [**18**]) define the reciprocal lattice as $\Lambda^\star = \{2\pi m\,\boldsymbol{d}_1, 2\pi n\,\boldsymbol{d}_2\}_{m,n\in\mathbb{Z}}$, so that for any $\boldsymbol{l} \in \Lambda$ and $\boldsymbol{d} \in \Lambda^*$, it follows that $\boldsymbol{l}\cdot\boldsymbol{d} = 2K\pi$ for some integer K and hence $e^{i\boldsymbol{l}\cdot\boldsymbol{d}} = 1$. The form of the Poisson summation formula will then differ slightly from* (6.4).

By applying (6.4) to (6.3), it follows that the sum over the reciprocal lattice consists of free-space Green's functions in the Fourier domain, and we will split each Green's function in the Fourier domain into two parts in order to obtain a rapidly converging series. In $\mathbb{R}^2$, we write the Fourier transform pair as

$$\hat{f}(\boldsymbol{p}) = \int_{\mathbb{R}^2} f(\mathbf{x})\, e^{-i\mathbf{x}\cdot\boldsymbol{p}}\,\mathrm{d}\mathbf{x}\,, \qquad f(\mathbf{x}) = \frac{1}{4\pi^2}\int_{\mathbb{R}^2} \hat{f}(\boldsymbol{p})\, e^{i\boldsymbol{p}\cdot\mathbf{x}}\,\mathrm{d}\boldsymbol{p}\,. \tag{6.5}$$

The free space Green's function satisfies $\Delta G_{\rm free} = -\delta(\mathbf{x})$. By taking Fourier transforms, we get $-|\boldsymbol{p}|^2\,\hat{G}_{\rm free}(\boldsymbol{p}) = -1$, so that

$$\hat{G}_{\rm free}(\boldsymbol{p}) = \frac{1}{|\boldsymbol{p}|^2}\,. \tag{6.6}$$

With the right-hand side of the Poisson summation formula (6.4) in mind, we write

$$\frac{1}{V}\sum_{\boldsymbol{d}\in\Lambda^*} \hat{G}_{\rm free}(2\pi\boldsymbol{d}-\boldsymbol{k})\, e^{i\mathbf{x}\cdot(2\pi\boldsymbol{d}-\boldsymbol{k})} = \sum_{\boldsymbol{d}\in\Lambda^*} \frac{e^{i\mathbf{x}\cdot(2\pi\boldsymbol{d}-\boldsymbol{k})}}{|2\pi\boldsymbol{d}-\boldsymbol{k}|^2}\,, \tag{6.7}$$

since $V = 1$. To obtain a rapidly converging series expansion, we introduce the decomposition

$$\hat{G}_{\rm free}(2\pi\boldsymbol{d}-\boldsymbol{k}) = \alpha(2\pi\boldsymbol{d}-\boldsymbol{k},\eta)\,\hat{G}_{\rm free}(2\pi\boldsymbol{d}-\boldsymbol{k}) + \Big(1-\alpha(2\pi\boldsymbol{d}-\boldsymbol{k},\eta)\Big)\,\hat{G}_{\rm free}(2\pi\boldsymbol{d}-\boldsymbol{k})\,, \tag{6.8}$$

for some function $\alpha(2\pi\boldsymbol{d}-\boldsymbol{k},\eta)$. We choose $\alpha(2\pi\boldsymbol{d}-\boldsymbol{k},\eta)$ so that the sum over $\boldsymbol{d}\in\Lambda^*$ of the first set of terms converges absolutely. We apply (6.5) to the second set of terms after first writing $(1-\alpha)\,\hat{G}_{\rm free}$ as an integral. In the decomposition (6.8) we choose the function α as

$$\alpha(2\pi\boldsymbol{d}-\boldsymbol{k},\eta) = \exp\!\left(-\frac{|2\pi\boldsymbol{d}-\boldsymbol{k}|^2}{4\eta^2}\right)\,, \tag{6.9}$$

where $\eta>0$ is a cutoff parameter to be chosen. We readily observe that

$$\lim_{\eta\to 0}\alpha(2\pi\boldsymbol{d}-\boldsymbol{k},\eta)=0\,;\qquad \lim_{\eta\to\infty}\alpha(2\pi\boldsymbol{d}-\boldsymbol{k},\eta)=1\,;\qquad \frac{\partial\alpha}{\partial\eta}=\frac{|2\pi\boldsymbol{d}-\boldsymbol{k}|^2\,\alpha}{2\eta^3}>0\,,\quad \text{since } \alpha>0\,,\ \ \eta>0\,,$$

which shows that $0<\alpha<1$ when $0<\eta<\infty$. Since $0<\alpha<1$, the choice of η determines the portion of the Green's function that is determined from the sum of terms in the reciprocal lattice Λ^* and the portion that is determined from the sum of terms in the lattice Λ.

With the expressions (6.9) for α and (6.6) for $\hat{G}_{\rm free}$, we get

$$\alpha(2\pi\boldsymbol{d}-\boldsymbol{k},\eta)\,\hat{G}_{\rm free}(2\pi\boldsymbol{d}-\boldsymbol{k})\,e^{i\mathbf{x}\cdot(2\pi\boldsymbol{d}-\boldsymbol{k})} = \exp\!\left(-\frac{|2\pi\boldsymbol{d}-\boldsymbol{k}|^2}{4\eta^2}\right)\,\frac{e^{i\mathbf{x}\cdot(2\pi\boldsymbol{d}-\boldsymbol{k})}}{|2\pi\boldsymbol{d}-\boldsymbol{k}|^2}\,. \tag{6.10}$$

Since $2\pi\boldsymbol{d}-\boldsymbol{k}\neq 0$, which follows since $\boldsymbol{k}/(2\pi)\in\Omega_B$, the sum of these terms over $\boldsymbol{d}\in\Lambda^*$ converges absolutely. Following [**3**], we define

$$G_{\rm fourier}(\mathbf{x}) \equiv \sum_{\boldsymbol{d}\in\Lambda^*}\exp\!\left(-\frac{|2\pi\boldsymbol{d}-\boldsymbol{k}|^2}{4\eta^2}\right)\,\frac{e^{i\mathbf{x}\cdot(2\pi\boldsymbol{d}-\boldsymbol{k})}}{|2\pi\boldsymbol{d}-\boldsymbol{k}|^2}\,. \tag{6.11}$$

For the $(1-\alpha)\,\hat{G}_{\rm free}$ term, we define ρ by $\rho\equiv|2\pi\boldsymbol{d}-\boldsymbol{k}|$, so that from (6.9), (6.6), and $\hat{G}_{\rm free}=\hat{G}_{\rm free}(|\boldsymbol{p}|)$, we get

$$\big(1-\alpha(2\pi\boldsymbol{d}-\boldsymbol{k},\eta)\big)\,\hat{G}_{\rm free}(2\pi\boldsymbol{d}-\boldsymbol{k}) = \frac{1}{\rho^2}\left(1-e^{-\rho^2/(4\eta^2)}\right)\,. \tag{6.12}$$

Since $\int e^{-\rho^2\,e^{2s}+2s}\,ds = -e^{-\rho^2\,e^{2s}}/(2\rho^2)$, the right hand side of (6.12) can be calculated as

$$2\int_{-\infty}^{-\log(2\eta)} e^{-\rho^2\,e^{2s}+2s}\,ds = \frac{1}{\rho^2}\left(1-e^{-\rho^2/(4\eta^2)}\right)\,,$$

so that

$$\big(1-\alpha(2\pi\boldsymbol{d}-\boldsymbol{k},\eta)\big)\,G_{\rm free}(2\pi\boldsymbol{d}-\boldsymbol{k}) = 2\int_{\log(2\eta)}^{\infty} e^{-\rho^2\,e^{-2s}-2s}\,ds\,. \tag{6.13}$$

To take the inverse Fourier transform of (6.13), we recall that the inverse Fourier transform of a radially symmetric function is the inverse Hankel transform of order zero (cf. [**23**]), so that $f(r)=(2\pi)^{-1}\int_0^\infty \hat{f}(\rho)\,J_0(\rho r)\,\rho\,d\rho$. Upon using the well-known inverse Hankel transform (cf. [**23**])

$$\int_0^\infty e^{-\rho^2\,e^{-2s}}\,\rho\,J_0(\rho r)\,\mathrm{d}\rho = \frac{1}{2}\,e^{2s-r^2\,e^{2s}/4}\,,$$

we calculate the inverse Fourier transform of (6.13) as

$$\frac{1}{2\pi}\int_0^{\infty}\int_{\log(2\eta)}^{\infty} 2\,e^{-\rho^2 e^{-2s}-2s}\,\rho\,J_0(\rho r)\,\mathrm{d}s\,d\rho = \frac{1}{\pi}\int_{\log(2\eta)}^{\infty} e^{-2s}\left(\int_0^{\infty} e^{-\rho^2\,e^{-2s}}\,\rho\,J_0(\rho r)\,\mathrm{d}\rho\right)ds$$
$$= \frac{1}{2\pi}\int_{\log(2\eta)}^{\infty} e^{-2s}\,e^{2s-\frac{r^2}{4}\,e^{2s}}\,ds = \frac{1}{2\pi}\int_{\log(2\eta))}^{\infty} e^{-\frac{r^2}{4}\,e^{2s}}\,ds\,.$$

In the notation of [**3**], we then define $F_{\rm sing}(\mathbf{x})$ as

$$F_{\rm sing}(\mathbf{x}) \equiv \frac{1}{2\pi}\int_{\log(2\eta)}^{\infty} e^{-\frac{|\mathbf{x}|^2}{4}\,e^{2s}}\,ds\,, \tag{6.14}$$

so that by the Poisson summation formula (6.4), we have

$$G_{\rm spatial}(\mathbf{x}) \equiv \sum_{\boldsymbol{l}\in\Lambda} e^{i\boldsymbol{k}\cdot\boldsymbol{l}}\,F_{\rm sing}(\mathbf{x}+\boldsymbol{l})\,. \tag{6.15}$$

In this way, for $\boldsymbol{k}/(2\pi)\in\Omega_B$, we write the Bloch Green's function in the spatial domain as the sum of (6.11) and (6.15)

$$G(\mathbf{x}) = \sum_{\boldsymbol{d}\in\Lambda^*}\exp\left(-\frac{|2\pi\boldsymbol{d}-\boldsymbol{k}|^2}{4\eta^2}\right)\frac{e^{i\mathbf{x}\cdot(2\pi\boldsymbol{d}-\boldsymbol{k})}}{|2\pi\boldsymbol{d}-\boldsymbol{k}|^2} + \frac{1}{2\pi}\sum_{\boldsymbol{l}\in\Lambda} e^{i\boldsymbol{k}\cdot\boldsymbol{l}}\int_{\log(2\eta)}^{\infty} e^{-\frac{|\mathbf{x}+\boldsymbol{l}|^2}{4}\,e^{2s}}\,ds\,. \tag{6.16}$$

From (6.11) and (6.15), it readily follows that $G_{\rm Fourier}\to 0$ as $\eta\to 0$, while $G_{\rm spatial}\to 0$ as $\eta\to\infty$.

Now consider the behaviour of the Bloch Green's function as $\mathbf{x}\to 0$. From (6.11), we have

$$G_{\rm Fourier}(0) = \sum_{\boldsymbol{d}\in\Lambda^*}\exp\left(-\frac{|2\pi\boldsymbol{d}-\boldsymbol{k}|^2}{4\eta^2}\right)\frac{1}{|2\pi\boldsymbol{d}-\boldsymbol{k}|^2}\,,\qquad \text{for}\quad \boldsymbol{k}/(2\pi)\in\Omega_B\,, \tag{6.17}$$

which is finite since $|2\pi\boldsymbol{d}-\boldsymbol{k}|\neq 0$ and $\eta<\infty$. It is also real-valued. Next, we decompose $G_{\rm spatial}$ in (6.15) as

$$G_{\rm spatial}(\mathbf{x}) = F_{\rm sing}(\mathbf{x}) + \sum_{\substack{\boldsymbol{l}\in\Lambda\\ \boldsymbol{l}\neq 0}} e^{i\boldsymbol{k}\cdot\boldsymbol{l}}\,F_{\rm sing}(\mathbf{x}+\boldsymbol{l})\,. \tag{6.18}$$

For the second term in (6.18), we can take the limit $\mathbf{x}\to 0$ since from (6.14) we have

$$\Big|\sum_{\substack{\boldsymbol{l}\in\Lambda\\ \boldsymbol{l}\neq 0}} e^{i\boldsymbol{k}\cdot\boldsymbol{l}}\,F_{\rm sing}(\boldsymbol{l})\Big| < \infty\,.$$

In contrast, $F_{\rm sing}(\mathbf{x})$ is singular at $\mathbf{x}=0$. To calculate its singular behavior as $\mathbf{x}\to 0$, we write $F_{\rm sing}(\mathbf{x}) = F_{\rm sing}(r)$, with $r=|\mathbf{x}|$, and convert $F_{\rm sing}(r)$ to an exponential integral by introducing u by $u = r^2e^{2s}/4$ in (6.14). This gives

$$F_{\rm sing}(r) = \frac{1}{2\pi}\int_{\log(2\eta)}^{\infty} e^{-\frac{r^2}{4}\,e^{2s}}\,ds = \frac{1}{4\pi}\int_{r^2\,\eta^2}^{\infty}\frac{e^{-u}}{u}\,du = \frac{1}{4\pi}\,E_1(r^2\eta^2)\,, \tag{6.19}$$

where $E_1(z)=\int_z^{\infty} t^{-1}e^{-t}\,dt$ is the exponential integral (cf. §5.1.1 of [**1**]). Upon using the series expansion of $E_1(z)$

$$E_1(z) = -\gamma - \log(z) - \sum_{n=1}^{\infty}\frac{(-1)^n\,z^n}{n\,n!}\,,\qquad \text{for}\quad |\arg z|<\pi\,, \tag{6.20}$$

as given in §5.1.11 of [**1**], where $\gamma = 0.57721\cdots$ is Euler's constant, we have from (6.19) and (6.20) that

$$F_{\rm sing}(r) \sim -\frac{\gamma}{4\pi} - \frac{\log\eta}{2\pi} - \frac{\log r}{2\pi} + o(1)\,,\qquad \text{as}\quad r\to 0\,. \tag{6.21}$$

$\mathbf{x}$	$G(\mathbf{x})$	$R(\mathbf{x})$
(.1,.1)	1.1027-.12568 i	.79138-.12568 i
(.01,01)	1.4730-.012593 i	.79526-.012593 i
$(10^{-3}, 10^{-3})$	1.8396-.0012593 i	.79531-.0012593 i
$(10^{-4}, 10^{-4})$	2.2060-.00012593 i	.79530-.00012593 i
$(10^{-5}, 10^{-5})$	2.5725-.000012593 i	.79529-.000012593 i
$(10^{-6}, 10^{-6})$	2.9389-.0000012593 i	.79531-.0000012593 i
$(10^{-7}, 10^{-7})$	3.3054-.00000012593 i	.79530-.00000012593 i
$(10^{-8}, 10^{-8})$	3.6719-.000000012593 i	.79531-.000000012593 i
$(10^{-9}, 10^{-9})$	4.0383-.0000000012593 i	.79529-.0000000012593 i
$(10^{-10}, 10^{-10})$	4.4048-.00000000012593 i	.79530-.00000000012593 i
$(10^{-11}, 10^{-11})$	4.7713-.000000000012594 i	.79529-.000000000012594 i

Table 1. The regular part $R(\mathbf{x})$ of the Bloch Green's function, as defined in (6.22), for $\mathbf{x}$ tending to the origin for a square lattice with unit area of the primitive cell and with $\eta = 2$ and $\boldsymbol{k} = (\sin\frac{\pi}{3}, \cos\frac{\pi}{3})$. Notice that the imaginary part of $R(\mathbf{x})$ becomes increasingly small as $\mathbf{x} \to 0$, as expected from Lemma 2.1 of § 2.2 where it was established that $R(0)$ is real-valued.

This shows that the Bloch Green's function in (6.16) has the expected logarithmic singularity as $\mathbf{x} \to 0$.

We write the Bloch Green's function as the sum of regular and singular parts as

$$G(\mathbf{x}) = -\frac{1}{2\pi}\,\log|\mathbf{x}| + R(\mathbf{x})\,, \qquad R(\mathbf{x}) = G_{\rm Fourier}(\mathbf{x}) + G_{\rm Spatial}(\mathbf{x}) + \frac{1}{2\pi}\,\log|\mathbf{x}|\,. \tag{6.22}$$

By letting $\mathbf{x} \to 0$, we have from (6.18), (6.21), (6.17), and (6.22), that for $\boldsymbol{k}/(2\pi) \in \Omega_B$

$$R(0) = \sum_{\boldsymbol{d}\in\Lambda^*} \exp\!\left(-\frac{|2\pi\boldsymbol{d}-\boldsymbol{k}|^2}{4\eta^2}\right)\,\frac{1}{|2\pi\boldsymbol{d}-\boldsymbol{k}|^2} + \sum_{\substack{\boldsymbol{l}\in\Lambda\\ \boldsymbol{l}\neq 0}} e^{i\boldsymbol{k}\cdot\boldsymbol{l}}\,F_{\rm sing}(\boldsymbol{l}) - \frac{\gamma}{4\pi} - \frac{\log\eta}{2\pi}\,, \tag{6.23}$$

where $F_{\rm sing}(\boldsymbol{l}) = E_1(|\boldsymbol{l}|^2\eta^2)/(4\pi)$.

For a square lattice, with unit area of the primitive cell and with $\eta = 2$ and $\boldsymbol{k} = (\sin\frac{\pi}{3}, \cos\frac{\pi}{3})$, in Table 1 we give numerical results for $R(\mathbf{x})$ for various values of $\mathbf{x}$ as $\mathbf{x} \to 0$. The computations show that $\mathrm{Im}\,(R(\mathbf{x})) \to 0$ as $\mathbf{x} \to 0$. This provides a partial check on the accuracy of our numerical scheme in the sense that from Lemma 2.1 of § 2.2 we must have that $R(0)$ is real-valued. From Table 1, our computations at $\mathbf{x} = (10^{-10}, 10^{-10})$ show that $R(\mathbf{x})$ is real-valued to within 9 decimal places.

6.1 An Optimal Lattice for Stability Thresholds

In this sub-section we determine the lattice that optimizes the stability thresholds given in Principal Results 3.2, 4.2, and 5.1, for the Schnakenburg, GM, and GS models, respectively. Recall that in the notation of §2–5, $R_{b0}(\boldsymbol{k}) = R(0)$, where $R(0)$ is given in (6.23). The minimum of $R(0)$ with respect to $\boldsymbol{k}$ is denoted by $R^{\star}_{b0}$.

In our numerical computations of $R(0)$ from (6.23) we truncate the direct and reciprocal lattices Λ and Λ^* by the subsets $\bar\Lambda$ and $\bar\Lambda^*$ of Λ and Λ^*, respectively, defined by

$$\bar\Lambda = \left\{n_1\boldsymbol{l}_1 + n_2\boldsymbol{l}_2 \,\middle|\, -M_1 < n_1, n_2 < M_1\right\}\,, \quad \bar\Lambda^* = \left\{n_1\boldsymbol{d}_1 + n_2\boldsymbol{d}_2 \,\middle|\, -M_2 < n_1, n_2 < M_2\right\}\,, \quad n_1, n_2 \in \mathbb{Z}\,.$$

For each lattice, we must pick M_1, M_2 and η so that G can be calculated accurately with relatively few terms in the sum. The computations were done in Maple, with these parameters found by numerical experimentation. For the two regular lattices (square, hexagonal) we used $(M_1, M_2, \eta) = (2, 5, 3)$. For an arbitrary oblique lattice with angle θ between $\boldsymbol{l}_1$ and $\boldsymbol{l}_2$ we took $M_1 = 5$, $M_2 = 3$, and we set $\eta = 3$. The numerical results given below in Table 2

Lattice	$R^\star_{b0}$	R_{0p}	$\mathcal{K}_{\rm s}$	$\mathcal{K}_{\rm gm}$
Square	-0.098259	-0.20706	-0.098259	0.06624
Hexagonal	-0.079124	-0.21027	-0.079124	0.32685

Table 2. Numerical values for $R^\star_{b0} = \min_{\boldsymbol{k}} R(0)$, where $R(0)$ is computed from (6.23), for the square and hexagonal lattice for which $|\Omega| = 1$. The third column is the regular part R_{0p} of the periodic source-neutral Green's function (3.6). The last two columns are $\mathcal{K}_{\rm s}$ and $\mathcal{K}_{\rm gm}$, as defined in Principal Results 3.2 and 4.2, respectively. Of the two lattices, the hexagonal lattice gives the largest values for $\mathcal{K}_{\rm s}$ and $\mathcal{K}_{\rm gm}$.

are believed to be correct to the number of digits shown. Increasing the values of M_1 and M_2 did not change these results.

In Table 2 we give numerical results for $R^\star_{b0}$ for the square and hexagonal lattices. These results show that $R^\star_{b0}$ is largest for the hexagonal lattice. For these two simple lattices, in Table 2 we also give numerical results for R_{0p}, defined by (3.6), as obtained from the explicit formula in Theorem 1 of [**7**] and §4 of [**7**]. In Theorem 2 of [**7**] it was proved that, within the class of oblique Bravais lattices with unit area of the primitive cell, R_{0p} is minimized for a hexagonal lattice. Finally, in the fourth and fifth columns of Table 2 we give numerical results for $\mathcal{K}_{\rm s}$ and $\mathcal{K}_{\rm gm}$, as defined in Principal Results 3.2 and 4.2. Of the two lattices, we conclude that $\mathcal{K}_{\rm s}$ and $\mathcal{K}_{\rm gm}$ are largest for the hexagonal lattice. In addition, since $R^\star_{b0}$ is maximized and R_{0p} is minimized for a hexagonal lattice, it follows that $\mathcal{K}_{\rm gs}$ in Principal Result 5.1 is also largest for a hexagonal lattice. Thus, with respect to the two simple lattices, we conclude that the optimal stability thresholds in Principal Results 3.2, 4.2, and 5.1, occur for a hexagonal lattice.

To show that the same conclusion regarding the optimal stability thresholds occurs for the class of oblique lattices, we need only show that $R^\star_{b0}$ is still maximized for the hexagonal lattice. This is done numerically below.

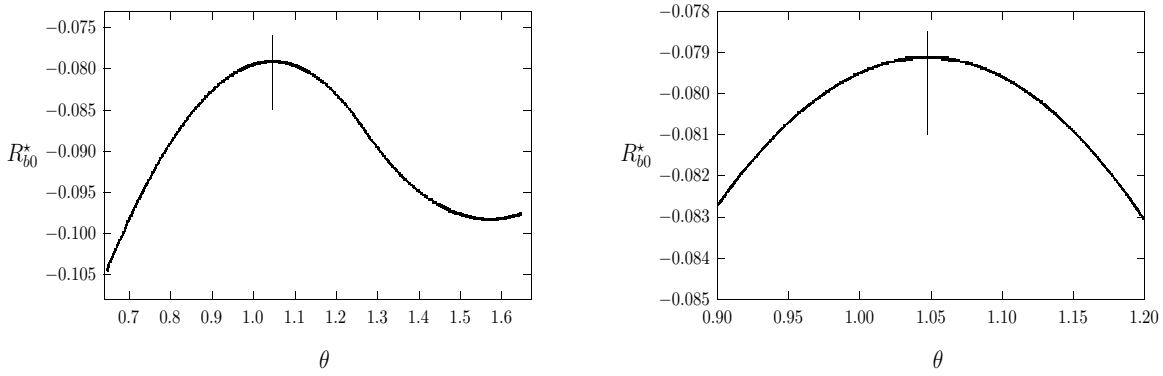

Figure 5. Minimum value $R^\star_{b0}$ of $R_{b0}(\boldsymbol{k})$ for all oblique lattices of unit area for which $\boldsymbol{l}_1 = (1/\sqrt{\sin(\theta)}, 0)$ and $\boldsymbol{l}_2 = (\cos(\theta)/\sqrt{\sin(\theta)}, \sqrt{\sin(\theta)})$, so that $|\boldsymbol{l}_1| = |\boldsymbol{l}_2|$ and $|\Omega| = 1$. The vertical line denotes the hexagonal lattice for which $\theta = \pi/3$. Left figure: the angle θ between the lattice vectors ranges over $0.6 < \theta < 1.7$. Right figure: enlargement of the left figure near $\theta = \pi/3$. The vertical line again denotes the hexagonal lattice.

We first consider lattices for which $|\boldsymbol{l}_1| = |\boldsymbol{l}_2|$. For this subclass of lattices, the lattice vectors are $\boldsymbol{l}_1 = (1/\sqrt{\sin(\theta)}, 0)$ and $\boldsymbol{l}_2 = (\cos(\theta)/\sqrt{\sin(\theta)}, \sqrt{\sin(\theta)})$. In our computations, we first use a coarse grid to find an approximate location in $\boldsymbol{k}$-space of the minimum of $R(0)$ and then we refine the search. After establishing by a coarse discretization that the minimum arises near a vertex of the adjoint lattice, we then sample more finely near this vertex. The finest

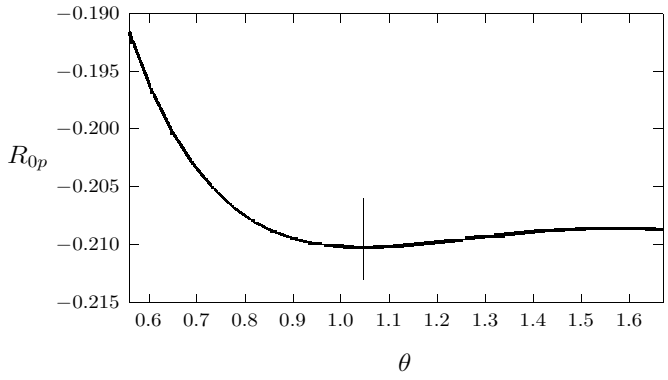

Figure 6. Plot of the the regular part R_{0p}, as given in (6.24) (cf. [**7**]), of the periodic source-neutral Green's function for all oblique lattices of unit area for which $\boldsymbol{l}_1 = (1/\sqrt{\sin(\theta)}, 0)$ and $\boldsymbol{l}_2 = (\cos(\theta)/\sqrt{\sin(\theta)}, \sqrt{\sin(\theta)})$, so that $|\boldsymbol{l}_1| = |\boldsymbol{l}_2|$ and $|\Omega| = 1$. The vertical line denotes the hexagonal lattice for which $\theta = \pi/3$. The minimum occurs for the hexagon.

mesh has a resolution of $\pi/100$. To determine the value of $R^\star_{b0}$ we interpolate a paraboloid through the approximate minimum and the four neighbouring points and evaluate the minimum of the paraboloid. As we vary the lattice by increasing θ, we use the approximate location of the previous minimum as an initial guess. The value of θ is increased by increments of 0.01. Our numerical results in Fig. 5 show that the optimum lattice where $R^\star_{b0} \equiv \min_{\boldsymbol{k}} R(0)$ is maximized occurs for the hexagonal lattice where $\theta = \pi/3$. In Fig. 6 we also plot R_{0p} versus θ (cf. Theorem 1 of [**7**]), given by

$$R_{0p} = -\frac{1}{2\pi}\log(2\pi) - \frac{1}{2\pi}\ln\left|\sqrt{\sin\theta}\, e\,(\xi/12)\prod_{n=1}^{\infty}\left(1-e(n\xi)\right)^2\right|, \quad e(z)\equiv e^{2\pi i z}, \quad \xi = e^{i\theta}. \tag{6.24}$$

Finally, we consider a more general sweep through the class of oblique Bravais lattices. We let $\boldsymbol{l}_1 = (a, 0)$ and $\boldsymbol{l}_2 = (b, c)$, so that with unit area of the primitive cell, we have $ac = 1$ and $b = a^{-1}\cot\theta$, where θ is the angle between $\boldsymbol{l}_1$ and $\boldsymbol{l}_2$. We introduce a parameter α by $a = (\sin\theta)^\alpha$ so that

$$c = (\sin\theta)^{-\alpha} \qquad \text{and} \qquad b = \cos\theta\,(\sin\theta)^{-\alpha-1}\,. \tag{6.25}$$

Then $|\boldsymbol{l}_1| = |\boldsymbol{l}_2|$ when $\alpha = -1/2$, $|\boldsymbol{l}_1| = 1$ (which is independent of θ) when $\alpha = 0$, and $|\boldsymbol{l}_2| = 1$ when $\alpha = -1$. In the left panel of Fig. 7, we plot $R^\star_{b0}$ versus θ for $\alpha = -.5, -.4, -.3, -.2, -.1, 0$. The angle, θ, at which the maximum occurs, increases from $\pi/3$ at $\alpha = -.5$ to about $1.107 = \pi/3 + .06$ for $\alpha = 0$. However, the value of the maximum is largest for $\alpha = -.5$ and decreases as α increases to zero. The regular hexagon occurs only at $\alpha = -.5$ and $\theta = \pi/3$. The vertical line in the plot is at $\theta = \pi/3$. Similarly, in the right panel of Fig. 7 we plot $R^\star_{b0}$ versus θ for $\alpha = -.5, -.6, -.7, -.8, -.9, -1.0$. Since there is no preferred angular orientation for the lattice and since the scale is arbitrary, the plot is identical to the previous plot, in the sense that the curves for $\alpha = -0.6$ and $\alpha = -0.4$ in Fig. 7 are identical. We conclude that it is the regular hexagon that maximizes $R^\star_{b0}$. These computational results lead to the following conjecture:

Conjecture 6.1 *Within the class of Bravais lattices of a common area, $R^\star_{b0}$ is maximized for a regular hexagonal lattice.*

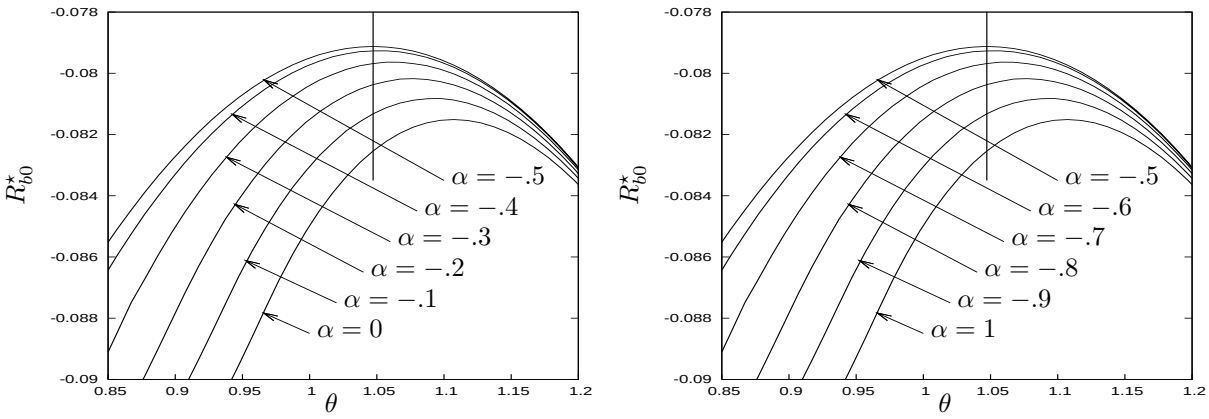

Figure 7. Plot of $R_{b0}^\star$ versus θ for oblique lattices with $\boldsymbol{l}_1 = (a, 0)$ and $\boldsymbol{l}_2 = (b, c)$, where $a = (\sin\theta)^\alpha$ with b and c given in (6.25). Left panel: plots are for $\alpha = -.5, -.4, -.3, -.2, -.1, 0$. Right panel: plots are for $\alpha = -.5, -.6, -.7, -.8, -.9, -1.0$.

7 Discussion

We have studied the linear stability of steady-state periodic patterns of localized spots for the GM and Schnakenburg RD models when the spots are centered for $\varepsilon \to 0$ at the lattice points of a Bravais lattice with constant area $|\Omega|$. To leading order in $\nu = -1/\log\varepsilon$, the linearization of the steady-state periodic spot pattern has a zero eigenvalue when $D = D_0/\nu$ for some D_0 independent of the lattice and the Bloch wavevector $\boldsymbol{k}$. The critical value D_0 can be identified from the leading-order NLEP theory of [**36**] and [**38**]. This zero eigenvalue corresponds to a competition instability of the spot amplitudes (cf. [**36**], [**12**], [**8**], and [**38**]). By using a combination of the method of matched asymptotic expansions, Floquet-Bloch theory, and the rigorous imposition of solvability conditions for perturbations of certain nonlocal eigenvalue problems, we have explicitly determined the continuous band of spectrum that lies within an $\mathcal{O}(\nu)$ neighborhood of the origin in the spectral plane when $D = D_0/\nu + D_1$, where $D_1 = \mathcal{O}(1)$ is a de-tuning parameter. This continuous band is real-valued, and depends on the regular part of the Bloch Green's function and D_1. In this way, for each RD model, we have derived a specific objective function that must be maximized in order to determine the specific periodic arrangement of localized spots that is linearly stable for the largest value of D. A simple alternative method to derive this objective function was also given and applied to the GS model. From a numerical computation, based on an Ewald-type algorithm, of the regular part of the Bloch Green's function that defines the objective function, we have shown within the class of oblique Bravais lattices that a hexagonal lattice arrangement of spots is the most stable to competition instabilities.

Although we have focused our analysis only on the Schnakenburg, GM, and GS models, our asymptotic methodology to derive the model-dependent objective function that determines the optimally stable lattice arrangement of spots is readily extended to general RD systems in the semi-strong interaction regime, such as the Brusselator RD model (cf. [**25**]). Either the simple method of §5, or the more elaborate but systematic method of § 3 and § 4, can then be used to derive the objective function.

There are a few open problems that warrant further investigation. One central issue is to place our formal asymptotic theory on a more rigorous footing. In this direction, it is an open problem to rigorously characterize the continuous band of spectrum that lies near the origin when D is near the critical value. In addition, is it possible to analytically prove Conjecture 6.1 that, within the class of oblique Bravais lattices of a common area, $R_{b0}^\star$ is maximized for a hexagonal lattice?

As possible extensions to this work, it would be interesting to characterize lattice arrangements of spots that maximize the Hopf bifurcation threshold in τ. To analyze this problem, one would have to calculate any continuous band of spectra that lies within an $\mathcal{O}(\nu)$ neighborhood of the Hopf bifurcation frequency $\lambda = i\lambda_{I0}$ when $\tau - \tau_I \ll 1$, where τ_I and λ_{I0} is the Hopf bifurcation threshold and frequency, respectively, on the Wigner-Seitz cell.

We remark that we have not analyzed any weak instabilities due to eigenvalues of order $\lambda = \mathcal{O}(\varepsilon^2)$ associated with the translation modes. It would be interesting to determine steady-state lattice arrangements of localized spots that optimize the linear stability properties of these modes. For these translation modes we might expect, in contrast to what we found in this paper for competition instabilities (see Remark 3.1 and Lemma 2.2), that it is the long-wavelength instabilities with $|\boldsymbol{k}| \ll 1$ that destabilize the pattern. Long-wavelength instabilities have been shown to be the destabilizing mechanism for periodic solutions on 3-D Bravais lattices of two-component RD systems in the weakly nonlinear Turing regime (cf. [**5**], [**6**]).

Finally, it would be interesting to examine the linear stability properties of a collection of $N \gg 1$ regularly-spaced localized spots on a large but finite domain with Neumann boundary conditions, and to compare the spectral properties of this finite domain problem with that of the periodic problem in $\mathbb{R}^2$. For the finite domain problem, we expect that there are N discrete eigenvalues (counting multiplicity) that are asymptotically close to the origin in the spectral plane when D is close to a critical threshold. Research in this direction is in progress.

Acknowledgements

D. I. and M. J. W. were supported by NSERC (Canada). Prof. Juncheng Wei was partially supported by an Earmarked Grant from RGC of Hong Kong and by NSERC (Canada). M.J.W. is grateful to Prof. Edgar Knobloch (U.C. Berkeley) for his comments regarding the de-stabilizing mechanisms of periodic weakly-nonlinear Turing patterns on lattices.

Appendix A Schnakenburg Model: Expansion of the Core Problem

We outline the derivation of the results of Lemma 3.1, as given in §6 of [**12**], and those of Lemma 5.1. To motivate the appropriate scaling for solutions U, V, and χ to (3.2) for $S \to 0$. Upon writing $U = \mathcal{U}S^{-p}$, $V = \mathcal{V}S^{p}$, where $\mathcal{U}$ and $\mathcal{V}$ are $\mathcal{O}(1)$ as $S \to 0$, we obtain that the V-equation in (3.2) is unchanged, but that the U equation becomes

$$\Delta_\rho \mathcal{U} = S^{2p}\,\mathcal{U}\mathcal{V}^2\,; \qquad \mathcal{U} \sim S^{1+p}\log\rho + S^p\chi \quad \text{as} \quad \rho \to \infty\,.$$

From equating powers of S after first applying the divergence theorem, we obtain that $2p = p + 1$, which yields $p = 1$. Then, to ensure that $\mathcal{U} = \mathcal{O}(1)$, we must have $\chi = \mathcal{O}(S^{-p})$. This shows that if $S = S_0\nu^{1/2}$ where $\nu \ll 1$, the appropriate scalings are $V = \mathcal{O}(\nu^{1/2})$, $U = \mathcal{O}(\nu^{-1/2})$, and $\chi = \mathcal{O}(\nu^{-1/2})$.

With this basic scaling, we then proceed to calculate higher order terms in the expansion of the solution to the core problem by writing $S = S_0\nu^{1/2} + S_1\nu^{3/2} + \cdots$ and then determining the first two terms in the asymptotic solution U, V, and χ to (3.2) in terms of S_0 and S_1. The appropriate expansion for these quantities is (see (6.2) of[**12**])

$$V \sim \nu^{1/2}\,(V_0 + \nu V_1 + \cdots)\,, \qquad (\chi\,, U) = \nu^{-1/2}\,[(\chi_0\,, U_0) + \nu\,(\chi_1\,, U_1) + \cdots]\,. \tag{A.1}$$

Upon substituting (A.1) into (3.2), and collecting powers of ν, we obtain that U_0 and V_0 satisfy

$$\begin{aligned} &\Delta_\rho V_0 - V_0 + U_0 V_0^2 = 0\,; \qquad \Delta_\rho U_0 = 0\,, \qquad 0 \le \rho < \infty\,, \\ &V_0 \to 0\,, \qquad U_0 \to \chi_0 \quad \text{as} \quad \rho \to \infty\,; \qquad V_0'(0) = U_0'(0) = 0\,, \end{aligned} \tag{A.2}$$

where $\Delta_\rho V_0 \equiv V_0'' + \rho^{-1} V_0'$. At next order, U_1 and V_1 satisfy

$$\Delta_\rho V_1 - V_1 + 2U_0V_0V_1 = -U_1V_0^2\,; \qquad \Delta_\rho U_1 = U_0V_0^2\,, \qquad 0 \le \rho < \infty\,,$$
$$V_1 \to 0\,, \qquad U_1 \to S_0 \log\rho + \chi_1 \quad \text{as} \quad \rho \to \infty\,; \qquad V_1'(0) = U_1'(0) = 0\,. \tag{A.3}$$

Then, at one higher order, we get that U_2 satisfies

$$\Delta_\rho U_2 = U_1V_0^2 + 2U_0V_0V_1\,, \qquad 0 \le \rho < \infty\,; \qquad U_2 \sim S_1\log\rho + \chi_2 \quad \text{as} \quad \rho \to \infty\,; \qquad U_2'(0) = 0\,. \tag{A.4}$$

The solution to (A.2) is simply $U_0 = \chi_0$ and $V_0 = w/\chi_0$, where $w(\rho) > 0$ is the unique radially symmetric solution of $\Delta_\rho w - w + w^2 = 0$ with $w(0) > 0$ and $w \to 0$ as $\rho \to \infty$. To determine χ_0 in terms of S_0 we apply the divergence theorem to the U_1 equation in (A.3) to obtain

$$S_0 = \int_0^\infty U_0V_0^2\,\rho\,d\rho = \frac{b}{\chi_0}\,, \qquad b \equiv \int_0^\infty \rho w^2\,d\rho\,. \tag{A.5}$$

It is then convenient to decompose U_1 and V_1 in terms of new variables U_{1p} and V_{1p} by

$$U_1 = \chi_1 + \frac{U_{1p}}{\chi_0}\,, \qquad V_1 = -\frac{\chi_1 w}{\chi_0^2} + \frac{V_{1p}}{\chi_0^3}\,. \tag{A.6}$$

Upon substituting $U_0 = \chi_0$, $V_0 = w/\chi_0$, (A.5), and (A.6) into (A.3), and by using $\Delta_\rho w - w + 2w^2 = w^2$, we readily obtain that U_{1p} and V_{1p} are the unique radially symmetric solutions of (3.7 c). Finally, we use the divergence theorem on the U_2 equation in (A.4) to determine χ_1 in terms of S_1 as

$$S_1 = \int_0^\infty \left(2U_0V_0V_1 + U_1V_0^2\right)\rho\,d\rho = -\frac{\chi_1}{\chi_0^2}\int_0^\infty w^2\rho\,d\rho + \frac{1}{\chi_0^3}\int_0^\infty \left(2wV_{1p} + w^2U_{1p}\right)\rho\,d\rho\,.$$

We then use $\Delta_\rho V_{1p} - V_{1p} = -w^2U_{1p} - 2wV_{1p}$ in the integral, as obtained from (3.7 c), and we simplify the resulting expression by using $U_0 = \chi_0$ and $V_0 = w/\chi_0$. This yields $S_1 = -b^{-1}\chi_1 S_0^2 + b^{-3}S_0^3\int_0^\infty V_{1p}\rho\,d\rho$, which gives (3.7 d) for χ_1. This completes the derivation of Lemma 3.1.

To obtain the result in Lemma 5.1, we set $S = S_0\nu^{1/2}$ and $S_1 = 0$ in (3.7) to obtain

$$V \sim \frac{S}{S_0}\left(\frac{w}{\chi_0} + \frac{S^2}{S_0^2}\left(-\frac{\chi_1 w}{\chi_0^2} + \frac{V_{1p}}{\chi_0^3}\right)\right)\,, \qquad U \sim \frac{S_0}{S}\left(\chi_0 + \frac{S^2}{S_0^2}\left(\chi_1 + \frac{U_{1p}}{\chi_0}\right)\right)\,, \qquad \chi \sim \frac{S_0\chi_0}{S} + \frac{S}{b^2}\int_0^\infty V_{1p}\rho\,d\rho\,, \tag{A.7}$$

since $\chi_1 = S_0 b^{-2}\int_0^\infty V_{1p}\rho\,d\rho$ from (3.7 d). Finally, since $S_0\chi_0 = b$ from (3.7 d), (A.7) reduces to (5.1) of Lemma 5.1.

Appendix B Gierer-Meinhardt Model: Expansion of the Core Problem

We outline the derivation of the results of Lemma 4.1 and Lemma 5.2. To motivate the scalings for the solution U, V, and χ to (4.2) as $S \to 0$, we write $U = \mathcal{U}S^p$, $V = \mathcal{V}S^p$, where $\mathcal{U}$ and $\mathcal{V}$ are $\mathcal{O}(1)$ as $S \to 0$. We obtain that the V-equation in (4.2) is unchanged, but that the U equation becomes

$$\Delta_\rho \mathcal{U} = -S^p\mathcal{V}^2\,; \qquad \mathcal{U} \sim -S^{1-p}\log\rho + S^{-p}\chi \quad \text{as} \quad \rho \to \infty\,.$$

From equating powers of S after applying the divergence theorem it follows that $p = 1 - p$, which yields $p = 1/2$. Then, $\chi = \mathcal{O}(S^{1/2})$ ensures that $\mathcal{U} = \mathcal{O}(1)$. This shows that if $S = S_0\nu^2$ where $\nu \ll 1$, the appropriate scalings are that V, U, and χ are all $\mathcal{O}(\nu)$. To obtain a two-term expansion for the solution to the core problem, as given in Lemma 4.1, we expand $S = S_0\nu^2 + S_1\nu^3 + \cdots$ and we seek to determine the solution U, V, and χ to (4.2) in terms

of S_0 and S_1. The appropriate expansion for these quantities has the form

$$(V\,,U\,,\chi) = \nu\,(V_0\,,U_0\,,\chi_0) + \nu^2\,(V_1\,,U_1\,,\chi_1) + \nu^3\,(V_2\,,U_2\,,\chi_2) + \cdots\,. \tag{B.1}$$

Upon substituting (B.1) into (4.2), and collecting powers of ν, we obtain that U_0 and V_0 satisfy

$$\begin{aligned} &\Delta_\rho V_0 - V_0 + V_0^2/U_0 = 0\,; \qquad \Delta_\rho U_0 = 0\,, \qquad 0 \le \rho < \infty\,, \\ &\qquad V_0 \to 0\,, \qquad U_0 \to \chi_0 \quad \text{as} \quad \rho \to \infty\,; \qquad V_0'(0) = U_0'(0) = 0\,, \end{aligned} \tag{B.2}$$

where $\Delta_\rho V_0 \equiv V_0'' + \rho^{-1} V_0'$. At next order, U_1 and V_1 satisfy

$$\begin{aligned} &\Delta_\rho V_1 - V_1 + \frac{2V_0}{U_0} V_1 = \frac{V_0^2}{U_0^2} U_1\,; \qquad \Delta_\rho U_1 = -V_0^2\,, \qquad 0 \le \rho < \infty\,, \\ &\qquad V_1 \to 0\,, \qquad U_1 \to -S_0 \log\rho + \chi_1 \quad \text{as} \quad \rho \to \infty\,; \qquad V_1'(0) = U_1'(0) = 0\,. \end{aligned} \tag{B.3}$$

Then, at one higher order, we get that U_2 satisfies

$$\Delta_\rho U_2 = -2V_0 V_1\,, \qquad 0 \le \rho < \infty\,; \qquad U_2 \sim -S_1 \log\rho + \chi_2 \quad \text{as} \quad \rho \to \infty\,; \qquad U_2'(0) = 0\,. \tag{B.4}$$

The solution to (B.2) is simply $U_0 = \chi_0$ and $V_0 = \chi_0 w$, where $w(\rho) > 0$ is the radially symmetric ground-state solution of $\Delta_\rho w - w + w^2 = 0$. Next, by applying the divergence theorem to the U_1 equation in (B.3) we obtain

$$S_0 = \int_0^\infty \rho V_0^2\, d\rho = \chi_0^2 b\,, \qquad b \equiv \int_0^\infty \rho w^2\, d\rho\,. \tag{B.5}$$

It is then convenient to decompose U_1 and V_1 in terms of new variables U_{1p} and V_{1p} by

$$U_1 = \chi_1 + S_0 U_{1p}\,, \qquad V_1 = \chi_1 w + S_0 V_{1p}\,. \tag{B.6}$$

Upon substituting $U_0 = \chi_0$, $V_0 = \chi_0 w$, (B.5), and (B.6) into (B.3), and by using $\Delta_\rho w - w + 2w^2 = w^2$, we readily obtain that U_{1p} and V_{1p} are the unique radially symmetric solutions of (4.8 *c*). Finally, we use the divergence theorem on the U_2 equation in (B.4) to obtain $2\chi_0\chi_1 b + 2\chi_0 S_0 \int_0^\infty w V_{1p}\rho\, d\rho = S_1$, which readily yields (4.8 *d*).

To obtain the result in Lemma 5.2, we set $S = S_0\nu^2$ and $S_1 = 0$ in (4.8), with $\chi_0^2 = S_0/b$ from (4.8 *d*), to get

$$V \sim \sqrt{\frac{S}{S_0}}\chi_0 w + \frac{S}{S_0}\,(\chi_1 w + S_0 V_{1p})\,, \qquad U \sim \sqrt{\frac{S}{S_0}}\chi_0 + \frac{S}{S_0}\,(\chi_1 + S_0 U_{1p})\,, \qquad \chi \sim \sqrt{\frac{S}{S_0}}\chi_0 + \frac{S}{S_0}\chi_1\,, \tag{B.7}$$

where $\chi_1 = -S_0 b^{-1} \int_0^\infty w V_{1p}\rho\, d\rho$ from (4.8 *d*). Since $S_0 = b\chi_0^2$ from (4.8 *d*), (B.7) reduces to (5.5) of Lemma 5.2.

References

[1] M. Abramowitz, I. Stegun, *Handbook of mathematical functions*, 9th edition, New York, NY, Dover Publications.

[2] N. Ashcroft, N. D. Mermin, *Solid state physics*, HRW International Relations, CBS Publishing Asia Ltd (1976).

[3] G. Beylkin, C. Kurcz, L. Monzón, *Fast algorithms for Helmholtz Green's functions*, Proc. R. Soc. A, **464**, (2008), pp. 3301-3326.

[4] G. Beylkin, C. Kurcz, L. Monzón, *Fast convolution with the free space Helmholtz Green's functions*, J. Comput. Phys., **228**(8), (2009), pp. 2770-2791.

[5] T. K. Callahan, E. Knobloch, *Symmetry-breaking bifurcations on cubic lattices*, Nonlinearity, **10**(5), (1997), pp. 1179-1216.

[6] T. K. Callahan, E. Knobloch, *Long-wavelength instabilities of three dimensional patterns*, Phys. Rev. E., **64**(3), 036214, (2001).

[7] X. Chen, Y. Oshita, *An application of the modular function in nonlocal variational problems*, Arch. Rational Mech. Anal., **186**(1), (2007), pp. 109-132.

[8] W. Chen, M. J. Ward, *The stability and dynamics of localized spot patterns in the two-dimensional Gray-Scott model*, SIAM J. Appl. Dyn. Sys., **10**(2), (2011), pp. 582–666.

[9] A. Doelman, R. A. Gardner, T. Kaper, *Large stable pulse solutions in reaction-diffusion equations*, Indiana U. Math. Journ., **50**(1), (2001), pp. 443-507.

[10] A. Doelman, R. A. Gardner, T. Kaper, *A stability index analysis of 1-D patterns of the Gray-Scott model*, Memoirs of the AMS **155** (737), (2002).
[11] D. Iron, M. J. Ward and J. Wei, *The stability of spike solutions to the one-dimensional Gierer-Meinhardt model*, Physica D, **150**(1-2), (2001), pp. 25–62.
[12] T. Kolokolnikov, M. J. Ward, J. Wei, *Spot self-replication and dynamics for the Schnakenberg Model in a two-dimensional domain*, J. Nonlinear Sci., **19**(1), (2009), pp. 1–56.
[13] T. Kolokolnikov, M. S. Titcombe, M. J. Ward, *Optimizing the fundamental Neumann eigenvalue for the Laplacian in a domain with small traps*, European J. Appl. Math., **16**(2), (2005), pp. 161–200.
[14] E. Knobloch, *Spatially localized structures in dissipative systems: open problems*, Nonlinearity, **21**(1), (2008), pp. T45–T60.
[15] I. M. Krichever, *Spectral theory of two-dimensional periodic operators and its applications*, Russian Mathematical Surveys, **44**(2), (1989), pp. 145–225.
[16] P. Kuchment, *Floquet theory for partial differential equations*, Birkhauser, Basel, 1993.
[17] C. M. Linton, *Lattice sums for the Helmholtz equation*, SIAM Rev., **52**(4), (2010), pp. 630–674.
[18] A. Moroz, *Quasi-periodic Green's functions of the Helmholz and Laplace equations*, J. Phys. A: Math. Gen., **39**(36), (2006), pp. 11247-11282.
[19] C. Muratov, V. V. Osipov, *Static spike autosolitons in the Gray-Scott model*, J. Phys. A: Math Gen. **33**, (2000), pp. 8893–8916.
[20] C. Muratov, V. V. Osipov, *Spike autosolitons and pattern formation scenarios in the two-dimensional Gray-Scott model*, Eur. Phys. J. B. **22**, (2001), pp. 213–221.
[21] C. Muratov and V. V. Osipov, *Stability of static spike autosolitons in the Gray-Scott model*, SIAM J. Appl. Math., **62**(5), (2002), pp. 1463–1487.
[22] Y. Nishiura, *Far-from equilibrium dynamics, translations of mathematical monographs*, Vol. **209**, AMS Publications, Providence, Rhode Island, (2002).
[23] R. Piessens, "The Hankel Transform.", *The transforms and applications handbook: second edition* Editor: Alexander D. Poularikas Boca Raton: CRC Press LLC, 2000.
[24] S. Pillay, M. J. Ward, A. Pierce, T. Kolokolnikov, *An asymptotic analysis of the mean first passage time for narrow escape problems: Part I: two-dimensional domains*, SIAM Multiscale Modeling and Simul., **8**(3), (2010), pp. 803–835.
[25] I. Rozada, S. Ruuth, M. J. Ward, *The stability of localized spot patterns for the Brusselator on the sphere*, submitted, SIADS, (August 2013), (51 pages).
[26] E. Sandier, S. Serfaty, *From the Ginzburg-Landau model to vortex lattice problems*, Comm. Math. Phys., **313**(3), (2012), pp. 635–743.
[27] I. M. Sigal, T. Tzaneteas, *Abrikosov vortex lattices at weak magnetic fields*, J. Funct. Anal. **263**(3), (2012), pp. 675–702.
[28] I. M. Sigal, T. Tzaneteas, *Stability of Abrikosov lattices under gauge-periodic perturbations*, Nonlinearity **25**(4), (2012), pp. 1187–1210.
[29] H. Van der Ploeg, A. Doelman, *Stability of spatially periodic pulse patterns in a class of singularly perturbed reaction-diffusion equations*, Indiana Univ. Math. J., **54**(5), (2005), pp. 1219-1301.
[30] V. K. Vanag, I. R. Epstein, *Localized patterns in reaction-diffusion systems*, Chaos, **17**(3), 037110, (2007).
[31] A. G. Vladimirov, J. M. McSloy, D. S. Skryabin, W. J. Firth, *Two-dimensional clusters of solitary structures in driven optical cavities*, Phys. Rev. E., **65** 046606, (2002)
[32] M. J. Ward, W. D. Henshaw, J. Keller, *Summing logarithmic expansions for singularly perturbed eigenvalue problems*, SIAM J. Appl. Math, **53**(3), (1993), pp. 799–828.
[33] M. J. Ward, J. Wei, *Hopf bifurcations and oscillatory instabilities of spike solutions for the one-dimensional Gierer-Meinhardt model*, J. Nonlinear Science, **13**(2), (2003), pp. 209–264.
[34] J. Wei, *On single interior spike solutions for the Gierer-Meinhardt system: uniqueness and stability estimates*, Europ. J. Appl. Math., **10**(4), (1999), pp. 353-378.
[35] J. Wei, *Existence and stability of spikes for the Gierer-Meinhardt system*, book chapter in *Handbook of Differential Equations, Stationary Partial Differential Equations*, Vol. 5 (M. Chipot ed.), Elsevier, (2008), pp. 489–581.
[36] J. Wei, M. Winter, *Spikes for the two-dimensional Gierer-Meinhardt system: the weak coupling case*, J. Nonlinear Sci., **11**(6), (2001), pp. 415–458.
[37] J. Wei, M. Winter, *Existence and stability of multiple spot solutions for the Gray-Scott model in* $\mathbb{R}^2$, Physica D, **176**(3-4), (2003), pp. 147–180.
[38] J. Wei, M. Winter, *Stationary multiple spots for reaction-diffusion systems*, J. Math. Biol., **57**(1), (2008), pp. 53–89.